Geochemistry, Geophysics, Geosystems®

AGU ADVANCING EARTH AND SPACE SCIENCES

RESEARCH ARTICLE
10.1029/2023GC011025

Key Points:

- The availability of magma storage depth constraints along the Cascade arc is highly variable and not well correlated to volcano threat level
- Available geophysical, mineral-melt and melt inclusion (MI) constraints cluster at 0–15 km depth (~2 ± 2 kbar), consistent with global compilations
- Investigating the potential for deeper storage of the most mafic magmas will require studies accounting for MI vapor bubble CO_2

Supporting Information:

Supporting Information may be found in the online version of this article.

Correspondence to:

P. E. Wieser,
Penny_wieser@berkeley.edu

Citation:

Wieser, P. E., Kent, A. J. R., Till, C. B., & Abers, G. A. (2023). Geophysical and geochemical constraints on magma storage depths along the Cascade arc: Knowns and unknowns. *Geochemistry, Geophysics, Geosystems*, *24*, e2023GC011025. https://doi.org/10.1029/2023GC011025

Received 26 APR 2023
Accepted 2 SEP 2023

Author Contributions:

Conceptualization: Penny E. Wieser, Adam J. R. Kent, Christy B. Till, Geoff A. Abers
Data curation: Penny E. Wieser, Geoff A. Abers
Formal analysis: Penny E. Wieser
Funding acquisition: Adam J. R. Kent, Christy B. Till, Geoff A. Abers
Investigation: Penny E. Wieser, Geoff A. Abers

Geophysical and Geochemical Constraints on Magma Storage Depths Along the Cascade Arc: Knowns and Unknowns

Penny E. Wieser[1,2], Adam J. R. Kent[2], Christy B. Till[3], and Geoff A. Abers[4]

[1]Department of Earth and Planetary Sciences, UC Berkeley, Berkeley, CA, USA, [2]College of Earth, Ocean, and Atmospheric Sciences, Oregon State University, Corvallis, OR, USA, [3]School of Earth and Space Exploration, Arizona State University, Tempe, AZ, USA, [4]Earth and Atmospheric Sciences, Cornell University, Ithaca, NY, USA

Abstract The iconic volcanoes of the Cascade arc stretch from Lassen Volcanic Center in northern California, through Oregon and Washington, to the Garibaldi Volcanic Belt in British Columbia. Recent studies have reviewed differences in the distribution and eruptive volumes of vents, as well as variations in geochemical compositions and heat flux along strike (amongst other characteristics). We investigate whether these along-arc trends manifest as variations in magma storage conditions. We compile available constraints on magma storage depths from InSAR, geodetics, seismic inversions, and magnetotellurics for each major edifice and compare these to melt inclusion saturation pressures, pressures calculated using mineral-only barometers, and constraints from experimental petrology. The availability of magma storage depth estimates varies greatly along the arc, with abundant geochemical and geophysical data available for some systems (e.g., Lassen Volcanic Center, Mount St. Helens) and very limited data available for other volcanoes, including many which are classified as "very high threat" by the USGS (e.g., Glacier Peak, Mount Baker, Mount Hood, Three Sisters). Acknowledging the limitations of data availability and the large uncertainties associated with certain methods, available data are indicative of magma storage within the upper 15 km of the crust (~2 ± 2 kbar) beneath the main edifices. These findings are consistent with previous work recognizing barometric estimates cluster within the upper crust in many arcs worldwide. There are no clear offsets in magma storage between arc segments that are in extension, transtension or compression, although substantially more petrological work is needed for fine scale evaluation of storage pressures.

Plain Language Summary The Cascade arc contains a number of large volcanoes, which present a significant hazard to human populations and infrastructure (e.g., Mount St. Helens, Mount Rainier). Until now, there has been no wide-scale review of where magma (molten rock) is stored in the crust beneath these volcanoes, even though understanding where magma is stored is very important to help monitor unrest at these volcanoes and to predict future activity. We compile all available data on magma storage for each volcano, and find that many volcanoes have had very few studies investigating them, despite the risk they pose to society. The available data (albeit sparse) suggest that most magma is stored at 0–15 km depth before eruption.

1. Introduction

Determining the depths at which magmas are stored in continental arcs is a key parameter to help inform models of the formation and evolution of the continental crust (e.g., Ducea et al., 2015; Lee & Anderson, 2015; Rudnick, 1995), as well as to aid our understanding of volcanic eruptions and hazards. For example, precise determinations of magma storage depths help to distinguish between end-member models, where magmas may be distributed in a mush zone spanning the entire crust (Cashman et al., 2017), or concentrated in distinct magma storage reservoirs, such as Kilauea Volcano (Poland et al., 2014; Wieser et al., 2021), and Bezymianny Volcano (Turner et al., 2013). Magma storage depths also influence the eruptive style, size and frequency of volcanic eruptions (Huber et al., 2019), and can be used to help interpret signals of volcanic unrest in monitoring data (Pritchard et al., 2019). Integration of petrological and geophysical constraints on magma storage depths was also identified as vital to improve our understanding of magma storage, staging and transport by the Subduction Zones in 4D (SZ4D) initiative (Hilley et al., 2022).

The Cascade arc presents an interesting case study to investigate magma storage depths, because of the wide variability in volcano morphology, magma compositions, and parameters relating to magma production along the arc (Hildreth, 2007; Till et al., 2019). The Cascade arc trends North-South along the Western margin of the

Methodology: Penny E. Wieser
Project Administration: Adam J. R. Kent, Christy B. Till, Geoff A. Abers
Resources: Penny E. Wieser, Adam J. R. Kent, Christy B. Till
Software: Penny E. Wieser
Supervision: Adam J. R. Kent, Christy B. Till
Validation: Penny E. Wieser
Visualization: Penny E. Wieser
Writing – original draft: Penny E. Wieser
Writing – review & editing: Penny E. Wieser, Adam J. R. Kent, Christy B. Till, Geoff A. Abers

US and Canada, forming as the result of the eastward subduction of the Juan de Fuca and Gorda plates beneath the North American plate. Quaternary activity in the Cascades has occurred at >2,300 individual vents, with at least 30 topographically prominent edifices representing longer-lived magmatic systems (Hildreth, 2007). These larger edifices stretch from Lassen Peak in North California (USA) to Mount Meager in British Columbia (Canada) along an approximately linear trend, erupting mostly intermediate and silicic magmas (Figure 1). The more distributed off-axis fields of smaller, often monogenetic vents are characterized by more mafic compositions (O'Hara et al., 2020). In addition to activity focused around the arc axis, there are also three prominent rear-arc volcanoes/volcanic fields (Simcoe Mountains, Newberry Volcano, and Medicine Lake; Donnelly-Nolan et al., 2008; Hildreth & Fierstein, 2015; Sherrod et al., 1997). This off axis volcanism is thought to be associated with the impingement of the Basin and Range extensional province on the eastern limit of Cascade volcanism (Guffanti & Weaver, 1988; Priest et al., 2013).

Volcanism in the Cascades presents a significant societal hazard. Fourteen Cascade edifices have been active since the late Holocene. 10 are classified by the USGS National Volcanic Threat assessment as "Very High Threat" (Mount St. Helens, Mount Rainier, Mount Shasta, Mount Hood, Three Sisters, Lassen Volcanic Center, Newberry Volcano, Mount Baker, Glacier Peak, Crater Lake; Ewert et al., 2018), while Mount Adams and Medicine Lake are listed as "High Threat" (Figure 1).

Over the last few decades, a number of studies have reviewed various aspects of Cascade volcanism on an arc-scale. Hildreth (2007) provided a comprehensive summary of the number, location, and distribution of Quaternary vents, along with descriptions of eruptive activity and approximate volume estimates of different vents along the arc. Poland et al. (2017) reviewed geodetic data collected over several decades in the Cascades to investigate the diverse causes of surface deformation. From a geochemical perspective, Schmidt et al. (2008) and Pitcher and

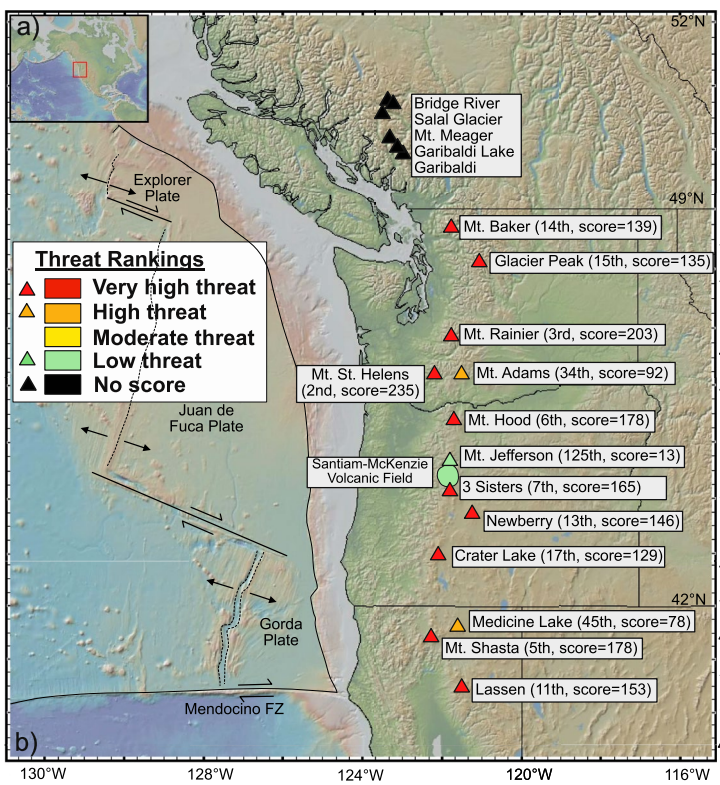

X No data
93 # of measurements
? Data exists but link to magmatic system unclear
✓ Data places constraint on depth

c)

	Petrology						Geophysics				
	MI +Quant VB	MI no Quant VB	Cpx	Amp	Cpx-Opx	ExpPet	Geodetics	Magneto-tellurics	Seismics	LPs	3bb at <20 km
Canadian GVB	X	93	15	X	X	X	X	X	X	X	X
Baker	X	8	230	10	X	X	✓	X	X	31	1
Glacier Peak	X	16	18	X	X	X	X	X	X	8	X
Mt. Rainier	X	X	79	16	X	✓	X	iMUSH Regional + local		18	13
Mt. Adams	X	X	1214	30	X	X	X			X	X
Mt. St. Helens	X	65	64	993	X	✓	✓	✓		8	16
Mt. Hood	X	38	56	274	X	X	X	X	X	X	8
Mt. Jefferson	X	X	35	323	25	X	X	X	X	X	X
Santiam VF	X	77	X	X	X	X	X	X	X	X	X
3 Sisters	X	X	17	X	X	X	✓	X	X	1	4
Newberry	X	X	X	X	X	?	?	✓	✓	✓	8
Crater Lake	X	144	333	245	X	X	X	X	X	1	4
Medicine Lake	X	X	21	7	X	✓	?	X	✓	1	X
Mt. Shasta	X	45	328	X	116	✓	X	X	?	X	4
Lassen	13	192	535	542	X	✓	?	✓	?	20	1

Figure 1. Schematic diagram showing the available barometric constraints along the Cascade arc. The locations of the major volcanoes from the USGS Holocene catalog (Hildreth, 2007) are overlain on a GeoMapApp base image (Ryan et al., 2009) with triangles colored by the USGS threat rankings. The numbers show the threat score and threat rank out of 161 US volcanoes included in the assessment (first being the most hazardous). The Santiam-Mckenzie volcanic field is not given a score, but the report says that it has a similar threat level to the individual low-threat centers (Blue Lake, Belknap etc.). The table schematic shows the availability of different types of data at each volcano. 3bb is the number of broadband seismometers within 20 km. Numbers show mineral analyses remaining after filtering described in Section 3. These numbers differ slightly from the number of calculated pressures shown on later figures, as some compositions return NaNs with certain barometers.

Kent (2019) reviewed the major, trace and isotopic composition of samples to assess compositional variability along the arc. Integrating geophysics and geochemistry, Till et al. (2019) examined variations in erupted volumes and compositions, heat budget, and seismic velocities along the Cascade arc to investigate the influence of crustal processes (e.g., tectonic stress state) versus mantle processes (e.g., magma generation, variations in subduction parameters, mantle wedge dynamics) on Cascade variability.

While geophysical and petrological studies have been performed at individual centers to investigate the pressures, temperatures and timescales associated with the magmatic plumbing system, there has been no detailed arc-scale review of magma storage conditions. A brief compilation was presented by Dufek et al. (2022, their Figure 3). However, data sources and uncertainty associated with each estimate were not discussed, and we have identified many additional constraints, both from the literature and our own petrological calculations. Based on the correlation between low seismic phase velocities and crustal heat flow, Till et al. (2019) suggested that crustal seismic structure and heat flow are primarily controlled by magmatic processes and advection of heat occurring in the upper mantle/deepest crust, and that the flux of mantle-derived basalt varies by a factor of two along strike in the Quaternary Cascades. In ocean-island basalts, it has been shown that volcanoes with longer repose periods (a proxy for magma supply rate) are characterized by deeper magma storage (Gleeson et al., 2021). This correlation may indicate that large melts fluxes are required to maintain active crustal storage reservoirs in the cooler upper crust. Thus, it may be expected that shallower magma storage depths are found in regions of the arc with higher mantle supply. Alternatively, magma storage in the Cascades may be controlled by crustal processes such as the crustal stress state, prominent lithological or density boundaries within the crust (Chaussard & Amelung, 2014), or magmatic H_2O contents (Rasmussen et al., 2022).

Numerous methods have been used to determine magma storage depths in the Cascades and elsewhere. These can broadly be subdivided into geophysical and petrological methods. One common petrological method is thermobarometry, which relies on pressure-sensitivity of the exchange of chemical components within a single mineral, between two minerals, or between minerals and the liquid from which they crystallize or re-equilibrate with (see Putirka, 2008). In the Cascades, equilibrium between clinopyroxene and liquid (Cpx-Liq), clinopyroxene-orthopyroxene (Cpx-Opx), and amphibole-liquid (Amp-Liq), as well as liquid compositions themselves have been used to determine magma storage conditions (e.g., Blundy, 2022; Hollyday et al., 2020; Scruggs & Putirka, 2018). Melt inclusion (MI) barometry is another petrological technique that has been applied to the Cascades (e.g., Aster et al., 2016; Ruscitto et al., 2010; Wright et al., 2012), which relies on the strong relationship between pressure and the concentration of CO_2 and H_2O in a volatile-saturated silicate melt (e.g., Dixon, 1997; Ghiorso & Gualda, 2015; Shishkina et al., 2014). After determining the volatile (and major element) contents of MIs at the time at which these pockets of melt were trapped within crystals, a mixed fluid solubility model can be used to calculate the minimum pressure at which the magma was volatile saturated. Finally, experimental petrology can be used to determine the conditions of magma storage, by comparing the chemistry of erupted products to experiments conducted at varying pressure, temperature and fluid compositions (e.g., Mandler et al., 2014; Quinn, 2014).

Various geophysical methods for imaging magma bodies have been applied to the Cascades. Magnetotellurics images the conductivity structure of the crust, which can help identify regions of melt and fluid, as well as hot intrusions (e.g., Bedrosian et al., 2018; Bowles-Martinez & Schultz, 2020). Seismic tomography using natural earthquakes or controlled sources (e.g., Kiser et al., 2016; Moran et al., 1999; Ulberg et al., 2020; Zucca & Evans, 1992) and methods that use the ambient seismic noise wavefield (e.g., Flinders & Shen, 2017; Heath et al., 2018; Jiang et al., 2023) are used to probe the elastic velocity structure of the crust. Seismic wave velocities are sensitive to composition and mineralogy, temperature, and the presence of melt or other fluids, while the attenuation of seismic waves is relatively more sensitive to temperature and fluids (Abers & Hacker, 2016; Magee et al., 2018).

A variety of geodetic methods (e.g., tilt, leveling, GPS and InSAR; Dzurisin et al., 2009; Mastin et al., 2008; Poland et al., 2017) have been used to identify changes in the ground surface around volcanoes, which can help identify intrusion of new magma into the crust. Seismicity also provides an indicator of deformation associated with magma movement, delineating pathways of magma transport (e.g., Jones & Malone, 2005). However, as for petrological methods, many caveats exist for these geophysical methods. For example, ground deformation and earthquakes can arise from both volcanic and tectonic processes (Dzurisin et al., 2006; Jones & Malone, 2005; Poland et al., 2006), and it can be difficult to robustly distinguish crustal velocity and conductivity anomalies from magma versus hot but solidified intrusions versus other compositional variations such as sedimentary units (e.g., Bedrosian et al., 2018 vs. Bowles-Martinez & Schultz, 2020; Flinders & Shen, 2017).

Here, we compile available geophysical and geochemical magma storage depths for the main Cascade volcanic centers (Figure 1). We anticipate that this review will serve several purposes. First, it can be used as a reference of available storage depths at each volcano. Perhaps more importantly, it is very helpful to identify high threat volcanoes where data is very sparse, and future work should be prioritized.

2. Methods

When compiling and collating magma storage depths along the arc into a single coherent database, it is important to ensure consistency between published depth estimates from different volcanoes. We discuss the approaches used below for each proxy to ensure consistency along-arc.

3. Mineral Barometry

For mineral-based barometry, we compile Amp and Cpx compositions from a wide variety of studies, along with a smaller number of matched Opx-Cpx analyses. In many cases, we could not obtain contextual information of whether the analysis was taken at a core or rim. A notable exception is the data of Streck and Leeman (2018) who overlaid their measurements on thin section images. One problem with literature compilations of mineral compositions is that a number of published analyses are labeled as Cpx are actually Amp or Opx or vice versa. To automatically sort through these, we use a sklearn support vector classification machine learning algorithm (linear kernel) trained on a compilation of pyroxenes, feldspars, amphiboles, apatites, olivines, and oxides. Analyses classified as pyroxenes are further filtered to only use analyses with cation sum between 3.95 and 4.05, and Ca/(Ca + Mg + Fe) atomic ratios between 0.2 and 0.5 for Cpx and 0–0.06 for Opx (excluding pigeonites). We filter out Amp with cation sums outside of 15–16. All thermobarometry and filtering calculations were performed using the open-source Python3 tool Thermobar (Wieser et al., 2022c).

Cpx-based barometry in the Cascades has utilized a variety of models to convert measured phase compositions into pressures (and temperatures). Hollyday et al. (2020) and Scruggs and Putirka (2018) used the Cpx-Liq barometer of Neave and Putirka (2017) iterated with the Cpx-Liq thermometer of Putirka (2008, Equation 33). Sas et al. (2017) used the Cpx-Liq barometer from Putirka (2008, Equation 32c) with an unspecified thermometer. However, applying different Cpx-Liq barometry equations to the same Cpx-Liq pairs yield pressures that can differ by 3–12 kbar (~10–45 km, see Wieser et al., 2023b), which is an offset equivalent to the thickness of the Cascade crust (Das & Nolet, 1998). Additionally, Cpx-Liq barometry relies on identifying or reconstructing a liquid composition in equilibrium with each Cpx composition (Scruggs & Putirka, 2018), which is challenging in arcs where whole-rock compositions may not necessary represent true liquids (Kent et al., 2010) and many equilibrium tests perform badly (Wieser et al., 2023b). Given that Cpx-only and Cpx-Liq barometers show similar performance for a data set of arc-like experimental products (Wieser et al., 2023b), we avoid melt-matching complications by using the Cpx-only barometers of Jorgenson et al. (2022, hereafter J2022) and Wang et al. (2021 Equation 1, hereafter W2021). These two Cpx-only barometers show the best RMSE and R^2 values (J2022: $R^2 = 0.78$, RMSE = 1.9 kbar, W2021: $R^2 = 0.66$, RMSE = 2.4 kbar) and least systematic error when tested on several hundred experiments relevant to arc magmas conducted at 0–17 kbar that were not used in model calibration (ArcPL dataset, Wieser et al., 2023b). These RMSE mean that these two Cpx-only barometers can identify magma storage depths within ~15–18 km of the true value at 1σ confidence. The relatively thick crust in the Cascades (~40–50 km, Jiang et al., 2023; Kiser et al., 2016; Parsons et al., 1998; Shehata & Mizunaga, 2022) means that Cpx-based barometry can roughly distinguish between storage in the upper, mid and lower crust at best. Another advantage of these two barometers is that they are independent of temperature and H_2O content, which are difficult to estimate from Cpx compositions alone (Wieser et al., 2023b). An additional complication with literature compilations is that the quality of mineral analyses in our compilation is not known, as publications do not quote the analytical precision of each measurement. Analytical uncertainty related to the measurement of Na_2O in pyroxene can easily yield errors spanning 3–5 kbar on each individual Cpx measurement (Wieser et al., 2023c). Averaging multiple Cpx compositions at each volcano can help to mitigate these random analytical errors (Putirka et al., 1996), and results in a substantial improvement when applied to the experimental data investigated by Wieser et al. (2023b). Thus, we predominantly focus on median pressures calculated for each volcano.

Identifying equilibrium Amp-Liq pairs is even more challenging than for Cpx-Liq, because the only widely used equilibrium test to assess equilibrium is the exchange of Fe-Mg ($K_{D\ Fe\text{-}Mg}$). Tests on experiments in the ArcPL data set not used to calibrate the Amp-only barometer of Ridolfi (2021, hereafter R2021) returns RMSE = 2.7 kbar and $R^2 = 0.67$, which indicates that this barometer peforms moderately well as long as extreme care is taken to ensure that the barometer is being used within the P-T-X limits of the calibration (Wieser et al., 2023a). When displaying Amp-only pressures, gray kernel distributions and black crosses show amphiboles that pass the compositional filters of Ridolfi (2021, Figures 2–12). We also apply an additional filter to remove Amp with atomic proportions on the basis of 13 cations >6.8 for Si, and <1.1 for Al, which lie outside the calibration range of the Ridolfi model. These filtered pressures are shown with a green kernel distribution and gray crosses on Figures 2–12 (see also supporting Figures S1 and S2 in Supporting Information S1). In general, these two additional filters remove Amp with the lowest calculated pressures. A large number of Amp at Lassen ($N = 260$, Figure 2) are excluded using this filter, affecting the interpretation of magma storage, but at other volcanoes this filter has a minor influence on the median pressure.

For Cpx-Opx, we calculate pressures by iterating Putirka (2008) Equations 36(T)-39(P) and 37(T)-39(P). Using a new data set of arc mineral and liquid compositions not used to calibrate such models (ArcPL, Wieser et al., 2023b, 2023c) we find that these two-pyroxene barometers behave poorly for Cpx with Mg# < 0.68, so we filter out such pairs. Even for Mg# > 0.68, it should be noted that Cpx-Opx barometry has a large RMSE (3.7–4.1 kbar).

Blundy (2022) released a liquid-only thermobarometry method to calculate temperature, pressure and fluid composition (X_{H_2O}) from the composition of a liquid saturated in Cpx-Hornblende(Amp)-Opx-Magnetite-Plagiclase-Ilmenite (CHOMPI). They examined experiments specific to Mount St. Helens, and then additional experiments to produce an empirical expression which can be used to obtain the conditions of storage of CHOMPI-saturated magmas. They applied this method to the youngest rocks erupted from 16 Cascade volcanic centers. However, no independent test data set was used by Blundy (2022) to assess the performance of this model, and the influence of false positives was not widely assessed (e.g., the algorithm classifying the liquid as CHOMPI-saturated when it was not). By coding CHOMPI into Python3 (available in Thermobar, Wieser et al., 2022c), we are able to perform such independent tests. Using the same filtering criteria Blundy (2022) use for the Cascades, CHOMPI calculations returned a false positive rate of ~46% on the ArcPL dataset, and a very poor relationship between experimental and CHOMPI pressure (see Text S1, Figure S3 in Supporting Information S1). Thus, we do not discuss the results from this method further.

We also compile experimental constraints where directly relevant to a specific Cascade edifice. We quote these pressures as published.

4. Melt Inclusion Saturation Pressures

Solubility models can be used to estimate the pressure at which a melt with a given major element composition, volatile content and temperature becomes volatile-saturated. Thus, assuming a MI was trapped from a volatile-saturated magma, the pressure at the time of MI entrapment can be calculated. However, Cascade MI studies have used a wide variety of solubility models (see Table S1 in Supporting Information S1). Because the calibration data sets of many of these models span a limited compositional range, calculated saturation pressures can easily differ by a factor of two or more (Wieser et al., 2022b). Thus, the use of different models at different volcanoes adds considerable uncertainty when comparing depths. For consistency, we use published major element and volatile contents to recalculate all saturation pressures using the solubility model MagmaSat implemented in the Open-source Python3 tool VESIcal (Iacovino et al., 2021), Wieser et al. (2022b) show that this model best recreates experimental data for andesitic and dacitic compositions, and has the largest calibration data set of all available models.

MI saturation pressures have other limitations. If crystals are growing and trapping MIs during storage in the crust, the distribution of MI saturation pressures will reveal the main magma storage regions. However, MIs can also form during ascent toward the surface, because degassing of H_2O is often accompanied by crystallization (Applegarth et al., 2013; Lipman et al., 1985). This can result in substantial "smearing" of saturation pressures toward shallower pressures. It is also becoming increasingly apparent from Raman spectroscopic analyses that a large proportion of the total CO_2 in a MI is held within the vapor bubble in olivine-hosted MIs in arc magmas (e.g., Mironov et al., 2020; L. R. Moore et al., 2015, 2018). Accurate Raman measurements require each laboratory to carefully determine the relationship between Raman spectral features and CO_2 densities using an optical apparatus where CO_2 gas is held at varying pressure conditions and temperature is closely controlled (DeVitre et al., 2021;

Lamadrid et al., 2017). Alternatively a calibration can be developed using reference materials measured in a laboratory with a calibration apparatus (e.g., Mironov et al., 2020; Wieser et al., 2021). Only the MI vapor bubbles from two cinder cones near Lassen Peak by Aster et al. (2016) have been measured on a calibrated Raman system. Venugopal et al. (2020) performed Raman measurements but used a literature calibration line rather than an instrument-specific calibration. The large number of their bubbles measured at room temperature with reported CO_2 densities above the thermodynamical limit indicates that their calibration may have overestimated CO_2 densities (DeVitre et al., 2023). Other studies reconstructed vapor bubbles in olivine-hosted MIs using bubble growth models (Johnson & Cashman, 2020; Walowski et al., 2019). However, these reconstructions require a precise estimate of the amount of post-entrapment crystallization (PEC) experienced by MIs, which in turn, requires accurate estimates of the initial FeO_t content of each MI (Danyushevsky & Plechov, 2011). Estimating initial FeO_t is very challenging for monogenetic cones, where the fractionation path is uncertain because only a very narrow range of liquid compositions were erupted. The remaining studies of olivine-hosted MIs do not measure or reconstruct the vapor bubble (e.g., Ruscitto et al., 2010; Walowski et al., 2016). As a result, saturation pressures obtained from published MI data must be interpreted with extreme caution, due to uncertainty regarding total CO_2 contents.

To obtain a self-consistent database, we calculate saturation pressures using bubble + glass CO_2 from Aster et al. (2016) and Venugopal et al. (2020), with the important caveat that the Venugopal et al. (2020) Raman measurements may have overestimated CO_2 because of the absence of an instrument-specific calibration. We do not use modeled bubble reconstructions from other papers, because of the wide variability of different approaches used, and the sensitivity of these methods to reliable estimates of the amount of PEC, H_2O-loss etc., which we do not have sufficient data to reliably estimate. Thus, it is important to recognize that the pressures shown for the mafic MI from studies other than Aster et al. and Venugopal et al. are very much minimum estimates, and the pressures would likely increase dramatically if bubble CO_2 were accounted for. For more silicic MIs, it is very difficult to assess the possible influence of the vapor bubble, given a lack of available measurements globally.

5. Trends at a Single Volcano

Ideally, we would look at trends in magma storage through time at each volcano, and variations in storage as a function of magma chemistry. Where possible, we split data by major volcanic phase (e.g., Figure 2—Lassen domefield vs. Brokeoff Volcano). We also indicate the mineral phase hosting MIs on figures (e.g., Ol-hosted MIs indicate storage of the most mafic magmas, Qtz-hosted the most silicic). Determining the relationship between storage and magma composition is particularly challenging with Cpx and Amp barometry. Given that magma mixing is ubiquitous in the Cascade arc, minerals erupted in a silicic magma cannot be assumed to have grown from that magma composition (and vice versa for minerals erupted in a mafic magma). In Supporting Information S1, we show Cpx barometry results plotted against Cpx Mg# and grouped by study. No robust trends appear, although there is a possible hint that the most mafic magmas are indeed stored deeper. We show using experimental data that calculating liquid compositions from Amp to compare to pressures generates spurious trends, because similar Amp components are used to calculate chemistry and pressure (Figure S5 in Supporting Information S1). Detailed work at each edifice would be required to resolve differences in magma storage as a function of magma chemistry that are not apparent in our literature compilation.

6. Calculating Depths and Reconciling Different Reference Levels

MI saturation pressure and mineral barometers yield pressures, which are then converted to depths (H) using assumptions about crustal density (e.g., $P = \rho gH$) or a crustal density model. Cascade MI and thermobarometry studies have used a wide variety of crustal densities to convert pressures into depths in the crust ($\rho = 2{,}200$ kg/m^3 by Bacon et al., 1992, $\rho = 2{,}700$ kg/m^3 by Hollyday et al., 2020, $\rho = 2{,}800$ kg/m^3 by Johnson & Cashman, 2020, $\rho = 2{,}200$ kg/m^3 for the first 2 km and $\rho = 2{,}800$ below that by Gardner et al., 1995). Here, we convert pressures to depths using a uniform crustal density of $\rho = 2{,}700$ kg/m^3.

In contrast, geophysical methods generally determine depths relative to a variety of reference levels. We abbreviate these as: below sea level (bsl), below ground level (bgl), below average station level (basl), and studies where the reference level is unknown (rlu). When comparing geophysical depths to one another, and to petrological estimates, it is important to account for different reference levels. For consistency, we adjust all measures to yield depth below the summit of each volcano. This means that geophysical estimates will match petrological estimates

if the magma chamber is centrally located. However, given evidence for magma reservoirs being offset from the volcanoes summit (Lerner et al., 2020), this correction could lead to a systematic offset between petrological and geophysical estimates. To allow visual assessment of these possible offsets, we include a topographic profile across each major edifice on each diagram, extracted from the ASTER global digital elevation model V003 using QGIS (NASA/METI/AIST/Japan Space systems and U.S./Japan ASTER Science Team, 2019; QGIS.org, 2022). Petrological and geophysical estimates could be displaced from one another by a vertical distance equivalent to the maximum height of the topographic profile.

7. Seismic Data Coverage

To obtain the km-scale resolution required to image magma bodies using seismic or magnetotelluric methods, it is normally necessary to obtain data using short-term high-density array deployments (e.g., Bedrosian et al., 2018; Kiser et al., 2018; Zucca & Evans, 1992). At relatively well-monitored volcanoes such as Mount Rainier and Mount St. Helens, these arrays can be used in conjunction with permanent volcano-monitoring networks (e.g., Moran et al., 1999; Ulberg et al., 2020; G. P. Waite & Moran, 2009). To help conceptualize the evolution in the quality and amount of seismic data available at different volcanoes, we plot the position of seismometers within ∼20 km (0.18°) of the summit of each major edifice on a map and a timeline for each major US Cascade volcano (Figures 2–14). The underlying station metadata was pulled from the IRIS GMAP server (http://ds.iris.edu/gmap/) and the Pacific Northwest Seismic Network (PNSN) compilation (https://pnsn.org/seismograms/map, both updated, 5 September 2022, http://ds.iris.edu/gmap/). We classify stations based on their station code as 1 component short period (1sp), 3 component short period (3sp) or 3 component broadband (3bb). Short-period stations are often older, analog-telemetered with limited dynamic range. Waveform-based measurements (such as ambient noise tomography, receiver functions, attenuation measurements) tend to be challenging using this data. Those stations are most useful for local earthquake travel-time tomography (e.g., Moran et al., 1999). Newer broadband stations, generally installed in the mid-late 2010s, provide more imaging options.

As permanent monitoring networks are densified and older 1- or 3-component seismometers are replaced with modern broadband seismometers, the potential for a new generation of imaging using only permanent installations increases, both through increased station density, and the potential for wavefield-based imaging methods using broadband data. For example, broadband data enables ambient-noise imaging, which provides high-accuracy estimates of shear-wave velocity (V_s) at the upper-crustal depths where magma storage frequently occurs (e.g., Crosbie et al., 2019; Jiang et al., 2023). We also summarize the presence and depth of Deep Long Period earthquakes (DLPs, Nichols et al., 2011), although exactly how these signals relate to the volcanic plumbing system is still enigmatic.

8. Results

Data coverage varies widely along the Cascades (Figures 1–15). Some edifices such as Mount St. Helens have an abundance of petrological and geophysical studies using a variety of methods (seismics, magnetotellurics, geodetics, Figure 10). Some volcanoes are relatively well studied using one method but not the other (e.g., very little petrology but moderate to good geophysical coverage at Newberry and Mount Rainier, Figures 7 and 12), while other volcanoes have very little data from either method (e.g., Three Sisters, Glacier Peak, Figures 6 and 13). The variability of available data reflects a combination of the heavy focus of research efforts on certain volcanoes (particularly for petrology), quiescence or noisy geophysical signals at certain centers (Poland et al., 2017), and often-insurmountable issues associated with permitting any monitoring equipment within protected wilderness areas and parks (Moran & Benjamin, 2021). It is interesting that there is no apparent correlation between the estimated threat level or ranking out of all US volcanoes and the availability of data (Ewert et al., 2018; Figure 1).

9. Lassen Volcanic Center

Activity at Lassen Volcanic Center is subdivided into three main eruptive stages: (a) the Rockland Caldera Complex (825–609 ka), (b) Brokeoff Volcano (590–385 ka), and (c) the Lassen domefield (∼300 ka to present, Clynne et al., 2008). Three dominant Holocene eruptions have occurred during the Lassen domefield stage; Chaos Crags (∼850 CE, Clynne et al., 2008), Cinder Cone (1666 CE, Sheppard et al., 2009), and Lassen Peak (1914–1917 CE; Clynne, 1999). There are also abundant mafic cinder cones within the Lassen segment of the Cascades, with both calc alkaline and tholeiite compositions (Walowski et al., 2019).

9.1. Mineral Compositions

Unpublished Cpx compositions were obtained from M. Clynne and B. Platt for samples from a range of formations from Brokeoff Volcano described in Bullen and Clynne (1990) and Clynne et al. (2008). These include andesites from the Diller sequence (470–385 Kyr ago, e.g., Rice Creek, Mount Diller) and the Mill Canyon sequence (470–590 Kyr, Clynne & Muffler, 2010). Platt (2020) measured core-rim traverses for Cpx crystals from Brokeoff Volcano. We extract core and rim compositions from these profiles, except for the longest traverses, where we extract core, intermediate and rim analyses for Cpx-only calculations.

Underwood et al. (2012) analyzed Amp from the several Lassen domefield stage eruptions for hydrogen isotopes, water contents and ferric/ferrous ratios and major elements which we use for Amp-only barometry ($N = 313$). These units represented by these analyses are the ∼35 ka Kings Creek unit, 28.3 ka dacite dome on Lassen Peak, 850 CE Chaos Crags, and 1914–1917 CE Lassen Peak.

Hollyday et al. (2020) performed Cpx-Liq thermobarometry calculations on samples from a cinder cone from the basaltic-andesite of Box Canyon (middle Pleistocene age). They combined $N = 20$ core analyses with a primitive MI composition from the basalt of Big Lake (BBL) from Walowski et al. (2016), and obtained pressures of 460–700 MPa using the Cpx-Liq barometer of Neave and Putirka (2017). However, we were not able to obtain the exact liquid composition used by the authors and could not recreate these pressures. Considering all PEC-corrected MIs from BBL, we instead obtain pressures distributed between −0.5 and ∼2.5 kbar (regardless of the exact equilibrium tests used). This discrepancy makes the inference from Hollyday et al. (2020) of lower crustal storage difficult to validate.

Overall, after applying the filters described in Section 3, Cpx-only barometry using W2021 yields median pressures of ∼0.6 kbar for Brokeoff volcano, and ∼1.9 kbar for the Lassen domefield. Pressures using J2022 are slightly deeper compared to W2021 for both formations (median = 1.4 kbar for Brokeoff, 2.6 kbar for the domefield). These deeper pressures likely result from the fact that extra-tree regression strategies used by J2022 never yield negative numbers, skewing averages toward anomalously high pressures. If Amp-only pressures are calculated using just the filters of Ridolfi (2021), the median pressure is 1.2 kbar. However, if we also discard amphiboles with Al and Si cation fractions outside the range of the calibration data set, we obtain substantially higher pressures (3.2 kbar). We favor the deeper, more extensively filtered median pressures (∼3.2 kbar), as none of the experiments used to calculate the R2021 barometer were performed at <1.3 kbar. Overall, considering the errors on these methods, Amp- and Cpx-only barometry are broadly consistent with magma storage in the upper ∼0.5–4 kbar of the crust at Lassen Volcanic Center. It is possible that a small number of erupted minerals originated deeper, but this is hard to distinguish from uncertainty given the lack of analytical metadata (Wieser et al., 2023c).

9.2. Melt Inclusions

The majority of MI measurements in mafic samples have focused on the cinder cones surrounding Lassen, rather than the main edifice. Saturation pressures may be representative of the storage depths of the most mafic magmas supplied to the edifice. Aster et al. (2016) analyzed olivine-hosted MIs from two cinder cones near Lassen (Basalt of Round Valley Butte—BRVB, and Basalt of old Railroad Grade—BORG). They measured CO_2 and H_2O in the melt phase using FTIR, and performed the first measurements of vapor bubble CO_2 in the Cascades using Raman Spectroscopy. The limited number of MIs where both the bubble was measured, and the MI was large enough for FTIR analyses yielded only $N = 9$ analyses from BORG and $N = 4$ analyses from BRVB where both phases were directly measured in the same inclusion. In addition to direct Raman measurements, Aster et al. (2016) produced a model to reconstruct vapor bubble CO_2, tracking the volume of a growing vapor bubble during PEC using volume and density information from crystallization simulations in rhyoliteMELTS (Gualda et al., 2012). The composition of the vapor phase in the modeled bubble volume was then calculated using the solubility model of Iacono-Marziano et al. (2012). While there is a broad correlation between modeled and reconstructed vapor bubble CO_2 contents when all samples are considered (Cascades, Parícutin, and Jorullo), the correlation for Lassen samples is poor ($R^2 = 0.01$, gradient = 0.09). Model-reconstructed values both over and underestimate the amount of CO_2 measured by Raman spectroscopy, and there is no clear association between this discrepancy and whether the bubble contained carbonates. We suggest that discrepancies between Raman measurements and models may result from large uncertainties in determining the exact amount of PEC experienced by each MI (which controls the calculated bubble volume), as well as the quench rate, and the amount of H_2O loss. The reconstructions of Aster et al. used Petrolog3 to perform PEC corrections, which requires the user to estimate the initial FeO_t content of each MI, a quantity that is

very challenging to estimate in volcanic fields/systems where there is no single liquid line of descent. This is particularly true at Lassen, where different eruptive centers have a wide range of FeO_t contents at similar MgO contents (Clynne, 1999). Thus, we do not calculate pressures for the Aster et al. (2016) MIs where they reconstruct the bubble using their model, and only consider those where the bubble was directly measured by Raman spectroscopy.

Walowski et al. (2016) performed FTIR measurements of olivine-hosted MIs ($N = 115$) from a wide variety of Quaternary cinder cones in a large volcanic field surrounding Lassen Peak. Walowski et al. (2019) performed FTIR measurements of olivine-hosted MIs from the 1666 CE eruption of Cinder Cone. Neither study performed direct vapor bubble CO_2 measurements, but Walowski et al. (2019) performed reconstructions using the method of Aster et al. (2016). Specifically, they calculated the amount of PEC assuming an initial FeO_t content of 7 wt%. However, as described above, a similar method performed poorly for the Lassen samples of Aster et al. (2016), and is very sensitive to the amount of PEC (and thus the initial FeO_t content of the MI). Cinder Cone lavas and tephra samples have FeO_t contents ranging from 5.5 to 7 wt%. Using Petrolog3, MI LCC-9–OL-01 has experienced 9.9 wt% PEC if reconstructed to 7 wt% FeOt, but only 2.8% PEC if reconstructed to 5.5 wt% FeO (most MIs have differences of 6%–7% PEC). The resulting change in temperature (ΔT), and therefore the volume of the bubble, and the total mass of bubble CO_2, is 2.5× less if FeOt is set at 5.5 wt% versus 7 wt%. Given the large uncertainties associated with bubble reconstructions, we only show measured H_2O-CO_2 contents for Walowski et al. (2016, 2019) MIs, with the caveat that they are very much minimum estimates.

When all MI saturation pressures are recalculated using MagmaSat (Ghiorso & Gualda, 2015), the measurements of Aster et al. (2016) yield pressures spanning 1.4–5.5 kbar. Melt-only saturation pressures from Walowski et al. (2016, 2019) are significantly shallower, as expected, and are likely not a useful constraint on magma storage.

The only MI constraint on storage beneath the main edifice comes from FTIR analyses of Qtz-hosted MIs from the Chaos Craggs rhyodacite by Quinn (2014). Discarding MIs with <3 wt% H_2O which they suggest have undergone leakage leaves 34 MIs, which yield pressures of ∼1–2 kbar. Vapor bubbles are not mentioned in this study, so it is difficult to assess the impact of bubbles on CO_2 contents. If these vapor bubbles are CO_2-poor, these results may indicate that more evolved magmas are stored at shallower depths than the regional basaltic magma supply examined by Aster et al. (2016).

9.3. Experimental Petrology

Schwab and Castro (2007) performed H_2O-saturated experiments to determine pre-eruptive storage conditions for the dacitic pumice erupted in 1915 from Lassen Peak. Comparison of natural and experimental products indicated that the dacitic magma equilibrated at 0.5 kbar and 800–875°C prior to mixing with an andesitic end member. Quinn (2014) performed H_2O-saturated experiments to assess the pre-eruptive storage conditions of the rhyodacitic magma erupted at Chaos Crags. By comparing textures and phase assemblages in natural samples with experimental products, they inferred that the most probable conditions of magma storage for these silicic magmas was 1.45 ± 0.25 kbar and 770 ± 10°C.

9.4. Geophysics

The first geophysical interpretation of magma storage under Lassen Volcanic Center came from Benz et al. (1992), who used teleseismic *P*-wave arrival times to investigate lithosphere structure in northern California. They invoked a low-velocity zone (average −7.2%) beneath Lassen Volcanic Center (as well as Medicine Lake) within Layer 1 of their model, which spans 0–15 km depth. More precise depth estimates cannot be obtained from such teleseismic models. However, the low is displaced 30–50 km NE from Lassen, and extends to depths of 70 km, perhaps as an artifact of vertical smearing (Thurber et al., 2009). Park and Ostos (2013) showed *P*-wave tomography from an MSci thesis (Reeg, 2008) investigating measurements conducted using the Sierra Nevada EarthScope project (2005–2007) which imaged a 600 km × 150 km area, with Lassen National Park in the north. They identified a low velocity zone, although they could not determine whether it was a mantle or crustal feature based on the wide station spacing (Park & Ostos, 2013). Overall, these teleseismic studies do not have sufficient resolution to reliably image small crustal magma chambers beneath Lassen Peak.

Park and Ostos (2013) examined a 250-km long broadband and long period magnetotelluric line "LASS" along the 40.5°N parallel. This survey line passed 20 km north of Lassen Peak (40.488°N). No large crustal conductor

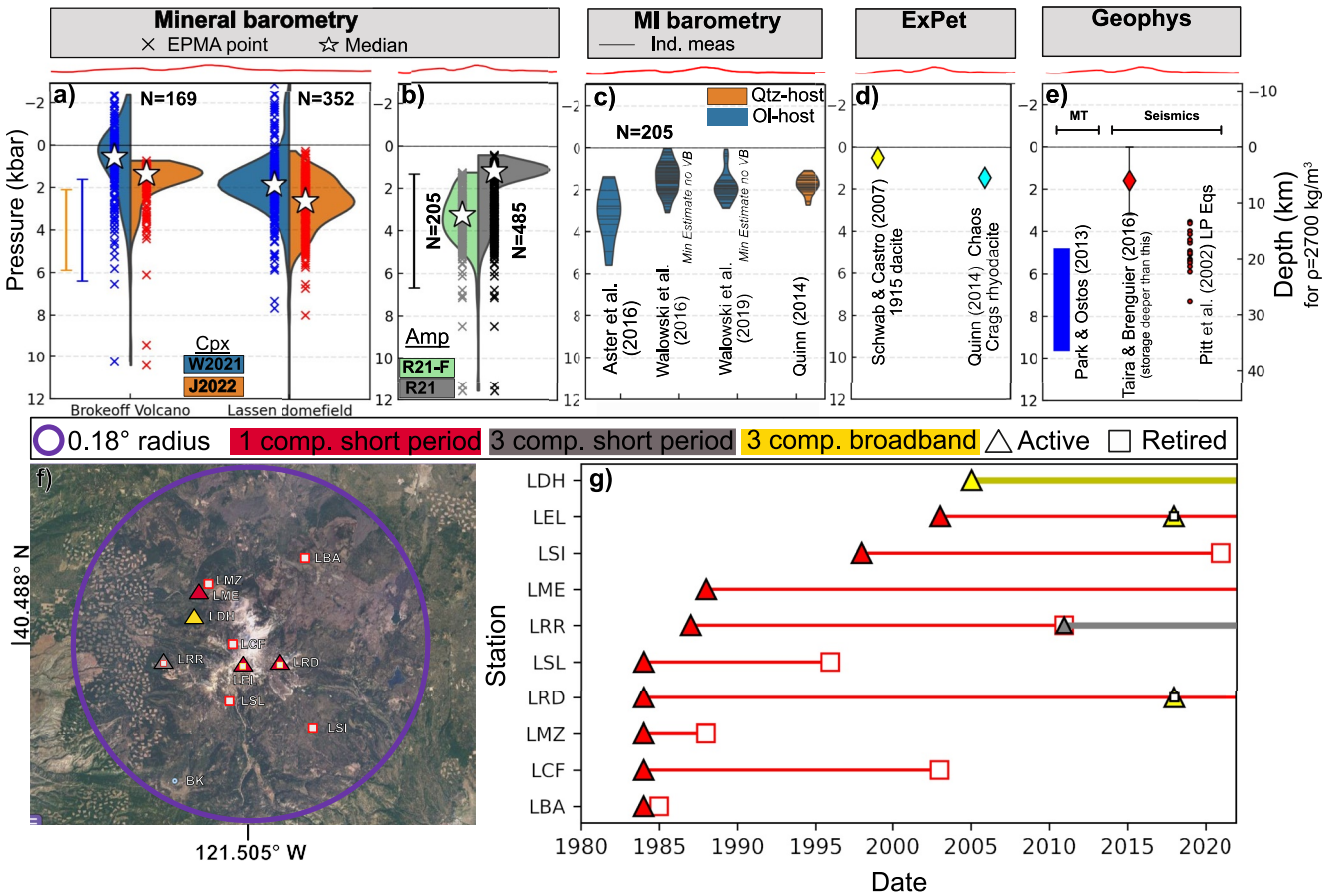

Figure 2. Compilation of magma storage depths at Lassen Volcanic Center (a–e) and summary of the seismic network (f–g). Violin plots show the distribution of pressures estimated from Cpx and Amp barometry, with individual pressures shown as crosses, and the median pressure shown with a white start. We overlay the ±RMSE error of each barometry method estimated from an experimental test dataset of arc magma compositions (Wieser et al., 2023a, 2023b). The depth axis on panels (a–e) is relative to the volcanoes summit. The red profile shows the height above sea level (the top of the chart) across a W-E section spanning 15 km section transecting the summit. As we could not obtain the exact earthquake catalog used by Taira and Brenguier (2016), we show the peak of their histogram ± the minimum and maximum values present with error bars. Magma is likely stored deeper than these earthquakes (red diamond). (f) Map of seismic stations within 0.18° (~20 km) of Lassen Peak's summit. (g) Schematic showing seismic station types versus time (lines changing color show station upgrades), within a circle with radius of 0.18° of the latitude and longitude shown on panel (f). Data from IRIS.org.

was observed beneath Lassen Peak, supporting our assertion that the teleseismic studies described above cannot provide useful constraints on upper crustal magma storage. However, they did identify three small conductors within the Lassen Volcanic Center at ~15–30 km (rlu, presumed bsl), which they suggest are basaltic reservoirs that may heat and melt the lower crust.

Another possible constraint comes from a compilation of the depths of earthquakes recorded from 1984 to 2016 (see Figure 6b of Taira & Brenguier, 2016). These depths showed a prominent peak at ~4–6 km (rlu). Such high-frequency or volcano-tectonic earthquakes require brittle (velocity-weakening) conditions, indicating temperatures far below the solidus, and are usually seen at a few km from sites of eruption (e.g., White & McCausland, 2016). The simplest interpretation is that the main magma storage region must be deeper than this high-frequency seismicity.

Pitt et al. (2002) reported the depths of $N = 20$ long-period earthquakes ranging from ~12 to 27 km depth (basl), which may represent magma recharge (indicating that the main magma storage region is above these). The absence of further seismic constraints at Lassen results from the fact that the permanent network is very small (Figures 2f and 2g), and that no high-resolution study has even been performed in the region.

Unfortunately, geodetic measurements at Lassen Volcanic Center do not help constrain magma storage depths. Lassen Volcanic Center has experienced broad, regional subsidence since 1992, consistent with a point source at ~8 km depth. However, the source of this subsidence is unclear, with dominant contributions likely from regional extension, changes in the location of hydrothermal/magmatic fluids, and a possible minor influence

of the cooling and crystallization of a magma body (Parker et al., 2016; Poland et al., 2004). Regional GPS will likely be vital to deconvolve the relative role of crustal extension compared to hydrothermal and magmatic processes. Given the ambiguity, we do not include this deformation source on Figure 2.

9.5. Summary and Future Work

Cpx-only and Amp-only barometry, Qtz-hosted MI saturation pressures, and available experimental constraints indicate that the majority of magma storage surrounding Lassen is within the upper crust (<4 kbar, <15 km). These depths are not inconsistent with the distribution of shallow earthquakes thought to overly the magma chamber, but further geophysical constraints from short-term high-density arrays, and/or the addition of more broadband seismometers providing an opportunity for passive-source tomography, would help to confirm the location of the shallow magma reservoir. Based on the downward spread of Cpx-only and Amp-only pressures, the presence of higher saturation pressures from Aster et al. (2016), and the seismic results of Park and Ostos (2013), further work is certainly needed to investigate whether there is deeper storage of more mafic magmas. This could be targeted through a study focusing on vapor bubble CO_2 in a large suite of MIs, experiments on relevant starting compositions, or a local high resolution seismic survey.

10. Mount Shasta

The position of Mount Shasta west of the Cascade arc axis and only ~70 km above the subducting plate means that it could be considered a fore-arc volcano (Christiansen et al., 2017; McCrory et al., 2012). Mount Shasta is a composite edifice, mostly comprised of five cones (Sand Flat, Sargents Ridge, Misery Hill, Hotlum and Shastina, Christiansen et al., 2020) which have a primarily calc-alkaline, high-silica-andesitic to low-silica-dacitic composition (60–67 wt% SiO_2). Quenched mafic inclusions of more MgO-rich magma are common. The last 10 Kyr of eruptive history at Mount Shasta indicates that eruptions occur every 600–800 years, with the most likely hazards being ash, lava flows, domes, pyroclastic flows and debris flows (Christiansen et al., 2017; USGS, 2022). Tephra is rare, with most pyroclastic deposits resulting from dome collapse (Christiansen et al., 2020). In addition to the main volcanic edifice, Mount Shasta is surrounded by a number of basaltic-andesite to andesitic shields (Ash Creek Butte, The Whaleback, Deer Mountain, Miller Mountain etc.), and less common basaltic to basaltic-andesitic cinder cones (Christiansen et al., 2017). While the majority of erupted material has a more evolved composition, small amounts of primitive magnesian andesite, high magnesian andesite (HMA) and high-alumina olivine tholeiite with high Mg#s are found in cinder cones and on Mount Shasta's flanks (Christiansen et al., 2013).

10.1. Mineral Compositions

Recent petrological work around Mount Shasta has largely focused on the HMA erupted at the S17 cinder cone near The Whaleback, ~20 km NNE of the main edifice. Interest in this cinder cone reflects a long-standing debate over whether HMAs are near primary mantle melts (Baker et al., 1994; Barr et al., 2007; Grove et al., 2002) or the result of magma mixing and crustal contamination (Streck & Leeman, 2018). Streck and Leeman (2018) displayed their EPMA data in an interactive tool overlain on a BSE image, allowing us to identify EPMA points on touching Opx-Cpx pairs. We assess all possible combinations of Cpx-Opx analyses for touching grains (e.g., for three EPMA spots on a Cpx, and two for a touching Opx, we obtain six pairs). This yields a total of $N = 116$ pairs. We also manually extract $N = 328$ Cpx analyses where the location in the crystal could be classified (core, rim). Phillips and Till (2022) measured Cpx and Opx compositions from the same HMA S17 cinder cone, although it was not possible to distinguish which analyses represent touching pairs. Given there is only one equilibrium test for Cpx-Opx (K_D, Fe-Mg) which shows limited success for hydrous experiments (Wieser et al., 2023a), we do not consider pairs when the textural context is unknown. Cpx-only pressures from these HMA are highly variable, ranging from 1 to 6 kbar (with very similar distributions and medians for J2022 and W2021). Cpx-Opx pressures are offset ~2–3 kbar deeper, but certainly overlap with the distribution of Cpx-only pressures (particularly given the 2–4 kbar RMSE on each method, Wieser et al., 2023a).

Baker et al. (1994) performed mineral analyses on a series of basaltic andesite lavas associated with the Sargents Ridge and Misery Hill dome building episodes, located ~15 km to the N and NW of Shasta's summit clustered around Highway 97 (e.g., at ~4,000″, summit at ~14,000″). They reported $N = 3$ representative Cpx compositions. However, M. Baker (written coms) said that these analyses were low precision, with the WDS background only

being collected once per thin section, so should not be used for barometry. Grove et al. (2005) measured mineral compositions in a wide variety of lavas representing the Hotlum, Shastina, Misery, and Sargents eruptive phases from on/around the main Shasta edifice. However only representative mineral composition are reported (a total of $N = 4$ Cpx, $N = 2$ Amp). Given the sparsity of available data, we do not perform any barometry on the main edifice, as these numbers are too small to sufficiently average out random analytical error (Wieser et al., 2023c).

10.2. Melt Inclusions

A. T. Anderson (1974) performed EPMA analyses on olivine-hosted MIs from the S17 cinder cone, and calculated H_2O by volatiles by difference. Sisson and Layne (1993) measured H_2O in MI from Goosenest volcano and Copco Cone, ∼35 and ∼60 km North of Shasta by SIMS. However, because of the lack of glass (and bubble) CO_2 measurements, as well as uncertainties associated with volatile-by-difference methods (see Hughes et al., 2019), we do not calculate saturation pressures for these inclusions.

Le Voyer et al. (2010) performed SIMS measurements of reheated olivine-hosted MIs from H_2O-poor high aluminum olivine tholeiites and H_2O-rich basaltic andesites from mafic flank eruptions from Mount Shasta. Their measured basaltic-andesite H_2O contents are lower than estimated by Baker et al. (1994), which may reflect diffusive loss from the olivine (adding uncertainty to the saturation pressure). We calculate saturation pressures for the $N = 25$ MIs with major element and volatile data.

Ruscitto et al. (2011) performed FTIR measurements of naturally quenched primitive basaltic andesite and HMA olivine-hosted MIs from the S17 cinder cone. We calculate saturation pressures for the $N = 20$ MIs with major element and volatile data. Both data sets yield pressures spanning ∼0–2 kbar. However, all Shasta MI studies note the presence of abundant vapor bubbles, many of which remain even after experimental homogenization (Le Voyer et al., 2010). Thus, it is very likely that these calculated saturation pressures are very much minimum estimates for storage of mafic magmas at Mount Shasta.

10.3. Experimental Phase Equilibrium

Grove et al. (2005) compared whole-rock and mineral compositions from the main edifice of Mount Shasta to the experiments of Grove et al. (2003), inferring shallow crustal differentiation of plagioclase (Plag) and pyroxene (Px) in a reservoir at 1–2 kbar (3–6 km, see also Baker et al., 1994). In the schematic model presented in Grove et al. (2005, their Figure 14), two additional storage zones are depicted: (a) a reservoir fractionating Olivine (Ol) + Px at 7–10 km, and (b) a reservoir fractionating Ol + Amp + Px at 15–25 km (based on high amphibole Mg#s and H_2O-rich MIs). Krawczynski et al. (2012) performed additional experiments at 200, 500 and 800 MPa, and used these experiments to calibrate a barometer estimating P_{H_2O} from the highest measured Amp Mg# in a given suite of samples. By applying this equation to Shasta Amps, P_{H_2O} values of 2.8–9.5 kbar were obtained. However, these pressures may be significant underestimates if CO_2 is present in the exsolved fluid at depth, such that $P_{tot} \neq P_{H_2O}$. Additionally, their Figure 8 shows that the simple relationship between Amp Mg# and P is more complex in mixed H_2O-CO_2 fluid experiments (and mafic melts beneath Shasta are likely in equilibrium with a mixed fluid).

10.4. Geophysics

Thurber et al. (2009) presented a regional 3D tomographic model of *P*-wave velocity for all of Northern California using a double-difference tomography algorithm (Zhang et al., 2004) with nodes 15–20 km apart. They imaged a low velocity zone (∼5.5 km/s, 5% reduction) beneath Mount Shasta centered at ∼12 km depth (bsl). However, the 40-km horizontal extent of this body makes it impossible to distinguish thermal versus magmatic contributions to the local velocity low. The lack of high resolution, local seismic inversions reflects the fact that no high density temporary deployments have ever been deployed around Shasta to our knowledge (unlike iMUSH at Mount St. Helens). Additionally, Shasta also shows relatively few earthquakes (Weaver et al., 1990), despite a long-lived short-period monitoring network. This network has been recently upgraded with four three component broadband seismometers (Figure 3g). Meaningful inversions on this new network will be reliant on recording sufficient earthquakes. From a geodetic perspective, there has been no detectable deformation at Mount Shasta since at least the 1980s (Poland et al., 2017). To our knowledge, there are no other geophysical constraints on magma storage beneath Shasta.

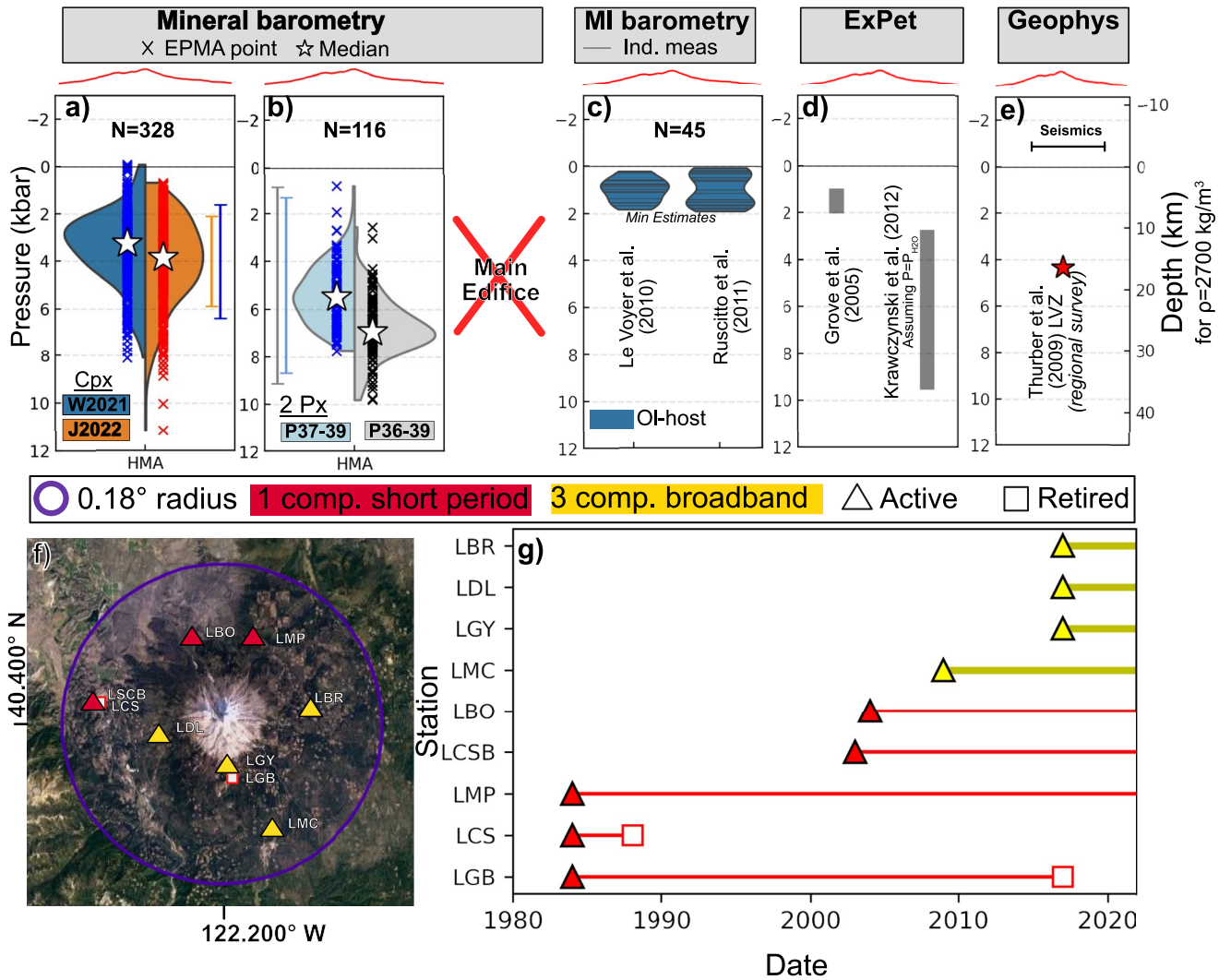

Figure 3. Compilation of magma storage depths at Mt. Shasta and the surrounding area (a–e) and a summary of the seismic network (f–g). Symbols, errorbars and seismic stations as in Figure 2. The red profile shows the height above sea level across a W-E section spanning 15 km section transecting the summit.

10.5. Summary and Future Work

Despite the clear hazard potential of the main edifice of Mount Shasta (ranked as the fifth most hazardous US volcano), we have remarkably few constraints on the magmatic plumbing system feeding the main edifice. While the S17 HMA cinder cone is academically interesting from the perspective of the generation of arc magma compositions, this cone has little relevance to future eruptions at Mount Shasta given the relative paucity of these high-magnesian andesite compositions in this volcanic field and its age pre-dating construction of the modern edifice (see Phillips & Till, 2022). We suggest that further work targeting MIs, mineral compositions and phase equilibration experiments in the presence of mixed fluids from the main edifice is needed. From a geophysical perspective, a high-density temporary deployment of seismometers using active sources would help, although permitting would be non-trivial. Soon, we expect sufficient earthquakes to been collected on the upgraded seismic network for a first-order seismicity assessment.

11. Medicine Lake

Medicine Lake Volcano is located ~50 km E-NE of Mount Shasta and the main Cascade front, on the western edge of the Basin and Range extensional province (Donnelly-Nolan et al., 2008). It has a broad shield shape, and

is the most voluminous volcano in the Cascades. It has erupted a wide variety of magma compositions, ranging from hydrous calc-alkaline magmas (basalt to rhyolite), to relatively anhydrous, high-aluminum olivine tholeiites. In general, basalts and andesites form the flank of the volcano, with rhyolites and small volumes of dacites occurring at the summit (Donnelly-Nolan, 2008).

11.1. Mineral Compositions

Despite a number of detailed petrological studies, there is a notable paucity of published mineral data after filtering ($N = 21$ Cpx, $N = 7$ Amp), with most papers only publishing representative analyses:

- Gerlach and Grove (1982) reported $N = 6$ Cpx from a variety of units (Modoc basaltic-andesite, older and later platy olivine andesite, Medicine Lake Dacite, Glass Mountain Rhyolite).
- Grove and Donnelly-Nolan (1986) reported $N = 4$ Cpx and $N = 4$ Amp from three types of magmatic inclusions from Pleistocene-Holocene silicic flows.
- Grove et al. (1997) reported data from $N = 1$ Cpx and $N = 3$ Amp from the Glass Mountain rhyolite.
- Grove et al. (1988) reported $N = 4$ Cpx analyses from the Burnt Lava flow.
- Kinzler (1985) and Kinzler et al. (2000) reported the composition of a $N = 5$ Cpx and $N = 1$ Cpx respectively from the Callahan lavas.

Cpx return a median pressure of 0.8 kbar using W2021, and 1.7 kbar using J2022. Amp return a median pressure of ∼2.5 kbar.

11.2. Melt Inclusions

Sisson and Layne (1993) measured a H_2O content of ∼0.2 wt% from Black Crater MIs using SIMS. Kinzler et al. (2000) reported an Amp crystal present in an olivine-hosted MI with ∼3 wt% H_2O. No CO_2 data exists for either the melt phase or the bubble in these studies. Thus, we do not calculate saturation pressures for these inclusions. MI work analyzing the melt and vapor phase for H_2O and CO_2 in the Paint Pot basaltic deposit is currently in progress (see Couperthwaite et al., 2022). To our knowledge, there has been no MI work performed on the more silicic compositions at Medicine Lake. This may reflect the paucity of rapidly quenched tephra at this volcano dominated by lava flows; only two ash falls are documented from the Holocene (Heiken, 1978).

11.3. Experimental Phase Equilibrium

Grove et al. (1982) conducted experiments investigating the origin of the calc-alkaline series at Medicine Lake. However, other than demonstrating that P_{H_2O} must be greater than 1 kbar to generate calc-alkaline compositions, no further constraints were placed on magma storage depths. Wagner et al. (1995) performed experiments on the Late Pleistocene Lake Basalt, reproducing lava compositions and phenocrysts in 1 kbar H_2O-saturated experiments. However, they did not perform experiments at different pressures, so the same relationships may be have reproduced at other pressures (e.g., 0.5, 2 kbar). Grove et al. (1997) performed experiments at 1, 1.5, and 2 kbar to investigate the origin of the Rhyolite of Glass Mountain. They suggested that the presence of Amp in more mafic inclusions indicates crystallization at >2 kbar, while Ol-Plag and Ol-Plag-Cpx inclusions indicate crystallization at near H_2O-saturated conditions at ≤1 kbar. Finally, Bartels et al. (1991) performed experiments at 1 atm, 10 and 15 kbar on high-aluminum basalts from Medicine Lake, demonstrating that these liquid compositions are close to equilibrium with a mantle lherzolite source. However, the high-pressure nature of these experiments mean they do not provide insights into the depth at which magma is stored in the crust beneath Medicine Lake.

11.4. Geophysics

J. R. Evans and Zucca (1988) and Chiarabba et al. (1995) used active source seismic topography (the NeHT experiment of 1985) and seismic refraction studies conducted in 1982 and 1984 to image P-wave velocity and attenuation beneath Medicine Lake. J. R. Evans and Zucca (1988) obtained ∼1–2 km depth resolution in the upper 5–7 km of the crust, and imaged a low Q (high attenuation), low velocity region in their layer 3 beneath the east central caldera with a volume of a few 10 s of km^3 (1.2–3.25 km depth bsl, 3.6–5.6 km bgl). Chiarabba

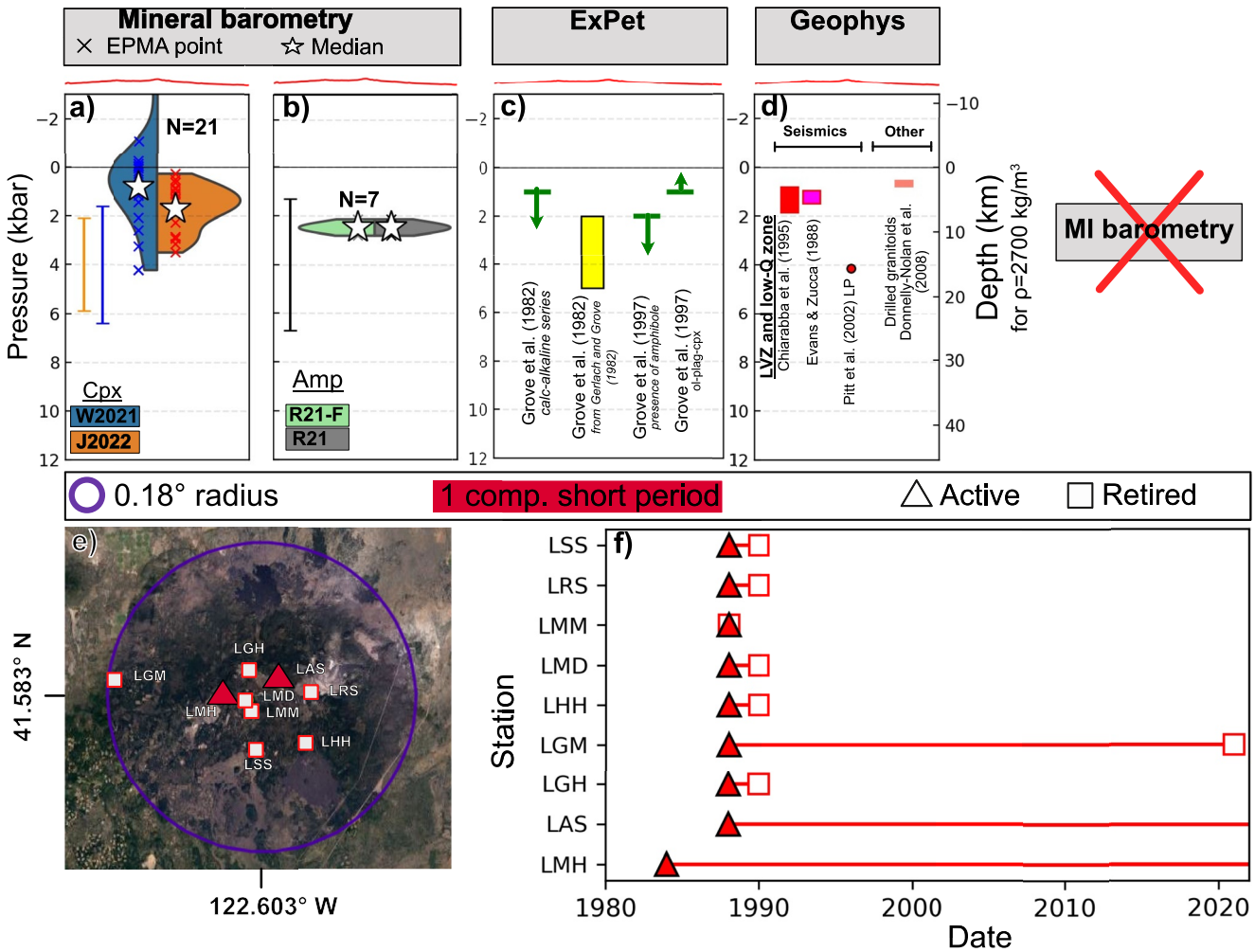

Figure 4. Compilation of magma storage depths at Medicine Lake Volcano (a–d) and summary of the seismic network (e–f). The red profile shows the height above sea level across an N-S section spanning 30 km transecting the summit.

et al. (1995) experimented with alternative inversion strategies and found that the low-velocity body was well resolved at 3–5 km depth (bgl), although some less-stable inversion strategies suggested that the low velocity zone is deeper (>6.8 km). Overall, Chiarabba et al. (1995) concluded that the low velocity zone likely occured at 3–4 km depth (bgl), but could exist as deep as 7 km depth. The small size of the low velocity anomaly identified in these two seismic studies, roughly 10 km wide horizontally, can account for the fact it was not seen in teleseismic studies (e.g., Ritter & Evans, 1997).

Pitt et al. (2002) reported 1 LP EQ beneath Medicine Lake in Dec 1989 (15 km basl). The notable paucity of seismometers (particularly three component broadband) means that there have not been any more recent investigations of magma storage using passive source techniques since the flurry of geothermal exploration in the 1980s (Figure 4g).

Interpreting geodetic data is complicated by the fact that Medicine Lake impinges on the western edge of the Basin and Range, meaning it is subject to regional extension. Additionally, Medicine Lake's large volume, and therefore mass, means that it loads and deforms the surrounding crust. These "background" signals make it difficult to distinguish the smaller signals resulting from inflation and deflation of crustal magma chambers (Dzurisin et al., 1991; Poland et al., 2006). Dzurisin et al. (1991, 2002) examined leveling surveys from 1954 to 1989, a small summit survey from 1988, and seismicity occurring 1978, 1981, and 1988. They infer that regional/loading signals overwhelm the minor amount of signal which may arise from crystallization and magma withdrawal.

Poland et al. (2006) investigated campaign GPS data and InSAR data from Medicine Lake Volcano. InSAR identifies ~10 mm/yr of approximately radially symmetric subsidence centered on the caldera region (consistent with GPS and leveling data). They showed that the GPS horizontal displacements are inconsistent with the model of Dzurisin et al. (2002) of volume being lost at 10–11 km depth, because this should produce radially inward horizontal deformation up to 40 km radius. Instead, they inverted for a Mogi point source at shallower depths (~6 km) to explain the fact that only GPS stations within ~10 km of the summit showed inward deformation. This deformation source can also be fitted as a deflating sill at 5 km depth. However, this sill fit has a higher misfit, and doesn't effectively recreate the vertical deformation of the 1954–1989 leveling survey of Dzurisin et al. (1991). Overall, Poland et al. (2006) suggested the dominant signal is edifice loading and extension of a hot weak crust, rather than magma withdrawal. Similarly, Parker et al. (2014) examined additional InSAR data (up to 2011), suggesting that deformation is caused by tectonic extension and gravitational loading, with a possible role for cooling and crystallization of an intrusive body at depth (rather than an active magma chamber). Given that geodetic signals appear not to represent magmatic processes at Medicine lake, we do not include them on Figure 4.

11.5. Other

Another possible constraint on magma storage depths comes from geothermal exploration drilling, which encountered hydrothermally altered granitoid rocks at 2–2.9 km depth below the summit caldera (Zircon dates of ~332 ka, Donnelly-Nolan et al., 2008; Lowenstern, 2003). While down dropping of the caldera and erosion over 100s of Kyr can alter the current depth versus the emplacement depth, down dropping is thought to have been limited to ~240–440 m, and erosion is relatively negligible in the high desert (Donnelly-Nolan et al., 2008, Donnelly-Nolan written communications).

11.6. Summary and Future Directions

We suggest that the most precise constraints on magma storage beneath Medicine Lake could be obtained by performing detailed MI studies on rapidly quenched material where available. For slower-cooled lava flows, detailed analysis of minerals and any fresh glasses could help provide barometric constraints to supplement the small amounts of publicly available mineral data. Without densification of the seismic network with three component broadband seismometers, or targeted local studies, additional geophysical constraints are unlikely to be obtained in the near future.

12. Crater Lake/Mount Mazama

The climatic eruption of Mount Mazama at ~7.7 ka produced the modern-day caldera known as Crater Lake. Activity at Mount Mazama began around ~420 ka, producing basaltic andesite, medium-K andesites and dacites. The first preclimactic rhyodacites erupted at ~27 ka, and the evolution of this silicic reservoir was terminated by the massive climatic eruption of ~50 km^3 at 7.7 ka (Bacon & Lanphere, 2006). Post-caldera volcanism was dominated by andesite for 200–500 years after the climatic event, followed by an eruption of a rhyodacite at 4.8 Kyr. There are also 20 cinder cones within Crater Lake National Park (Prueher & McBirney, 1988).

12.1. Mineral Compositions

We obtain the following mineral data after filtering:

- $N = 16$ Cpx from preclimatic rhyodacites from Nakada et al. (1994).
- $N = 124$ Cpx analyses from the eight dacitic-rhyodacitic deposits spanning 71–7.7 ka described in Wright et al. (2012, kindly provided by the authors).
- $N = 193$ Cpx and $N = 245$ Amp from the original handwritten datasheets of EPMA analyses for the climatic samples described in Druitt and Bacon (1989).

The dacitic-rhyodacitic deposits at Crater Lake are outside the calibration range of the W2021 barometer, which could explain why calculated pressures are so shallow (median = −0.2 kbar). The median pressure

for the J2022 barometer is ∼1.2 kbar, with a skewed distribution to higher pressures (this barometer does not return very shallow pressures). Si-Al filtered Amp pressures are very similar to those unfiltered, with median pressures of ∼3 kbar. There is also a small cluster of Amp-only pressures at ∼7 kbar, from samples 80c444 (Ol-Px rich scoria from top of the climatic ignimbrite), 82C882 (high-Sr scoria from top of climatic ignimbrite), 82C938 (high-Sr enclave from Llao rock) and 1290 (low-Sr scoria from the top of the climatic ignimbrite), all from Druitt and Bacon (1989). It is difficult to interpret the single Cpx measurement from Wright et al. (2012) yielding a pressures in a similar range to these high Mg# amphiboles without detailed information on the analytical uncertainty associated with these measurements (see Wieser et al., 2023c). Additional mineral analyses will be vital to pin down the possibility of a deeper region of more mafic magma storage.

12.2. Melt Inclusions

Bacon et al. (1992) analyzed plagioclase-hosted MIs from three rhyodacitic Holocene eruptions (∼7–6.8 Kyr BP) from Crater Lake by FTIR (Llao Rock, Cleetwood, and the climatic event). CO_2 concentrations in these MIs are <25 ppm, and often undetectable by FTIR. We remove MIs with low H_2O contents (<3.1 wt%) which the authors suggest may have a connection to the outside, leaving $N = 10$ MIs. Mandeville et al. (2009) analyzed plagioclase and pyroxene-hosted MIs from the same three eruptive episodes as Bacon et al. (1992), also using FTIR. None of the reported $N = 48$ MIs had visible connections to the outside or cracks, and CO_2 concentrations were below the FTIR detection limit. Wright et al. (2012) analyzed $N = 127$ plagioclase and pyroxene-hosted MIs from eight dacitic-rhyodacitic deposits spanning 71–7.7 ka using SIMS (along with a subset by FTIR). They identify high H_2O (3–4.6 wt%) and low H_2O (<2.4 wt%) populations of MIs. They suggest that the low-H_2O population likely reflects leakage, and diffusive re-equilibration. Thus, for consistency with Bacon et al. (1992), we do not calculate saturation pressures for inclusions with <3.1 wt% H_2O. Wright et al. (2012) only detect CO_2 significantly above detection limit in deposits from the 71 ka Pumice Castle. All Crater Lake MI saturation pressures cluster at ∼1 kbar. To our knowledge, no vapor bubbles have been measured in these more silicic MIs, although this doesn't mean they are CO_2-free.

12.3. Experimental Petrology

We are not aware of any published experimental petrology studies placing constraints on magma storage depths beneath Crater Lake.

12.4. Geophysics

The only seismic constraints at Crater Lake that we are aware of is a single LP at ∼32 km depth (Nichols et al., 2011), and a brief mention of a low velocity zone in the lower crust below Crater Lake in the regional teleseismic study by Harris et al. (1991). However, Harris et al. (1991) did not provide a depth or place any quantitative constraints on the size of this body, so we do not include this in our compilation. The lack of seismic constraints on magma storage is not surprising; the seismic network at Crater Lake was non-existent for more than 20 years in the late 1980s to mid 2000s (Figure 5g), and has only been upgraded very recently with three-component broadband seismometers. Once sufficient earthquakes have been measured on this new network, additional constraints on magma storage may be possible. Poland et al. (2017) summarized available geodetic constraints at Crater Lake, which show no deformation resolvable above survey noise since the 1980s.

12.5. Summary and Future Work

We suggest that further petrological and experimental work examining the postclimactic materials erupted at Wizard Island could provide useful insights into the likely storage depths of the next eruption at Crater Lake. Examination of CO_2 within more silicic MI vapor bubbles would also be a worthy target, as would MI measurements on the numerous mafic cinder cones, which have been suggested to tap magma bypassing the centrals silicic reservoir (Prueher & McBirney, 1988). Although permitting would certainly be a challenge, a higher resolution array with active sources could help provide additional geophysical constraints.

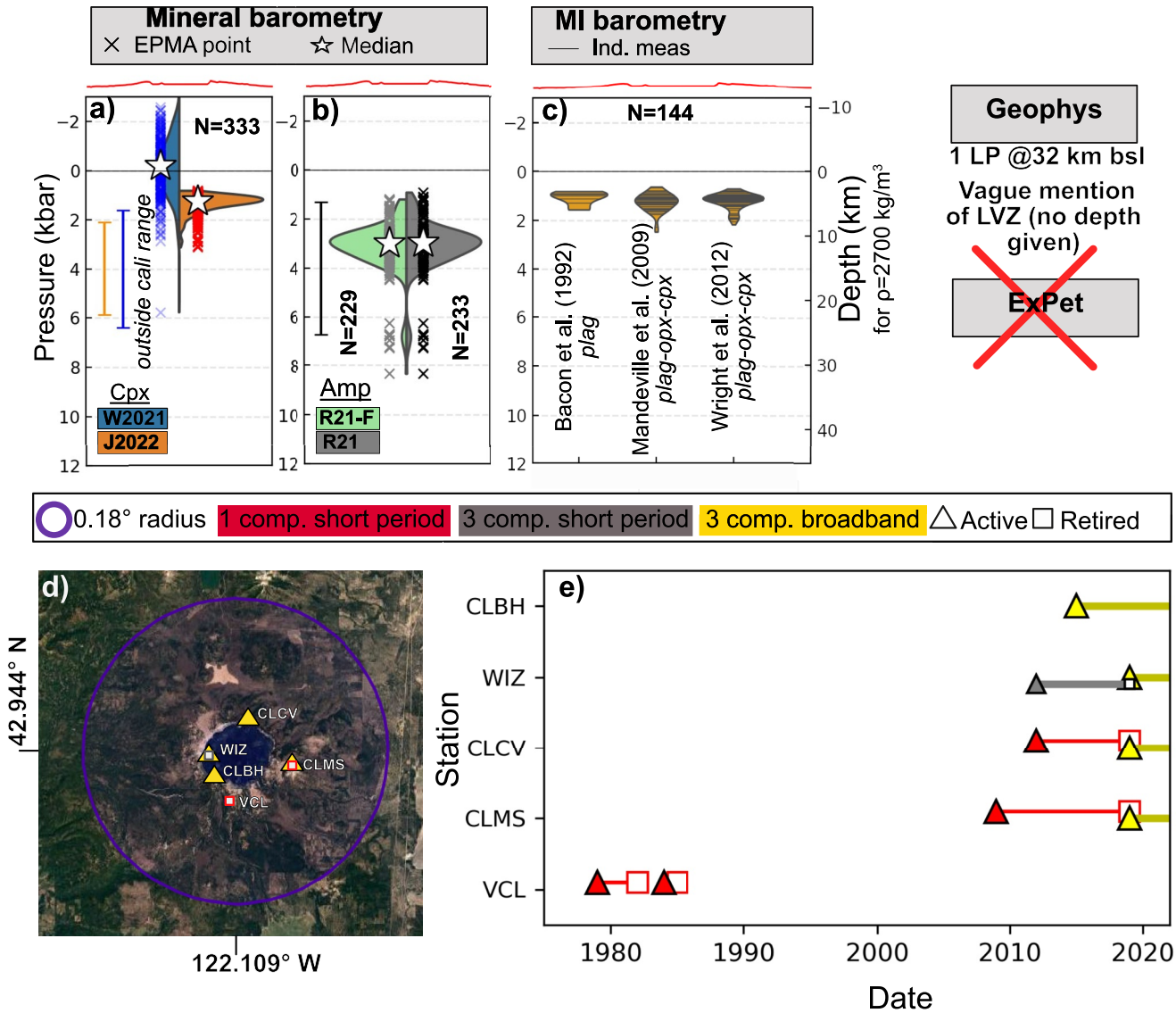

Figure 5. Compilation of magma storage depths at Crater Lake (a–c) and summary of the seismic network (d–e). The red profile shows the height above sea level across a W-E section spanning 30 km transecting the summit.

13. Three Sisters

The Three Sisters volcanic field consists of three prominent summits (North, Middle and South Sister), as well as a number of distributed vents. North Sister has a very monotonous basaltic-andesite composition, with activity between ~120 and 50 ka, including a small shield (Little Brother), and a string of fissures (Matthieu Lakes fissure, Fierstein et al., 2011; Schmidt & Grunder, 2011). Activity at Middle and South Sister has been largely contemporaneous, with Middle Sister erupting basalt-andesite and dacite, while South Sister erupts only intermediate to more felsic compositions. In general, relatively little petrological work has been done on this area.

13.1. Mineral Compositions

After filtering, we were only able to obtain $N = 6$ Cpx from the Matthieu Lakes Fissure transecting North Sister from Schmidt and Grunder (2011), and $N = 11$ Cpx from South Sister dacites from Waters et al. (2021). The small number of analyses make it harder to average out the effects of analytical uncertainty; the available data suggests storage centered around 1 kbar at North Sister and ~2 kbar at South Sister, although these differences are certainly within uncertainty of one another, and individual analyses show substantial overlap between the two centers.

13.2. Melt Inclusions

To our knowledge, there are no published MI analyses from South or Middle Sister. Mordensky and Wallace (2018) analyzed olivine-hosted MIs from North Sister using FTIR. 9/15 of these MIs had vapor bubbles. They calculated that minimal PEC had occurred (0%–2.3%, representing ΔT = ~20°C). They performed a bubble correction similar to that of Aster et al. (2016), inferring ~48%–78% of CO_2 was within the bubble. However, for such small amounts of PEC, where the vast majority of the bubble grows during syn-eruptive cooling, bubble reconstructions assuming re-equilibration between vapor bubble and melt can greatly overestimate bubble CO_2 contents (Wieser et al., 2021). Additionally, with such low amounts of PEC, the correction is heavily affected by the choice of FeO_t content, which shows scatter in local whole-rock compositions. Mordensky and Wallace (2018) reported PEC-corrected major element data for $N = 8$ North Sister MIs, six of which have CO_2 below-detection limit. Given the small number of analyses, low CO_2 contents in the glass, lack of published major element contents for many MIs, and lack of bubble CO_2 data, we do not perform saturation pressure calculations. Mercer and Johnston (2008) cited unpublished MI data from North Sister, which we were not able to obtain for this study.

13.3. Experimental Petrology

Mercer and Johnston (2008) performed experiments using a North Sister melt composition, mostly to constrain the lower crustal mineralogy the melt last equilibrated with. They propose based on phase relationships and the absence of garnet or amphibole signatures that mantle-derived melts likely stalled at ~12 kbar in a deep crustal hot zone, and then ascended to ~1 km where observed phases such as Ol, Plag, and Cpx crystallize. We do not include these depths in our compilation, as they are not precise constraints on magma storage locations, but instead constrain the likely ascent path based more on inference of crustal structure than precise experimental constraints on phase stability. While their experiments focus on Newberry Volcano, Mandler et al. (2014) drew comparisons with natural compositions erupted at the Three Sisters, indicating "damp" not wet magmas are present at Three Sisters along the arc front, as well as in the rear-arc.

13.4. Geophysics

We are not aware of any seismic constraints on magma storage at Three Sisters, and the PNSN only locates 0–3 earthquakes within 10 km per year. Seismic constraints are not helped by the fact that there are relatively few seismometers within a very broad area, and these were only upgraded to broadband seismometers relatively recently (Figure 6g).

The lightly vegetated flanks around Three Sisters makes it an attractive location for satellite-based geodetics (Poland et al., 2017). InSAR acquisitions between 1992 and 2000 reveal inflation over a broad area (10 × 20 km) centered ~6 km west of the South Sister summit (Wicks, 2002). InSAR was vital to identify this period of deformation, as it was offset to the west of the electro-optical distance meter (EDM) and tilt-leveling methods installed at the summit between 1985 and 1986. Wicks (2002) modeled this inflation with a Mogi point source at 6.5 ± 0.4 km depth (rlu), with a volume increase of 0.0023 ± 0.003 km^3. Dzurisin et al. (2006) supplemented InSAR observations with tilt surveys from 1985, 1986, and 2001, EDM surveys from 1985 to 1986, Campaign GPS surveys from 2001 to 2002, and leveling in 2002–2003 along survey lines intersecting the deformation center. They inverted these four data sets, investigating Mogi point sources, elliptical and dislocation sources, finding that the best fit is a shallowly dipping sill at 6.5 ± 2.5 km depth bgl. Dzurisin et al. (2009) further supplemented this data with InSAR, GPS, and leveling data collected up to 2006. This new data revealed that the inflation rate had been decreasing exponentially. They suggested that the best fit shallowly dipping sill proposed by Dzurisin et al. (2006) was caused by combining early InSAR data with later GPS data during this change in deformation, skewing the relative proportions of horizontal motion (which GPS is most sensitive to) and vertical deformation (which InSAR is most sensitive to). Dzurisin et al. (2009) instead proposed a vertical prolate source geometry, which provides better fits to the data once these temporal changes are accounted for. This source sits at 4.4 km depth bgl with an aspect ratio of 0.9, which is the best fit if network translation is ignored (the source is 5.4 km bgl with an aspect ratio of 0.86 when accounting for network translation). Riddick and Schmidt (2011) examined C-band InSAR from two satellites (ERS and ENVISAT), suggesting that deformation tails off following two separate linear trends (1998–2003, 2004–2010). Using a Mogi source, they obtained 5.5 km, 6.5 km using an ellipsoidal source, and 7 km using a sill source.

Wicks (2002) suggested that the deformation source could result from the injection of new magma, or pressurization of a hydrothermal system, with the former being more likely as hydrothermal activity is often accompanied

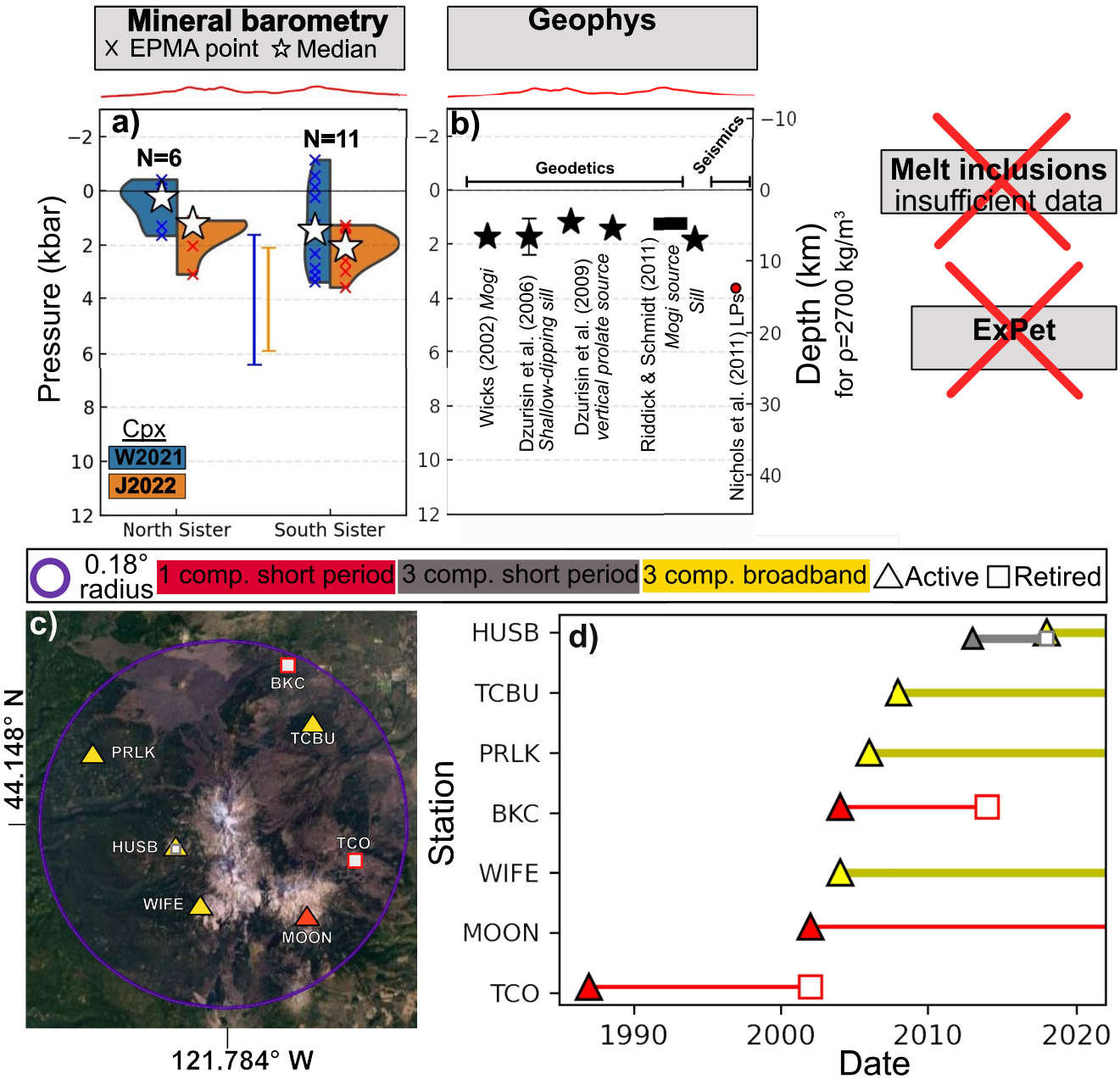

Figure 6. Compilation of magma storage depths at Three Sisters (a, b) and summary of the seismic network (c, d). The red line shows the height above sea level across an approximately N-S section spanning 17 km transecting all three summits. (c, d) Seismic stations versus time.

with seismic activity (and this episode was relatively aseismic). Dzurisin et al. (2009) also concluded based on spring chemistry that an intrusion of magma is a more likely cause of deformation than a hydrothermal system perturbation.

13.5. Summary and Future Work

Given recent renewed uplift ~5 km W of South Sister (January 2022) in addition to the deformation discussed above, more detailed petrological work on this edifice is warranted. In particular, MI constraints could help determine whether the depth inferred from geodetics is similar to that of magma reservoirs feeding past eruptive episodes. Unlike many Cascade volcanoes, South Sister has silicic tephra fall deposits suitable for such work—in fact local ash dispersion is one of the most probable future hazards in this area (Hildreth et al., 2012). In order to investigate the storage depths of the more mafic fissures and cinder cones of North

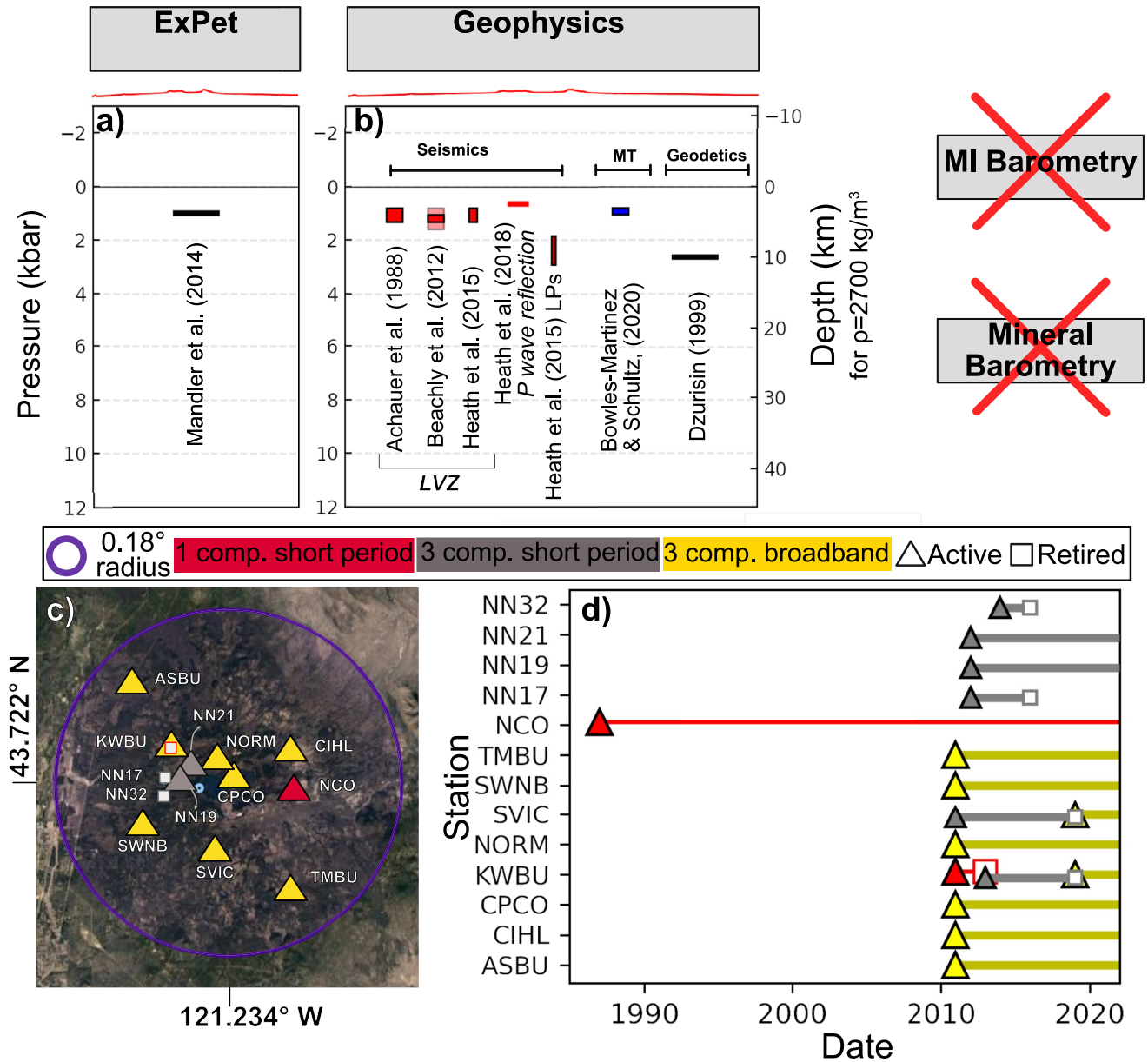

Figure 7. Compilation of magma storage depths at Newberry Volcano (a, b) and summary of the seismic network (c, d). The red line shows the height above sea level across an approximately N-S section 55 km section transecting the crater. The unlabeled blue dot in (c) is a strong motion station (HN).

Sister and the surrounding area, a detailed study of vapor bubble CO_2 in MIs is required. Experimental constraints could be used to investigate the relationship between mafic and silicic magmas, combined with new, high precision analyses of mineral compositions, to build a more coherent model of the magmatic plumbing system.

14. Newberry Volcano

Newberry Volcano lies ~50–60 km east of the main arc front and covers the largest area of all Cascade volcanoes. It is second in volume only to Medicine Lake. Newberry exhibits predominantly bimodal volcanism; intracaldera eruptions are rhyolitic, while its north-westerly trending rift zone hosts basaltic-andesite fissures and cinder cones. Newberry caldera was formed at ~75 ka with the eruption of a compositionally zoned basaltic-andesite to rhyolite tuff (Donnelly-Nolan et al., 2011).

14.1. Mineral Compositions/Melt Inclusions

We were unable to find any published mineral compositions or MIs from Newberry Volcano.

14.2. Experimental Petrology

Mandler et al. (2014) performed 1 bar (anhydrous) and H_2O-saturated 1–2 kbar experiments on the ∼75 ka caldera-forming tuff from Newberry Volcano. The 1 kbar experiments best reproduced the samples from the caldera-forming tuff, but they suggest that these experiments were conducted with too high H_2O contents, because differentiation was likely H_2O-undersaturated. They stated that it is difficult to constrain the pressure of storage in these undersaturated systems, where the effect of pressure on phase equilibria is small at crustal conditions. Overall, they concluded that differentiation occurred in the upper crust.

14.3. Geophysics

Extensive geophysical work has been performed at Newberry because of its geothermal potential. The teleseismic study of Stauber et al. (1988) indicated that no magma chamber was resolvable within the resolution of their study (e.g., ∼5 km width). Using active source tomography with higher resolution, Achauer et al. (1988) identified a low velocity body at 3–5 km depth bgl, which they interpreted to be a small silicic or stratified magma body, although the lower end of this body was difficult to resolve in their inversion. Zucca and Evans (1992) investigated P-wave attenuation using the same seismic data as Achauer et al. (1988). They found that the low velocity zone in their layer 3 had average attenuation, such that it may reflect a recently solidified, hot cracked pluton, rather than actual melt (which would have high attenuation). More recently, Beachly et al. (2012) used travel time tomography and forward modeling of arrival times and seismic amplitudes from an active-source seismic experiment with 75 three component seismometers in 2008. They identified a central low velocity anomaly at 3–6 km below the caldera floor. They found the best fit is a molten sill with a thin mush region at the bottom - in their schematic the melt body is located at ∼4–5 km depth beneath the caldera.

The seismic network at Newberry was densified with six new three component broadbands in 2011 and two further upgrades to 3 component short period stations in 2019, increasing the opportunity for passive source techniques when supplemented by data from the active source campaigns. Heath et al. (2015) combined active and passive source seismic data collected on the 2008 array to better constrain seismic velocity, with increased resolution at depths >6 km (the limit of the Beachly et al., 2012 study). They identified the main low velocity volume at 3–5 km depth below the crater floor, with horizontal dimensions of 5×3 km, and a vertical thickness of 2 km. They suggested that the location of this body is consistent with it hosting the rhyolitic magmas erupted in the caldera. Their model requires ∼10% melt with a minimum melt volume of 2.5 km^3 in this region. They also reported LPs from PNSN seismometers between 2012 and 2015 at 7–11 km depth (rlu). Finally, Heath et al. (2018) used seismic autocorrelation, finding a coherent P-wave reflection at 2.5 km depth beneath the caldera, which they inferred is generated at the top of the magma body.

Bowles-Martinez and Schultz (2020) used 3D magnetotellurics to identify a relatively resistive magma chamber beneath Newberry Volcano at 3–4 km depth below the crater floor. The relatively high resistivity of this body does not require melt and could be a fractured pluton. However, for consistency with the seismic studies described above, they showed that this body could be melt, if that melt was relatively water-poor (∼1.5 wt%). They suggested that such a low H_2O content is reasonable if the rhyolitic melt differentiated from a dryer basalt. However, mafic inclusions in the Big Obsidian Flow have a phase assemblage typical of relatively hydrous magmas (e.g., amphibole, two pyroxene and Fe-Ti oxides, Linneman & Myers, 1990). Additionally, melt inclusions indicate that differentiation of a basalt with ∼0.3–0.6 wt% H_2O to a dacite at Kilauea Volcano raises H_2O contents to 2 wt% (Wieser et al., 2022a). Thus, it seems unlikely that fractional crystallization at ∼3–5 km depth could produce such a dry rhyolite magma without a substantial contribution from melting of very anhydrous crustal material.

Dzurisin (1999) examined leveling data over a period of uplift between 1931 and 1994. They suggested that one possible mechanism for this uplift was the intrusion of 0.06 km^3 of magma ∼10 km below the crater floor. It is hard to investigate this deformation source further, because no measurable volcanic deformation has occurred at Newberry since the 1980s (Poland et al., 2017).

14.4. Summary and Future Work

Overall, Newberry Volcano has been subjective to extensive geophysical investigation. However, it is clear that substantially more petrological work involving mineral and MI compositions is required. In particular, MI work

constraining pre-eruptive H_2O contents will help inform geophysical inversions (e.g., determining whether rhyolitic melts are as dry as suggested by Bowles-Martinez & Schultz, 2020). Additional experiments conducted using volatile contents inferred from MIs could help constrain storage conditions further (Mandler et al., 2014).

15. Mount Jefferson

The area around Mount Jefferson has a complex volcanic history over 4–8 Myrs, with 160 separate units from monogenetic and composite cones, shields, and domes spread over 150 km^2 (Conrey, 1991). A transition from widespread mafic volcanism to more focused intermediate and silicic volcanism and the development of the modern edifice began at ∼300 ka (Conrey, 1991; DiGuilio, 2015). Erupted rocks are characterized by very complex, heterogenous crystal cargoes (Conrey, 1991; Ustunisik et al., 2016).

15.1. Mineral Compositions

We obtain the following mineral analyses after filtering:

- $N = 87$ Amp analyses from Conrey (1991) representing the last 200 Kyr of stratigraphy at Mt. Jefferson, from rhyodacites, dacites, and quenched mafic inclusions. While Conrey (1991) also present Cpx analyses, they do not report Na_2O data, so these measurements cannot be used with the J2022 and W2021 barometers.
- $N = 211$ Amp, $N = 24$ Cpx and $N = 26$ Opx-Cpx pairs from various intermediate units from DiGuilio (2015). This units include the Whitewater Creek intermediate domes (32 ka), the Park Butte Andesite (154 ka), and the Pleistocene age basaltic andesite of Whiskey Creek. Only $N = 3$ of these Opx-Cpx pairs are in high-T K_D equilibrium following Putirka (2008).
- $N = 25$ Amp analyses from the ∼10 ka Whitewater Creek andesite reported by Ustunisik et al. (2016).

The median Cpx-only pressure is ∼2.5 kbar using W2021 and ∼1.9 kbar using J2022. Amp-only median pressures (∼3 kbar) are reasonably similar to these Cpx pressures. In contrast, median Cpx-Opx pressures are 6.7 kbar using Equations 37–39 and 5.7 kbar using Equations 36–39 from Putirka (2008). Given the relatively poor performance of Cpx-Opx barometers in arc magmas (Wieser et al., 2023a) and the relatively small number of Opx-Cpx analyses, we suggest that more substantial evidence is needed to infer a deeper magma storage zone.

15.2. Melt Inclusions

The only MI measurements from Mount Jefferson to our knowledge are from Ustunisik et al. (2016). However, they do not measure MI H_2O or CO_2, so no barometric constraints can be obtained from these samples.

15.3. Experimental Petrology

To our knowledge, there are no experimental constraints on magma storage at Mount Jefferson.

15.4. Geophysics

We are not aware of literature describing seismic or magnetotelluric investigations of magma storage. Given that there is only a single one component short-period seismometer >10 km from the summit, and that the PNSN locates an average of 0 earthquakes per decade, the absence of seismic constraints on magma storage is unsurprising. No-ground based geodetic studies have been performed at Mount Jefferson. InSAR from the 1990s–2000s shows coherence, but no deformation (Poland et al., 2017).

15.5. Summary and Future Work

Further petrological work would help to further investigate the plumbing system, particularly MI or experimental petrology. However, the low threat ranking of Jefferson means that this work is not as urgent as similar data gaps at higher threat volcanoes (Figures 1 and 16).

16. Regional Mid Crustal Anomalies Around Mount Hood, Mount St. Helens, Mount Adams and Mount Rainier

To avoid repetition in the following sections, we discuss the regional anomalies in the mid to lower crust around Mount Hood, Mount St. Helens, Mount Adams and Mount Rainier here in a single section.

Stanley (1984) performed a regional magnetotelluric (MT) study, identifying a conductive zone in the region between Mount St. Helens, Mount Adam and Mount Rainier termed the Southern Washington Cascades Conductor (SWCC). He suggested that this feature reflects a band of conductive sediments and volcanic rocks of approximately Tertiary age. Hill et al. (2009) performed a higher-resolution MT study over a 35 km^2 area near Mount St. Helens, as well as a 2D line stretching from Mount St. Helens to just north of Mount Adams across the southern portion of the SWCC. They identified a conductor stretching beneath the summit of Mount St. Helens, merging with a thick conductive region at ∼15 km depth, and stretching across to Mount Adams, where it shows some weak upper crustal features. They interpret the shallow zone beneath Mount St. Helens as a magma conduit supplying the volcano, which was showing unrest during the survey. By extension, they suggest that the connected mid crustal feature also represents 2%–12% interconnected melt, which supplies the dacitic magmas erupted at Mount St. Helens and Mount Adams. Bedrosian et al. (2018) further investigated this region using new high density MT data from an array spanning the entire SWCC to determine whether the anomaly resulted from magma or sediments. They note that the conductor beneath MSH imaged by Hill et al. (2009) extends 10s of km away from the volcano, extending into a metasedimentary belt. They believe the conductivity of dacite partial melt would be dwarfed by the ∼10× higher conductivity of these metasediments, and as a result conclude MT techniques alone cannot unambiguously distinguish between regions of magma storage versus sedimentary deposits.

Flinders and Shen (2017) used 3D ambient-noise tomography to investigate the velocity structure of the SWCC, with a particular focus around Mount Rainier. They found a large low velocity zone in approximately the same region as the MT-defined SWCC, with its top at depths of ∼10 km bsl toward the northern extent closer to Mount Rainier, and ∼15 km depth closer to Mount St. Helens and Mount Adams. The base is likely unconstrained in the model but may extend to ∼27 km bsl. They also suggested that portions of the SWCC have seismic velocities most consistent with the presence of ∼6% melt, particularly in the context of the large number of Quaternary volcanic vents over this feature (>100).

In addition to local anomalies at Mount St. Helens, Ulberg et al. (2020) identified a broad region with low P-wave velocity at >10 km depth around Mount Rainier to Mount Adams. They speculated that this may indicate fluid or melt present, or high crustal temperatures.

Jiang et al. (2023) used ambient noise interferometry on a regional seismic network to further investigate the origin of these crustal anomalies. Crucially, their approach used data from the EarthScope array in addition to regional seismic networks, which helped to mitigate edge effects allowing them to expand their reconstruction to cover the area around Mount Hood. They identified two subparallel low V_s zones at 15–30 km depth bsl, which they interpreted as deep crustal magma sills with ∼2.5%–6% melt. One zone stretches from Mount Rainier to Mount Adams, and the other from Mount St. Helens to Mt Hood.

17. Mount Hood

Construction of the modern edifice at Mount Hood began at ∼500 ka. Activity has since been dominated by remarkably homogenous andesitic (and sometimes dacitic) lava flows and domes, with no evidence for explosive eruptions in the regional tephra record (W. E. Scott & Gardner, 2017). The three most recent eruptive episodes are Polallie (13–20 Kyr), Timberline (1.5 Kyr), and Old Maid (∼200 years, Koleszar et al., 2012), with the Main Stage preceding this (>29 Kyr, W. E. Scott et al., 1997). We also discuss analyses from the Parkdale flow (7.5–7.7 Kyr, W. E. Scott et al., 1997) and the Main Stage Cloud Cap lavas which erupted from satellite vents between ∼400 and 600 Kyr (Keith et al., 1985).

18. Mineral Compositions

We obtained the following mineral compositions after filtering:

- $N = 15$ Cpx analyses from the Main Stage and Parkdale Flow from Darr (2006).
- $N = 41$ Cpx analyses from the Main Stage Cloud Cap, Main Stage, and Polallie from Cribb (1997).
- $N = 274$ Amp compositions from Koleszar (2011), Koleszar et al. (2012) and Loewen (2012) from the Old Maid, Timberline and Polallie eruptive episodes.

The median Cpx-only pressure is ∼1.4 kbar for W2021, and ∼1.6 kbar for J2022, with W2021 extending as a tail to much shallower pressures (while J2022 shows the absence of very shallow pressures typical of this barometer).

The median Amp-only pressure is ~1.6 kbar regardless of filters, which is remarkably similar to the Cpx-only pressure estimates.

18.1. Melt Inclusions

Koleszar et al. (2012) presented Plag, Opx, and Cpx hosted MIs ($N = 38$) from the Old Maid, Timberline, and Polallie Stages. A subset of MIs that were large enough for double polishing ($N = 12$) were measured using FTIR and yielded no CO_2 above the detection limit. The remaining MIs (<60–80 μm diameter, $N = 28$) were measured by SIMS. These inclusions contained CO_2 contents up to 2,400 ppm, although they note that the lack of standards with >540 ppm CO_2 required their calibration line to be extrapolated for these measurements. These high CO_2 contents are unusual in such evolved materials, so Koleszar et al. (2012) suggested that they may result from the presence of undetected microcracks with CO_2 contamination during sample preparation. They also noted that many MIs contain vapor bubbles, which may contain additional CO_2. Their FTIR H_2O measurements range from 0.8 to 3.6 wt%, while SIMS measurements range from 0.9 to 5.4 wt%. The higher SIMS H_2O contents may reflect the superior ability of smaller MIs to retain high volatile contents (e.g., less resistant to cracking/rupturing), although it is possible this disagreement also reflects calibration issues. They note that there is a general trend toward lower H_2O contents with increasing SiO_2, indicating MI entrapment during degassing induced-crystallization, which makes it hard to apply a filter based on H_2O contents. Thus, considering the poorly constrained nature of CO_2, and the probable influence of degassing on H_2O, saturation pressure from these MIs are not a rigorous constraint on magma storage.

18.2. Experimental Petrology

While Mount Hood andesite has been used widely as an experimental starting material, we are not aware of any experimental studies directly relating to magma storage conditions beneath Mount Hood. Additionally, erupted Mt Hood andesites are mixed magmas and are thus not representative of a single multiply saturated liquid (Kent et al., 2010).

18.3. Geophysics

Weaver et al. (1982) reported the results from a 16-station seismic network established in 1977 at Mount Hood. They found no significant velocity anomalies beneath Mount Hood indicative of magma reservoirs. Use of earthquakes directly, rather than through inversions for crustal structure, has been hindered at Mount Hood by the fact that low frequency earthquakes and tremor are exceedingly rare. Jones and Malone (2005) summarized that most earthquakes detected on the Mount Hood seismic network have characteristics of tectonic earthquakes, likely reflecting the northern edge of regional Basin and Range seismicity. Following a M4.5 earthquake in June 2002 located ~4.6 km south of Mount Hood, there was a swarm of >200 aftershocks, which Jones and Malone (2005) subdivided into four groups. A small subset of these earthquakes (Group D) occurred at very shallow depths. Jones and Malone (2005) suggested that these earthquakes may reflect volcanic processes beneath Mount Hood, although they do not speculate further as to whether these represent magma or fluid movement. Other than the regional mid-crustal anomalies discussed above, there are no further seismic constraints on upper crustal storage to our knowledge. In part, this reflects the fact that no local high-resolution study has been conducted using modern instrumentation. Poland et al. (2017) summarize available geodetic constraints at Mount Hood, which show no consistent deformation patterns that can be associated with volcanic activity since the 1980s.

18.4. Summary and Future Work

Future work remeasuring CO_2 and H_2O in MIs and their vapor bubbles using more robust SIMS calibrations would help resolve whether the high-pressure MIs of Koleszar et al. (2012) represent a deeper magma storage region or an analytical artifact. Hints of higher-pressure storage (2–4 kbar) are perhaps seen in the Cpx and Amp pressures; coupled measurements of mineral chemistry and MIs within a single crystal would help to investigate this further. Like many of the volcanoes discussed so far, Mount Hood's seismic network has been recently densified with three-component broadband seismometers (Figure 9e). Once sufficient earthquakes have been recorded on this network, local, passive-source inversions should provide additional constraints on the presence/absence of magma storage regions and low velocity zones, and a greater understanding of the origin of earthquakes at Mount Hood (Jones & Malone, 2005).

19. Mount St. Helens

Mount St. Helens is located 53 km west of Mount Adams and 35–50 km W of the main arc front, so can be classified as a fore-arc volcano. It erupts primarily dacitic bulk compositions with plagioclase, pyroxene and amphibole phenocrysts (Hildreth, 2007), although erupted products range from basaltic to rhyodacite. Many display evidence of the mingling of basaltic and a dacitic magma (Pallister et al., 2017). It is one of the youngest and most active volcanoes in the Cascades, erupting more than half its 75 km^3 magma volume in the last 28 Kyr, and exhibiting five major explosive eruptions in the last 500 years. This high activity relative to other Cascade centers has been attributed to its location within a small pull-apart basin (Pallister et al., 2017). Following its Plinian eruption in 1980 and re-awakening in 2004–2008, it represents one of the best-studied Cascade volcanoes both in terms of petrology and geophysics (Figure 10).

19.1. Mineral Compositions

We obtain the following mineral data after filtering:

- $N = 41$ Cpx compositions from the Kalama (~1480 CE) and Castle Creek andesites (1.9–1.7 Kyr BP) from Cooper and Reid (2003).
- $N = 19$ Cpx from the 2004–2005 eruption from Rowe et al. (2008).
- $N = 4$ Cpx from the Castle Creek andesite from Smith and Leeman (1993).
- $N = 47$ Amp from the 2004–2005 episode obtained from the Rowe et al. (2008) USGS data repository, and an additional $N = 78$ analyses from Humphreys et al. (2019) attributed to Rowe et al. (2008).
- $N = 171$ Amp from the May 1980 cryptodome and pumice fall, the 12 June 1980 airfall, and the July 1980 pyroclastic flow from Humphreys et al. (2019).
- $N = 170$ Amp from the 1980 CE eruption from Loewen (2012).
- $N = 521$ Amp from samples spanning 1980–2004 CE from Thornber et al. (2008).
- $N = 54$ Amp from mafic Castle Creek samples from Wanke et al. (2019).

The median Cpx-only pressure is 2.3 kbar using W2021, and 1.8 kbar using J2022, with relatively similar distributions (although W2021 shows a deeper tail). Filtered and unfiltered Amp-only pressures are 3.1 and 3.2 kbar respectively, although, as for Cpx, the distributions are quite broad. In general, Amp pressures are offset~ 1 kbar deeper than Cpx, which is well within the uncertainty of these methods.

19.2. Melt Inclusions

Rutherford et al. (1985) measured H_2O in 57 plag-hosted MIs from the 18 May pumice using volatiles-by difference techniques (~4.6 wt%). Blundy and Cashman (2005) measured H_2O using SIMS in mostly Plag-hosted MIs (some Amp- and Opx-hosted) from blast deposits, pyroclastic flows and domes from May to October 1980. Texturally, many of these MIs show evidence for connection to the outside of the crystal, and there is a correlation between H_2O and SiO_2. These textural and chemical trends indicate decompression-induced degassing accompanying MI entrapment, meaning that MIs saturation pressures may be weighted toward recording processes occurring during magma ascent. Blundy and Cashman (2005) stated that their preliminary FTIR measurements indicated that CO_2 contents were very low, so pressures could be determined using H_2O-only saturation pressures. However, Blundy et al. (2010) supplemented the 2005 analyses with new SIMS analyses of CO_2 in $N = 77$ MIs from nine eruptive episodes between 1970 and 1984, and found CO_2 above the FTIR detection limit. We only use these later measurements. This is intriguingly similar to the scenario at Mount Hood where Koleszar et al. (2012) found no CO_2 using FTIR, but abundant CO_2 using SIMS. The SIMS analyses of Blundy et al. (2010) for MIs from the 1980 plinian episode have relatively low CO_2 (<400 ppm) and high H_2O (~4–6 wt%), while the later subplinian to vulcanian and effusive events have higher CO_2 and lower H_2O. They attributed these differences to CO_2-flushing as the eruption progressed. Four MIs have 0.4–1.7 wt% CO_2, which Blundy et al. (2010) link to much deeper magma storage.

19.3. Experimental Phase Equilibrium

Rutherford et al. (1985) performed experiments on a bulk sample of MSH dacitic pumice at 1–3.2 kbar, varying the fluid composition and oxygen fugacity. They showed that the observed phase assemblage and crystallinity of the 18 May 1980 magma can only be produced if $P_{H_2O} \neq P_{Total}$, requiring either H_2O-undersaturation, or a

relatively CO_2-rich melt. They concluded that the upper part of the MSH magma reservoir was at a pressure of 2.2 ± 0.3 kbar, P_{H_2O} was 50%–70% of P_{total}, and T was 930 ± 10°C. However, they noted that the exact storage pressure was not constrained because these conditions were not simultaneously satisfied in different experiments. Rutherford and Devine (1988) performed additional experiments at 920°C and 2.2 and 3.2 kbar, with variable fo_2 and X_{H_2O} to further investigate Amp stability. They found that the phase assemblage of the 1980 eruption including Amp was reproduced at $P = 2.2$ kbar, $T = 920$°C, and $X_{H_2O} \geq 0.67$, with a surge of Plag crystallization occurring when X_{H_2O} decreased just before eruption.

Gardner et al. (1995) performed experiments at 1, 1.5, 2.5, and 3.5 kbar and 850°C to determine storage pressures and water fugacity of six dacitic magmas from the last 4,000 years. For different dacite units, they invoked storage depths between ~3.5 and 1.5 kbar. Their results suggested that 4,000–3,000 years ago, dacites were H_2O-saturated (5.5–6.5 wt%), while more recently erupted dacites were H_2O-undersaturated (<5 wt% H_2O). They suggest this shift represents increasing mafic input, which dilutes H_2O and adds CO_2 (and also explains the appearance of andesitic bulk compositions). Constraints on magma storage are also provided by the stability of the mineral cummingtonite (a type of amphibole), which breaks down to orthopyroxene (Geschwind & Rutherford, 1992), indicating similar storage conditions to Gardner et al. (1995).

Rutherford and Devine (2008) performed experiments on the 2004–2006 dacite, suggesting that the Fe and Al-rich Amp cores formed at 2–3 kbar and 900°C, as Amp forming in experiments at <2 kbar had lower Al than observed products. They suggested the observed $An_{68\text{-}40}$ Plag compositions formed when pressure dropped to 2 kbar at 900°C, and the outer rims of some Amp phenocrysts may have formed at 1–2 kbar.

19.4. Geophysics

Scandone and Malone (1985) used subsidence recorded by electronic tiltmeters in June-November 1980 to make a first estimate of the reservoir depth supplying the 1980 eruption (~7–9 km, rlu). They also analyzed earthquake hypocenters accompanying each explosive event, identifying an aseismic zone at ~ 7 km depth (rlu) extending vertically for 6+ km which they suggested is a magma reservoir connected to the surface by a ~50 m wide conduit. Barker and Malone (1991) used earthquake focal mechanisms to identify an aseismic zone at 7–11 km bsl associated with magma storage. Musumeci et al. (2002) relocated 447 earthquakes from the late 90s to produce a 1D velocity structure beneath Mount Saint Helens, identifying a magma reservoir at ~5.5–10 km depth (bsl), and a thin vertical conduit similar to that invoked by Scandone and Malone (1985). More recently, G. P. Waite and Moran (2009) presented a *P*-wave travel time velocity model using earthquake data recorded on the local network over 25 years, supplemented by 19 temporary broadband seismometers from 2005 to 2006. They identified a low-velocity zone at ~2–3.5 km bsl which they attributed to a shallow magma storage zone. Their model had limited resolution beneath 6 km, but they identified low velocities at ~5.5–8 km bsl in an aseismic zone, which approximately aligns with the older estimates described above.

The numerous geophysical studies described above mostly imaged the upper crust, as travel time tomography struggles to produce high resolution images at >6 km depth. Kiser et al. (2016) presented results from the active source portion of the iMUSH (imaging Magma Under St. Helens) project. They identify a high V_p/V_s anomaly at 4–13 km bsl which they attributed to magma storage, and a low V_p column extending from 15 km to the Moho to the southeast of Mount St. Helens. Kiser et al. (2018) built on this study, using a finite-frequency tomographic method to place more detailed constraints on the geometry of the magma storage region. They identified a number of low V_p anomalies forming a near continuous body spanning 3.5–14 km bsl, with the highest amplitude V_p anomalies at 4–6 km bsl (interpreted to represent 10%–12% melt, dropping to ~8% at 7 km depth, and continuing to decrease downwards).

Ulberg et al. (2020) used local source V_s and V_p tomography as part of the iMUSH broadband array of 70 broadband seismometers to image the upper 20 km of the crust beneath Mount St. Helens. They identified a low *P*- and *S*-wave anomaly at 6–15 km depth bsl, with a diameter of 5–7 km, which they interpret as a magma storage region with ~3% partial melt over ~15–20 km^3. They also imaged the broader low *P*-wave velocity region discussed above in the section "*Regional mid crustal anomalies…*". Ambient noise imaging from the same array showed low-velocity lower-crustal anomalies between Mount St. Helens and Mount Adams (Crosbie et al., 2019).

Interestingly, neither Kiser et al. (2016, 2018), Ulberg et al. (2020), nor Crosbie et al. (2019) imaged the low velocity region at 2–3 km bsl identified by G. P. Waite and Moran (2009). Ulberg et al. (2020) suggested

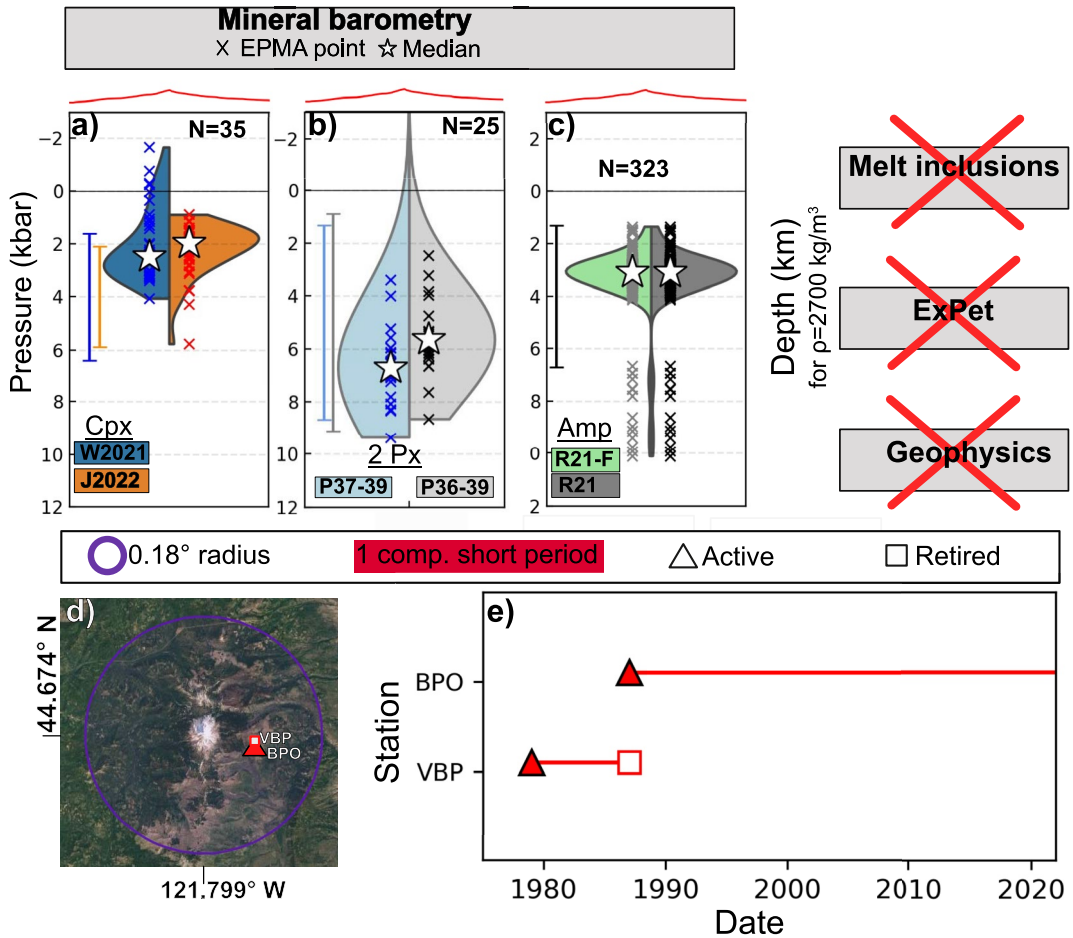

Figure 8. Compilation of magma storage depths at Mount Jefferson (a–c) and summary of the seismic network (d–e). The red line shows the height above sea level across an approximately W-E section spanning 10 km transecting the summit.

that differences between the inversion techniques in the two studies may explain this discrepancy, while Kiser et al. (2018) suggested that the low velocity zone may have been a temporary anomaly related to dome-forming activity between 2004 and 2008. Alternatively, the magma body may be too small to be resolved at the relatively long wavelengths of microseismic noise used in ambient noise imaging (Crosbie et al., 2019).

Lisowski et al. (2008) examined GPS deformation associated with the onset of unrest in 2004. They modeled the deformation in an elastic half space model arising from a vertically elongate magma reservoir centered at ~7–8 km (basl). Mastin et al. (2008) modeled geodetic data from eight continuous GPS stations as an ellipsoidal source with its top at 5 ± 1 km (basl), and the center offset 1.3–1.6 km east of the crater center. The base of this source is less well constrained; they place it somewhere below 10 km (likely 10–20 km basl).

K. Anderson and Segall (2013) inverted geodetic data from the 2004–2008 period, along with information on extruded lava dome geometry. Using a range of input parameters (e.g., melt H_2O), they showed a probabilistic estimate of magma chamber geometry from 100 randomly sampled outputs from their Markov-Chain Monte Carlo simulations. They estimated that the centroid of the magma chamber was ~11–18 km below the crater floor, with an aspect ratio of at least 2 (e.g., vertically elongated). On Figure 10, we show the extent of the magma chamber indicated on their Figure 11 within the 67% contour line of different simulations (e.g., 1σ, 5.5–20.5 km). Wong and Segall (2020) built on this approach using a time-dependent conduit flow model, inverting time series data for extruded dome volume, CO_2 emissions and ground deformation. Their model favors an elongate chamber (width:height = 0.13–0.55). Extracting depths from their contours on their Figure 8 to allow direct comparison with K. Anderson and Segall (2013) yields depths of ~5–17 km.

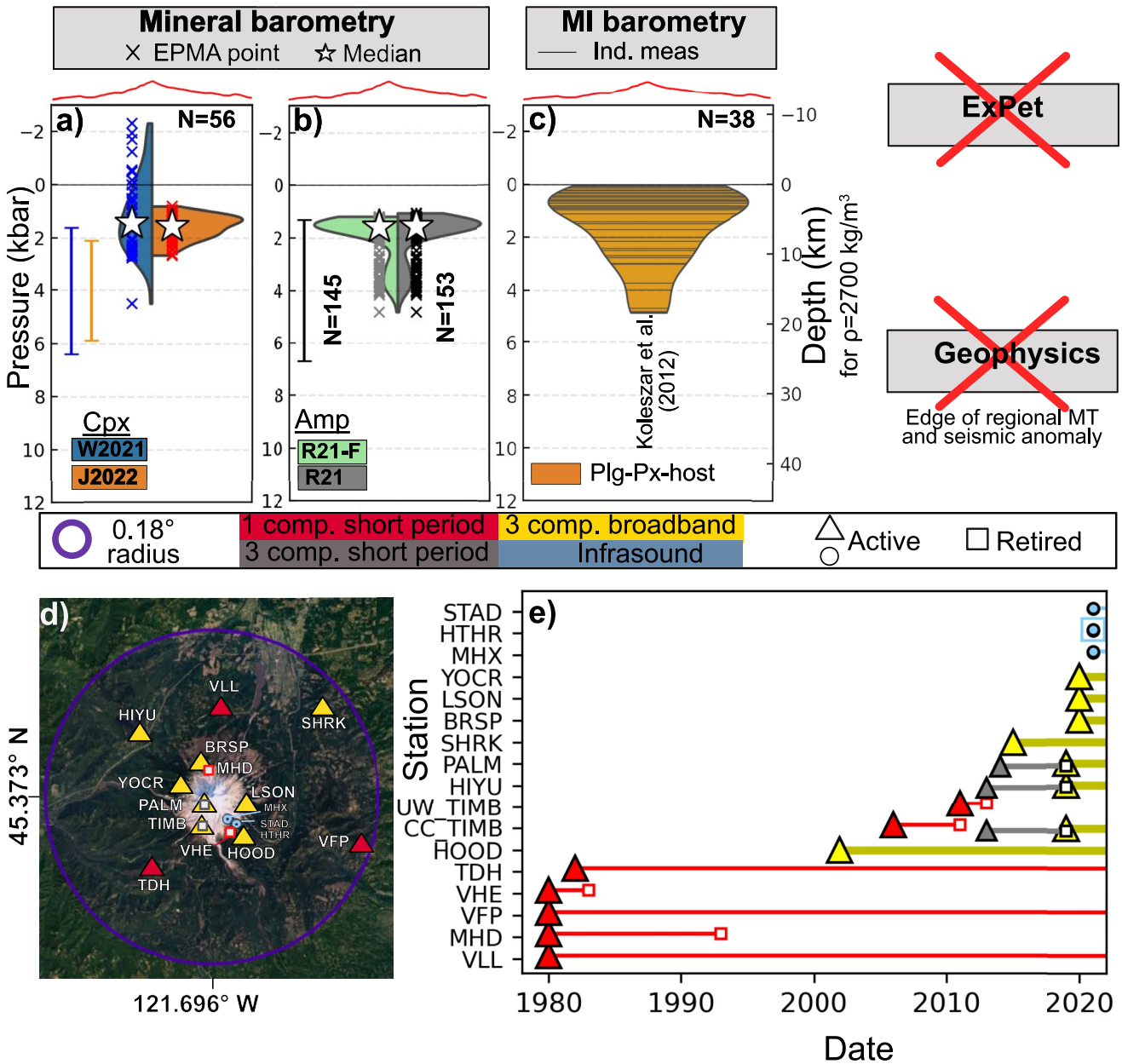

Figure 9. Compilation of magma storage depths at Mount Hood (a–c) and summary of the seismic network (d–e). The red line shows the height above sea level across an approximately W-E section spanning 20 km transecting the summit. Blue dots on map are infrasound stations.

19.5. Summary and Future Work

Relative to the rest of the Cascade arc, magma storage depths are well constrained at Mount St. Helens, with various methods delimiting a vertically extensive magmatic system ranging from ~5 to 12 km depth (Pallister et al., 2017). In general, the shallower geophysical anomalies cluster at ~2–4 kbar, which is reasonably consistent with the median pressures from mineral barometry, while MIs appear to record shallower processes, perhaps during ascent toward the surface. However, given experimental and MI evidence for the importance of CO_2, it would be worthwhile re-evaluating the CO_2 budget of Mount St. Helens MIs to account for any CO_2 which has partitioned into the vapor bubble. Further MI work on more mafic cones in the general area may provide petrological evidence for the geophysically imaged mid-crustal anomaly. The recent densification of three component broadband stations will greatly increase the potential for local, passive-source inversions. The biggest unanswered question revolves around whether the shallow low velocity anomaly of G. P. Waite and

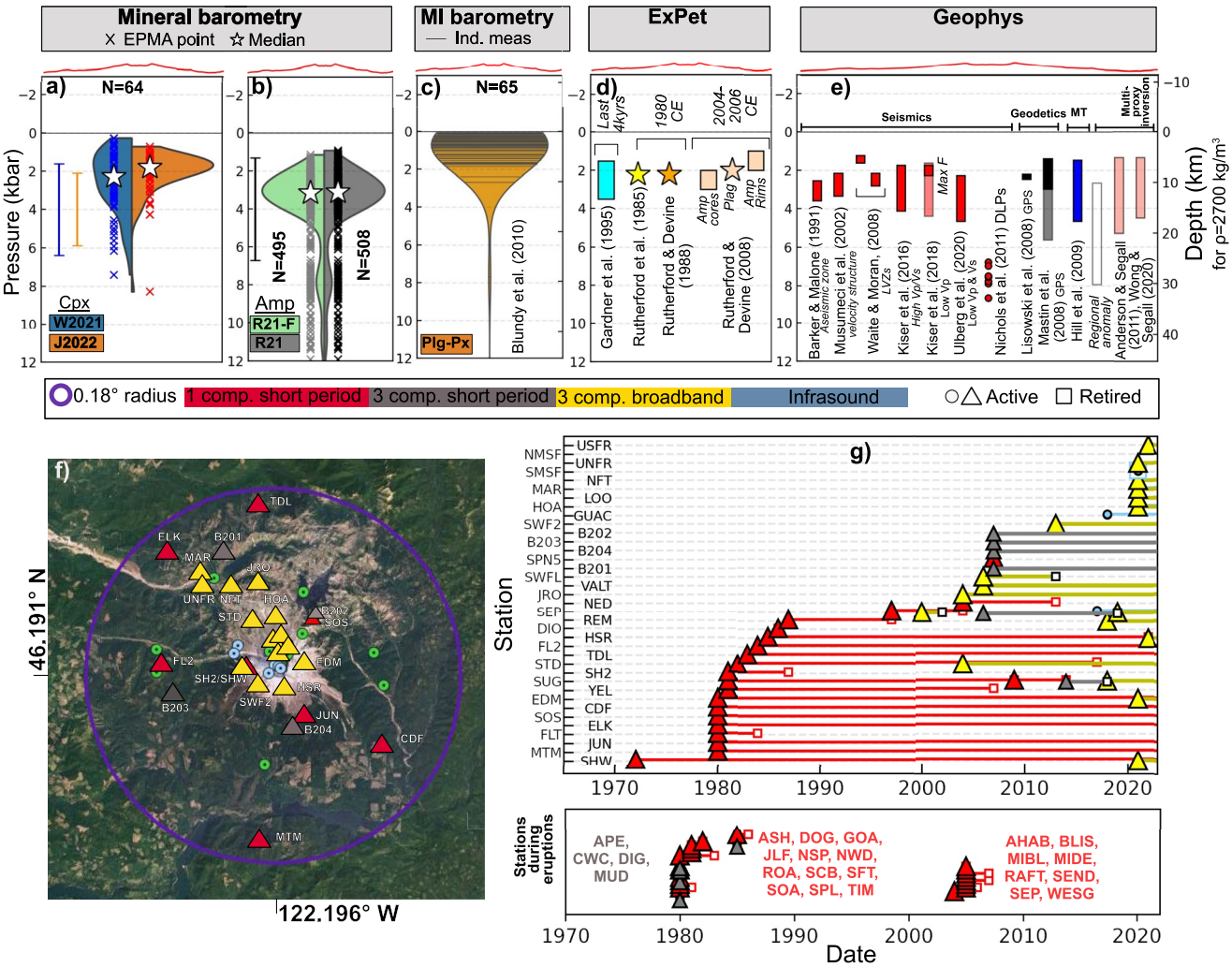

Figure 10. Compilation of magma storage depths at Mount St. Helens (a–e) and summary of the seismic network (f–g). The red line shows the height above sea level across an approximately W-E section spanning 15 km transecting the summit.

Moran (2009) was an ephemeral feature which was difficult to resolve by other methods, or whether it was an imaging artifact.

20. Mount Adams

Mount Adams is an andesitic-dacitic stratovolcano, located east of Mount St. Helens along the main arc-axis. The large edifice lies in the center of a larger volcanic field with ~120 spatter, scoria cones, and shield volcanoes. Vents within ~6 km of the summit are classified as flank vents because of compositional similarity to summit lavas, while those further away have basaltic or basaltic-andesitic compositions (Hildreth, 2007).

20.1. Mineral Compositions

J. Fierstein supplied previously unpublished analyses yielding N = 43 Amp and N = 1,214 Cpx from the post-glacial (0–15 kyr) period of Mount Adams after filtering (samples discussed in Hildreth & Fierstein, 1997). The median Cpx-only pressure is ~0.4 kbar for W2021 and ~1.3 kbar for J2022, which is a similar offset to that seen between these barometers at other edifices. In contrast, Amp-only pressures span a significantly greater range, from ~2 to 6 kbar, with a median pressure of 3.9 kbar.

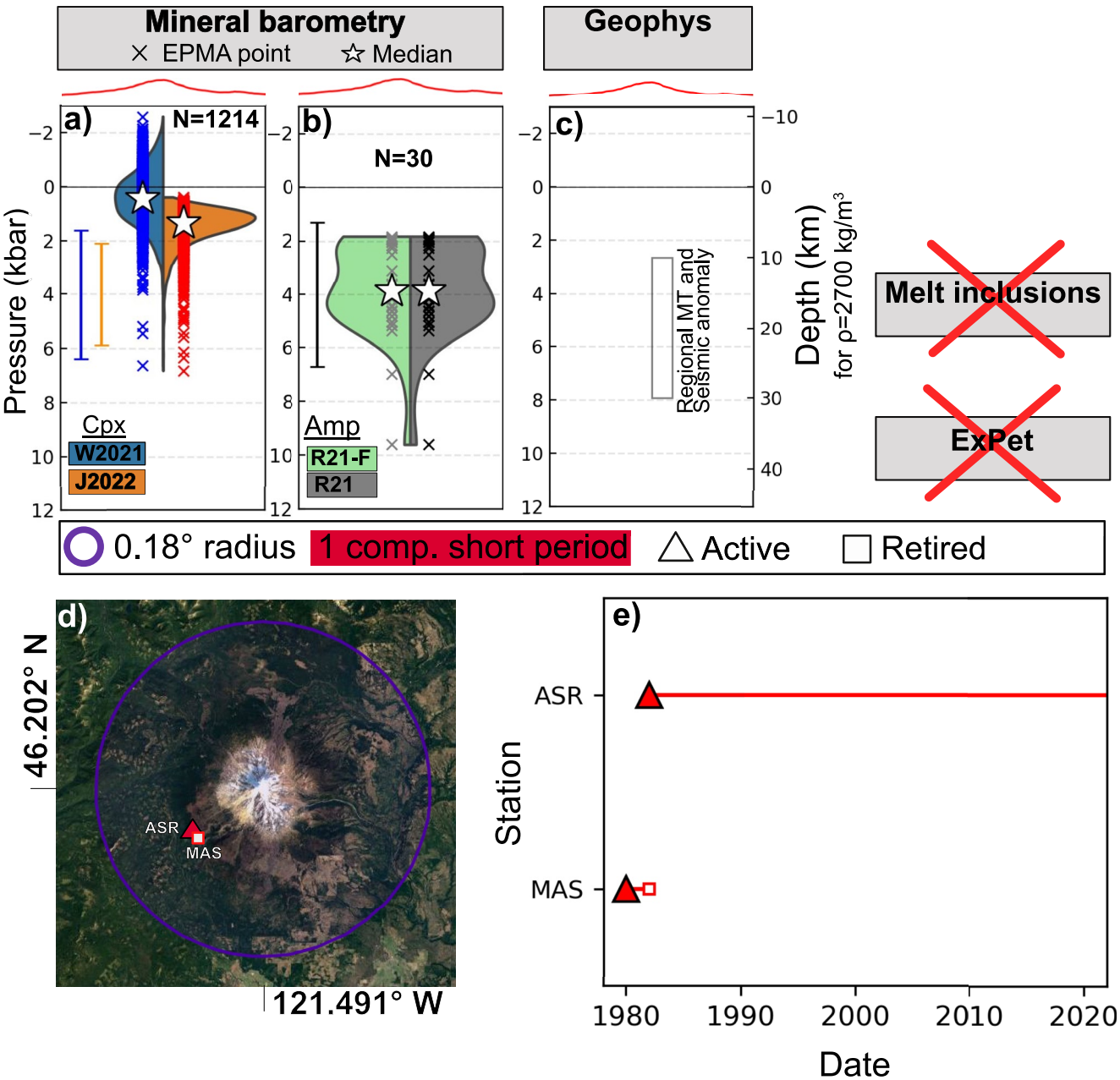

Figure 11. Compilation of magma storage depths at Mount Adams (a–c) and summary of the seismic network (d–e). The red line shows the height above sea level across an approximately W-E section spanning 15 km transecting the summit.

20.2. Experimental Phase Equilibrium and Melt Inclusions

We are not aware of any phase-equilibrium constraints for Mount Adams or MI studies.

20.3. Geophysics

Apart the regional mid crustal anomalies discussed above, there are no seismic constraints for magma storage at Mount Adams, reflecting the fact there is only a single 1 component short period seismometer installed in the area (Figure 11d), and no detailed local studies have been performed. The iMUSH array extends to the western flanks of Mount Adams, and does indicate potential for melt storage in the lower crust west of Adams (Crosbie

et al., 2019; Kiser et al., 2016; Ulberg et al., 2020). However, the lack of stations on or east of the summit, due to permitting constraints, makes it difficult to image a proximal magma system. In addition, no ground based geodetic studies have been performed at Mount Adams, and while InSAR shows coherence, there were no obvious signals of deformation in the 1990s to early 2000s (Poland et al., 2017).

20.4. Summary and Future Work

The absence of upper crustal geophysical constraints, MIs and experimental petrology is very concerning, particularly given Mount Adams is classified as high threat, and ranked the 34th most hazardous US volcano. While the difference in Cpx-only and Amp-only pressures may reflect different storage regions with different crystallizing phases, these barometers are too imprecise to be sure without other proxies for magma storage. A densified seismic network would be an important next step, along with more focused petrological studies specifically targeting magma storage depths (e.g., MIs).

21. Mount Rainier

Mount Rainier is the highest elevation Cascade peak, although the volume of volcanic material is smaller than it appears as a result of it being built on top of older underlying terrains (130 vs. 450 km^3 for Mount Shasta). The edifice is made predominantly of pyroxene andesites-dacites with minor amphibole (59–66 wt% SiO_2; Hildreth, 2007). Unlike other Cascade volcanoes with numerous peripheral vents, Rainier's activity primarily occurs on the main edifice. While lava flows dominate, two large pumice falls >10 km^3 from ∼190 and ∼380 ka have been identified as well as ∼10 post-glacial pumice deposits (Hildreth, 2007; Mullineaux, 1974; Sisson & Lanphere, 2000; Sisson & Vallance, 2009).

21.1. Mineral Compositions

We obtain the following mineral analyses after filtering:

- $N = 11$ Cpx and $N = 5$ Amp analyses from the large andesitic Burroughs Mountain lava flow, which is thought to have been emplaced at ∼496 Kyr at the beginning of activity at the modern edifice of Mount Rainier (Stockstill, 1999).
- Representative analyses ($N = 6$ Cpx and $N = 4$ Amp) from Venezky and Rutherford (1997) from the 2.2 ka tephra layer.
- Unpublished EPMA analyses ($N = 13$ Amp, $N = 35$ Cpx) from the Sunset Amphitheater dacite (∼85 ka, see Sisson et al., 2019) and cognate plutonic blocks from other Rainier lava flows (T. Sisson, Pers. Comms), and Cpx ($N = 27$) and Amp ($N = 9$) from K-rich spessartite samples (S. Scott, 2010), which occurs in small eruptions on the flank and vent, and are thought to bypass the main plumbing system (Sisson et al., 2014).

Considering all formations together, the median Cpx-only pressure is ∼2.7 kbar using W2021 and ∼2 kbar using J2022. While the number of analyses is relatively small for each formation, Cpx-only pressures from the spessartite samples are deeper than the mafic Sunset Amphitheater samples (median of 4.4 vs. 2.2 kbar using W2021, 2.9 vs. 1.4 kbar using J2022, Supporting Figure S4 in Supporting Information S1). This is consistent with the hypothesis that these spessartite melts bypass the main plumbing system. Burroughs Mountain shows a very broad distribution of pressures, overlapping with Sunset and spessartite samples (−2 to 10 kbar, Supporting Figure S4a in Supporting Information S1). For Amp-only barometry, the median pressure for all samples is 3.1 kbar. Only two spessartite-hosted Amp pass the quality checks of Ridolfi (2021)—these return pressures which are ∼1–2 kbar deeper than Sunset Amphitheater amphiboles, although far more analyses per formation than could be obtained from the literature are required to accurately resolve any differences in magma storage using mineral compositions (Figure S4b in Supporting Information S1).

21.2. Experimental Phase Equilibrium

Venezky and Rutherford (1997) investigated natural products from the 2.2 ka tephra layer C from Mount Rainier, and conducted experiments at 0.25–2.5 kbar. They interpreted the products of this eruption to form during mixing of an andesitic and dacitic magma. Their experiments on a powdered Rainier dacite showed that the matrix glass composition is produced at H_2O-saturated conditions at <0.5 kbar (∼2.4 km). Determining the storage conditions

of the andesitic melt is harder (see discussion in MI section below), although they suggest that the presence of Amp indicates storage at >7 km depth, which is reasonably consistent with the Amp-only pressures we obtain.

21.3. Melt Inclusions

We are not aware of any published MI work measuring both CO_2 and H_2O. Venezky and Rutherford (1997) described an "exhaustive" attempt to find suitable MIs, noting that most inclusions were either too small to analyze, or were partially crystallized. They analyzed 20 Plag- and Pyroxene-hosted MIs in the dacitic magma, obtaining H_2O contents of 2.4–3.3 wt% by volatiles by difference. For the andesitic magma, they obtain 4–6 wt% (although they acknowledge possible issues due to PEC). These H_2O contents were used to infer entrapment depths of ∼2.4 km for the dacite, and >7 km for the andesite. However, volatile-by-difference methods are associated with large uncertainties (Hughes et al., 2019). Additionally, ongoing MI work indicates that Rainier melts are relatively CO_2-rich and H_2O-poor (T. Sisson, Pers. Comms), so we do not believe it is insightful to calculate H_2O-only saturation pressures based on volatile-by-difference methods.

21.4. Geophysics

Moran et al. (1999) investigated P-wave velocities using a local earthquake tomography imaging experiment. They identified a ∼10–15 km wide low velocity zone at 1–14 km bsl. Based on the P-wave speeds (6 km s^{-1}) and the absence of earthquakes within this cylindrical anomaly, they suggested that this anomaly consists of hot fractured rock with the possible presence of small amounts of melt and fluid. The absence of significant S-wave attenuation indicates that no large, continuous bodies of melt or fluid exist in this volume. As well as the regional anomalies discussed above, Flinders and Shen (2017) also identify a slow *V*s zone 1–8 km bsl just East of Rainier.

McGary et al. (2014) used data from the CAFE (Cascade Array for Earthscope) experiment, which collocated seismic and magnetotelluric data in a E-W transect passing near Mount Rainier. While they mostly imaged the deeper structure down to the subducting slab, they do identify a crustal conductor they infer to represent a magma reservoir. However, this feature is offset 6–10 miles from the volcanoes summit, so further investigation of this feature is warranted to determine whether it is magma or another source of conductivity (Bonner, 2015). Obrebski et al. (2015) jointly inverted receiver functions and ambient-noise-derived phase-velocity dispersion curves. No unambiguous low-velocity bodies were detected in the upper crust, although signals were complicated and station spacing of >10 km probably cannot resolve a magma body the size of that imaged by Moran et al. (1999). There are also 18 LP earthquakes located by Nichols et al. (2011).

From a geodetic perspective, no deformation has been detected at Mount Rainier since at least the 1980s, despite numerous leveling and GPS surveys, CGPS sites and InSAR acquisitions (Poland et al., 2017). Overall, these geophysical constraints are reasonably consistent with depths from petrological methods, with no concrete evidence from either method for extensive magma storage below ∼6 kbar (or 20 km).

21.5. Summary and Future Work

Mount Rainier is the third most hazardous volcano in the US (Ewert et al., 2018; Figure 1), and while a lot of the hazard is somewhat decoupled from volcanic activity (e.g., edifice collapse, lahars from existing materials), its proximity to the major population centers of Seattle, Yakima, Tacoma and Portland should justify further petrological and geophysical study. Specifically, MI studies could provide insights into the storage conditions of the andesitic melt, perhaps focusing on the pumice deposits documented by Sisson and Vallance (2009). The recent densification of the seismic network (Figure 12f) should help to further constrain the origin of seismic anomalies beneath Mount Rainier, and determine whether or not these reflect melt.

22. Glacier Peak

Glacier Peak is a predominantly dacitic edifice that has substantially less topographic prominence above neighboring peaks than many US Cascade volcanoes (Figure 13d). The early history of Glacier Peak was eroded during the last major glaciation. Since glacial retreat at ca. ∼15 ka (R. Waite et al., 1995), Glacier Peak has produced at least 9 pumice layers indicative of large explosive eruptions and past eruptions have been characterized by numerous lahars. Thus, its activity more closely resembles Mount St. Helens rather than the many other effusion-dominated Cascade volcanoes.

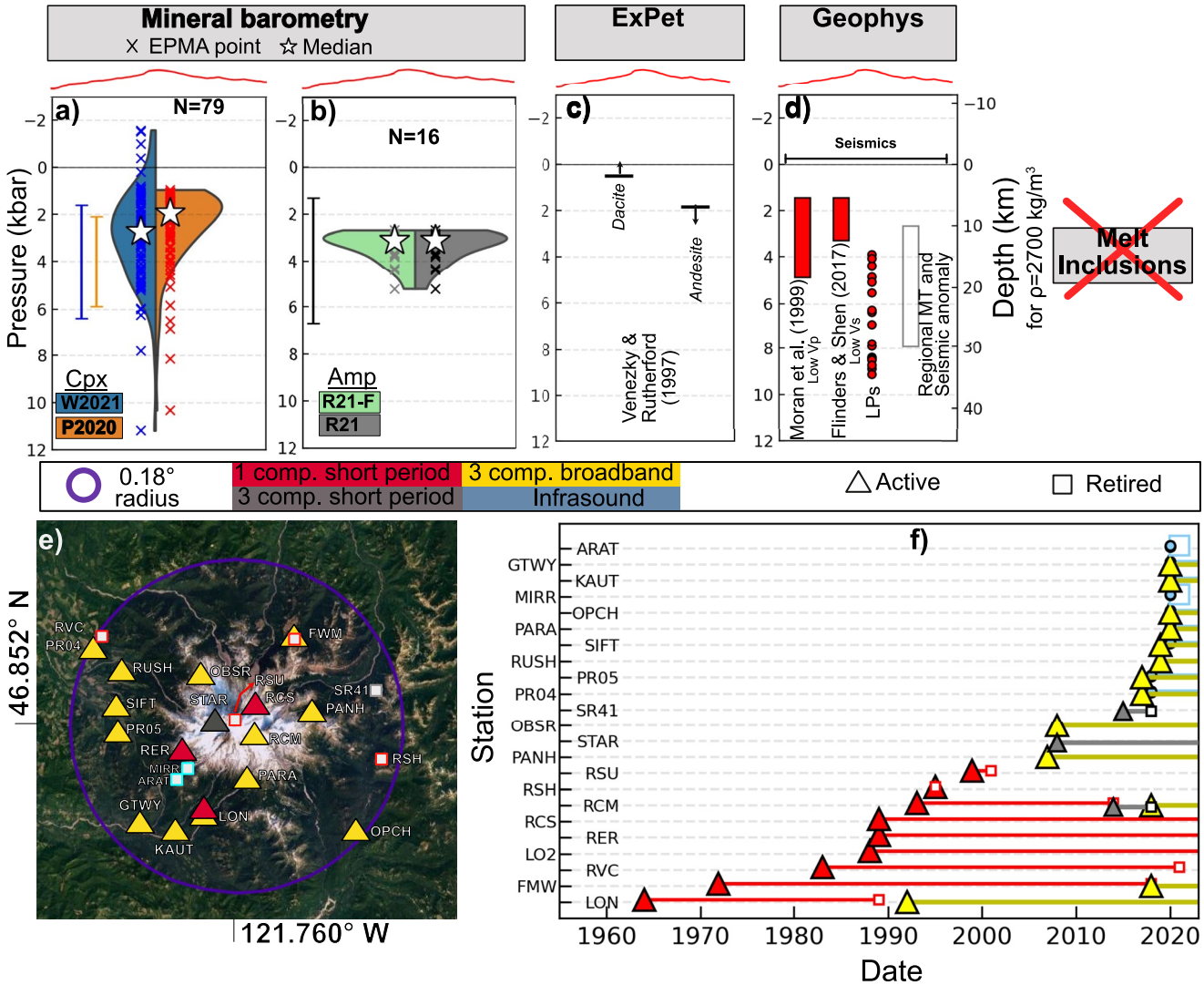

Figure 12. Compilation of magma storage depths at Mount Rainier (a–d) and summary of the seismic network (e–f). The red line shows the height above sea level across an approximately W-E section spanning 15 km transecting the summit.

22.1. Mineral Compositions

After filtering, we were only able to obtain $N = 18$ Cpx compositions from the Lightning Creek high magnesian basaltic andesite from Sas et al. (2017). The median Cpx-only pressure is ~2.2 kbar for both W2021 and J2022.

22.2. Melt Inclusions

Shaw (2011) measured 16 olivine-hosted MIs from a primitive calc-alkaline basalt and a primitive low-potassium olivine tholeiite cinder cone (data reported in Venugopal et al., 2020). However, Shaw (2011) did not measure CO_2 in MI vapor bubbles. Venugopal et al. (2020) make a prediction of the amount of bubble CO_2 by assuming the same proportion of melt-vapor partitioning as at their measurements at Mount Meager. However, the partitioning of CO_2 into a vapor bubble is very dependent on the amount of PEC varies to a large extent even within a single eruption (Wieser et al., 2021, 2023a), let alone between volcanoes. Thus, we favor stating minimum estimates using just glass volatile contents from Shaw (2011) rather than using the bubble reconstructions of Venugopal et al. (2020).

22.3. Experimental Phase Equilibrium

We are not aware of any phase equilibrium experiments relevant to Glacier Peak.

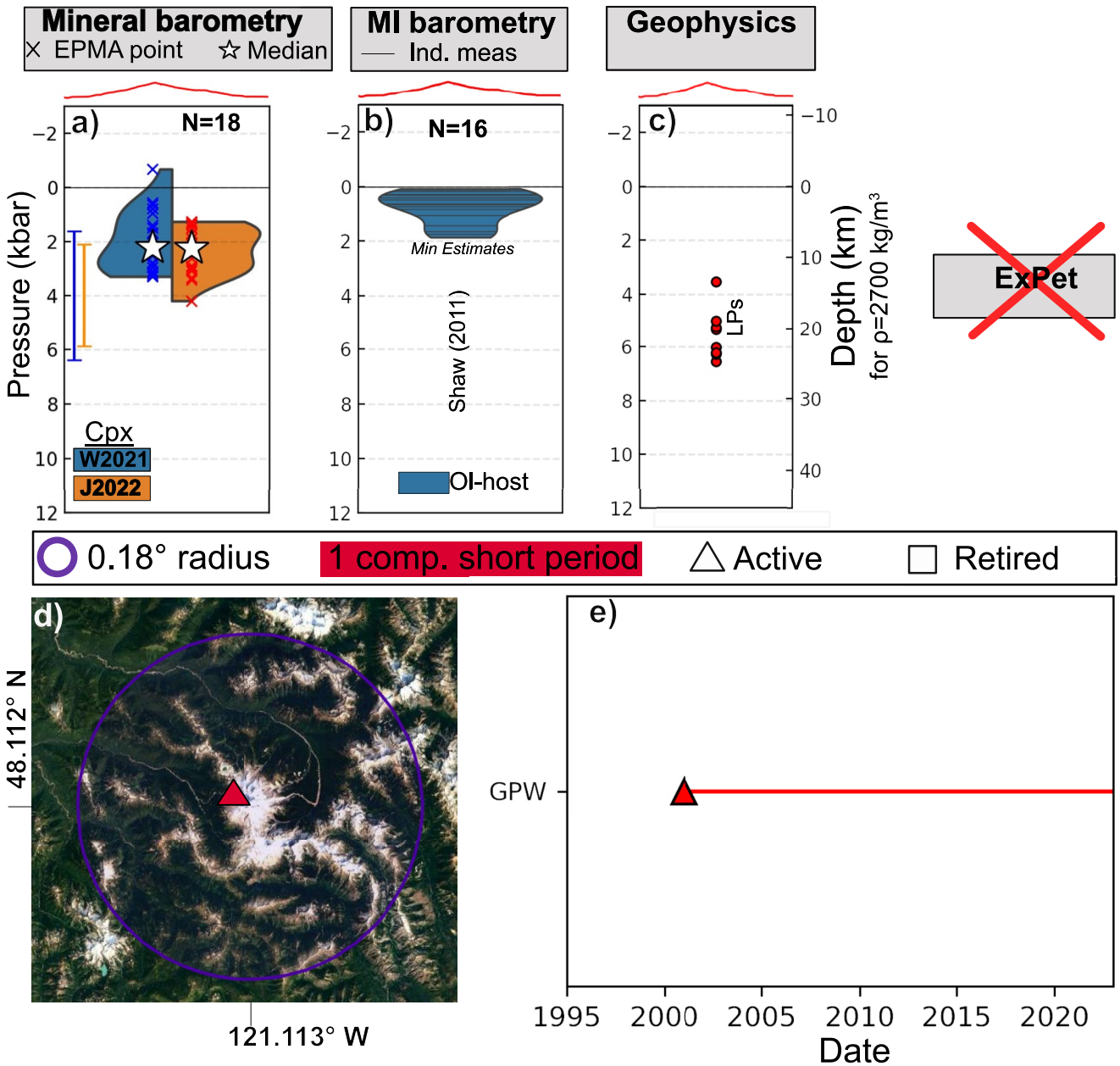

Figure 13. Compilation of magma storage depths at Glacier Peak (a–c) and summary of the seismic network (d–e). The red line shows the height above sea level across an approximately W-E section spanning 15 km transecting the summit.

22.4. Geophysics

We are not aware of any geophysical constraints on magma storage, other than identification of 8 LP earthquakes (Nichols et al., 2011). There is only a single one-component short-period seismometer, so the lack of seismic constraints other than LPs is not surprising (Figure 13). No ground-based geodetic studies have been attempted, and InSAR hasn't detected any deformation (although the ice-covered summit and heavily vegetated flanks make coherence challenging; Poland et al., 2006).

22.5. Summary and Future Work

Glacier Peak is ranked as very high threat, and the 15th most hazardous US volcano. The absence of petrological or geophysical constraints on magma storage is a very clear data gap to address with future work.

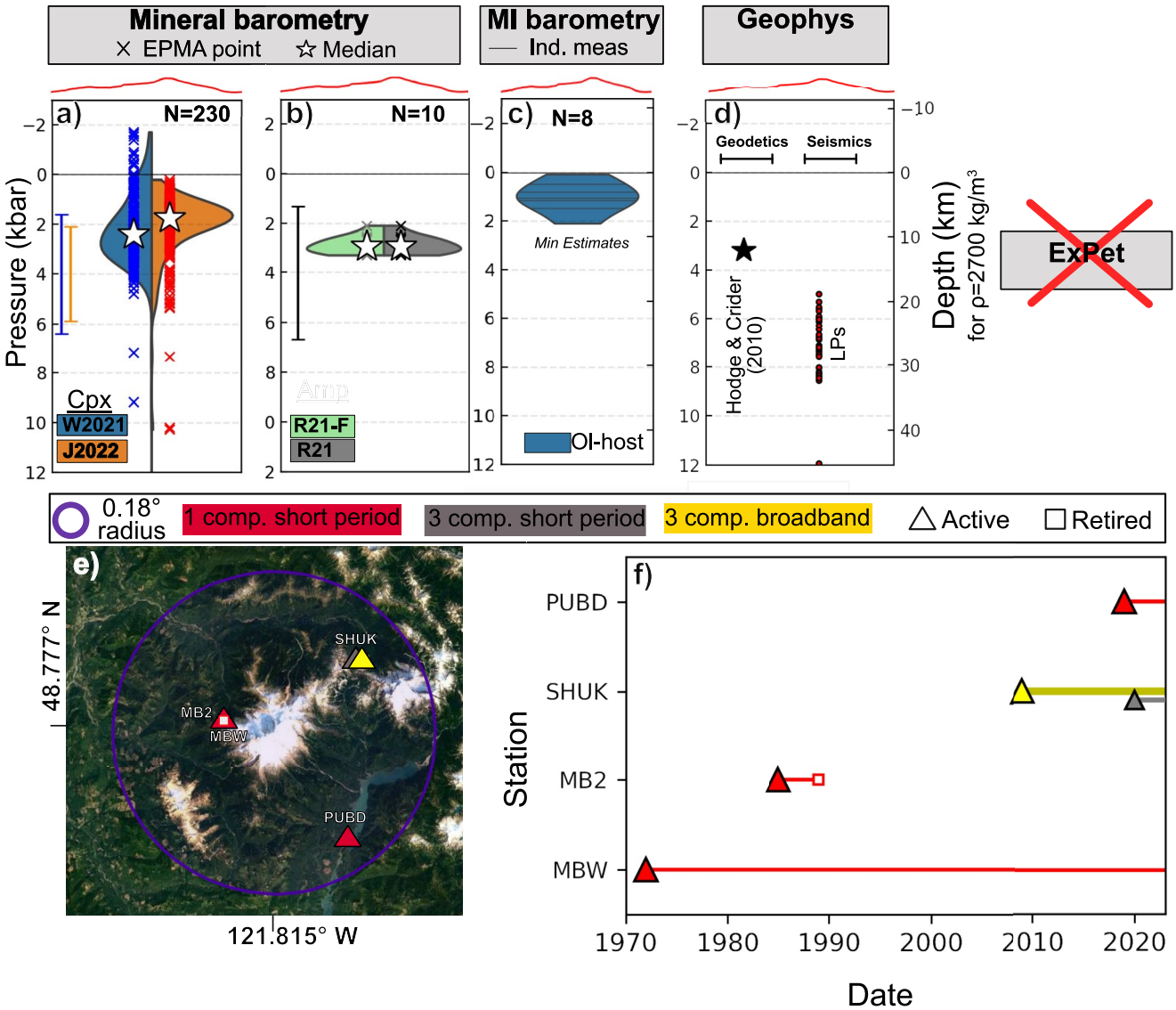

Figure 14. Compilation of magma storage depths at Mount Baker (a–d) and summary of the seismic network (e–f). The red line shows the height above sea level across an approximately W-E section spanning 12.5 km transecting the summit.

23. Mount Baker

Mount Baker is a stratocone situated within a larger multi-vent volcanic field that has been active since 1.3 Ma. It is one of the youngest volcanoes in the Cascades, with most of the modern edifice built over the last 40 ka (Hildreth et al., 2003). The larger volcanic field is predominantly andesitic and rhyodacitic in composition, with basalt and dacite making up only ~1%–3% of the total volume. Mt Baker itself comprises of andesites, two pyroxene dacites, with some olivine-bearing andesites (Hildreth et al., 2003).

23.1. Mineral Compositions

We obtained the following mineral analyses after filtering:

- $N = 12$ Amp and $N = 132$ Cpx reported in Gross (2012) from three mid Pleistocene dacitic lava flows Nooksack Falls (~149 ka), Cougar Divide (~613 ka) and Mazama Lake of uncertain age (Hildreth et al., 2003).
- Cpx from the more primitive basalts and Mg-rich andesites erupted at Mount Baker, with $N = 17$ Cpx from Baggerman and DeBari (2011), $N = 32$ Cpx from Sas et al. (2017), $N = 28$ Cpx from Mullen and McCallum (2014), and $N = 21$ Cpx from N. E. Moore and DeBari (2012).

The median Cpx-only pressure is 2.4 kbar for W2021 and 1.8 kbar for J2022. There is significant overlap between Cpx from dacitic and more mafic samples, with no consistent differences emerging for both W2021 and J2022 (Figure S6 in Supporting Information S1). The $N = 12$ Amp from the dacites examined by Gross (2012) yield a pressure of ∼2.9 kbar (between the median Cpx pressures of 1.7 and 2.9 kbar from J2022 and W2021 for these dacites).

23.2. Melt Inclusions

Shaw (2011) measured eight olivine-hosted MIs from Mount Baker (reported by Venugopal et al., 2020), with the same caveats regarding CO_2 as described for Glacier Peak. These MIs return pressures between 0 and 2 kbar, which represent minimum estimates as bubble CO_2 was not directly measured.

23.3. Experimental Phase Equilibrium

We are not aware of any phase equilibrium experiments relevant to Mount Baker.

23.4. Geophysics

Seismically, Mount Baker is relatively quiescent, with most shallow (<3 km) events thought to reflect activity of the glacier. We find one abstract describing a local seismic survey conducted at Mount Baker but no clear link to magma storage is made (Rohay & Malone, 1977). The lack of seismic data is unsurprising given the sparse coverage of the seismic network. At the time of writing, there is only a single three component broadband seismometer within 20 km. Nichols et al. (2011) report 31 LPs earthquakes from Mount Baker, more than any other Cascade volcano.

Mount Baker experienced a period of thermal unrest in 1975, investigated retrospectively by Crider et al. (2011). In 1975, a large area of snow-free ground was created in the crater, with high magmatic gas emissions, and an accompanying increase in gravity in the 30 years following this period. While there is some debate about whether this episode can be magmatic given the lack of seismicity, Crider et al. (2011) noted the presence of recent aseismic intrusions at other arc volcanoes worldwide (e.g., Z. Lu et al., 2000), indicating that an absence of seismicity doesn't necessarily mean an intrusion didn't happen. Unfortunately, there was insufficient monitoring data to place detailed constraints on this episode beyond the speculation that it was likely caused by intrusion into the mid crust.

Hodge and Crider (2010) investigated edifice deflation between 1981 and 2007 recorded by continuous GPS and EDM at Mount Baker. This deflation is best recreated by a source at ∼5.8 km depth (basl, ∼2,000 m), located 1.5 km to the E-NE of the summit. This aligns reasonably well with Cpx-only and Amp-only pressures. Poland et al. (2017) describe challenges relating to InSAR at Mount Baker as a result of poor coherent on the edifice because of ice and snow, and vegetation on the lower flanks, meaning data is only possible to collect over a narrow window in late summer on the mid flanks.

23.5. Summary and Future Work

The paucity of data for this very high threat volcano is a concern. Mount Baker is an obvious target for MI work given the presence of tephra layers. Experimental phase equilibrium would also help to place constrains on storage conditions. Without a concerted geophysical campaign, it is unlikely that meaningful magma storage information will be gleaned from the current seismic network without significant densification.

24. Canadian Garibaldi Volcanic Belt

The Garibaldi Volcanic Belt consists of 2,300 distinct vents, and 22 major edifices, including Glacier Peak and Mount Baker (Hildreth, 2007). Here, we focus our discussion of the available data for the Canadian segment of this volcanic belt, given differences in volcano monitoring on either side of the border. The major Canadian edifices and volcanic fields include Mount Garibaldi, Garibaldi Lake, Mount Meager, Salal Glacier, and Bridge River. A wide variety of compositions are present in this Canadian segment, with dacites and rhyodacites at Mount Garibaldi and Mount Cayley, and high Si rhyolites at Mount Garibaldi (Hildreth, 2007). These volcanoes also erupt olivine-bearing basalts and basaltic-andesites (Venugopal et al., 2020).

24.1. Mineral Compositions

We obtain $N = 15$ Cpx compositions from basaltic andesite samples from the Garibaldi Lake Volcanic Field (Fillmore, 2014). We were unable to find any other mineral data. W2021 yields median pressures of 0.19 kbar, and 1.8 kbar for J2022.

24.2. Experimental Phase Equilibrium

We are not aware of any experimental phase constraints on magma storage conditions in the Garibaldi Volcanic Belt.

24.3. Melt Inclusions

As mentioned in the introduction, Venugopal et al. (2020) performed glass and vapor bubble measurements, but do not use an instrument specific Raman calibration. Given that their high CO_2 densities are thermodynamically impossible at room temperature, it seems likely the amount of CO_2 in the vapor bubble was overestimated. We show their vapor-bubble reconstructed CO_2 alongside glass-only saturation pressures for completeness. Re-analysis of a subset of bubbles could be used to correct the original Raman data (as different Raman calibrations are reasonably parallel to one another, Lamadrid et al., 2017).

24.4. Geophysics

There are no geodetic constraints on magma storage in the Garibaldi Volcanic belt. No-ground based geodetic studies have been performed, and while C-band InSAR obtains some coherent images on the volcanoes flank, InSAR is generally hindered by vegetated slopes and ice-covered summits (Poland et al., 2017). We do not find any direct seismic constraints on magma storage beneath these volcanoes. Querying the IRIS database from 1975 to 2023 for the Canadian networks yields 4 seismometer stations in the general vicinity of the Garibaldi Volcanic Belt. The broader distribution of vents and less well defined summits relative to the US Cascades makes it harder to define clear query criteria. Instead, we show volcanic regions on Figure 15. There is a 3bb station close to Whistler (WSLR, 2013-present), and a second 3bb station is present near Squamish (WPB), ~27 km south of Mount Garibaldi (1bb 1996–2018, 3bb 2018-present). There was a 3bb station ~8 km W of Mount Meager and 10–15 km SW of Salal Glacier between 2016 and 2019, and a 3bb station about ~20 km ESE along the same river valley from 1993 to 1998, although it appears there are currently no stations in this area. L. Lu and Bostock (2022) use the record from these four stations to identify 48 deep long period earthquakes (DLPs) at ~4–45 km depth in the region near Mount Meager.

24.5. Summary and Future Work

The paucity of work on the Garibaldi Volcanic Belt likely reflects its relative inaccessibility, snow and ice cover, and the lower hazard compared to the more active, US-based volcanoes.

25. Arc-Scale Trends

25.1. Data Availability

Our compilation shows the presence of many concerning data gaps affecting our knowledge of magma storage depths along the Cascade Arc. The quantity of data available along the arc is highly variable, and is also poorly correlated with the USGS threat index for individual volcanoes (Figure 1; Ewert et al., 2018). Some systems are relatively well covered, but many high threat volcanoes show a disturbing paucity of geochemical and geophysical constraints on the nature of crustal magma storage. For example, at Mount Rainier, the second highest threat volcano in the Cascades and third highest threat volcano in the US we have no magma storage depth constraints from MIs, very few reported Amp and Cpx compositions, one experimental pressure constraint, and only two seismic constraints. Recent deployment of 13 broad band seismometers (Figure 12f) provides potential for better seismological imaging in future (e.g., receiver functions, P and S wave topography). Mount Hood (sixth highest threat in US) and Three Sisters (seventh highest threat in US) are also very understudied. Available MIs from Mount Hood are limited and potentially unreliable due to SIMS calibration issues, and there are no detailed geophysical or experimental constraints on magma storage depths. Similarly, the Three Sisters have no usable MI data, no seismic studies, and no experimental studies placing precise constraints on magma storage reservoir depths. The only real depth constraints at Three Sisters come from a geodetic inversion of the 1998 inflation episode. However, it has been suggested based on spring chemistry and the lack of surface volcanism <10 ka

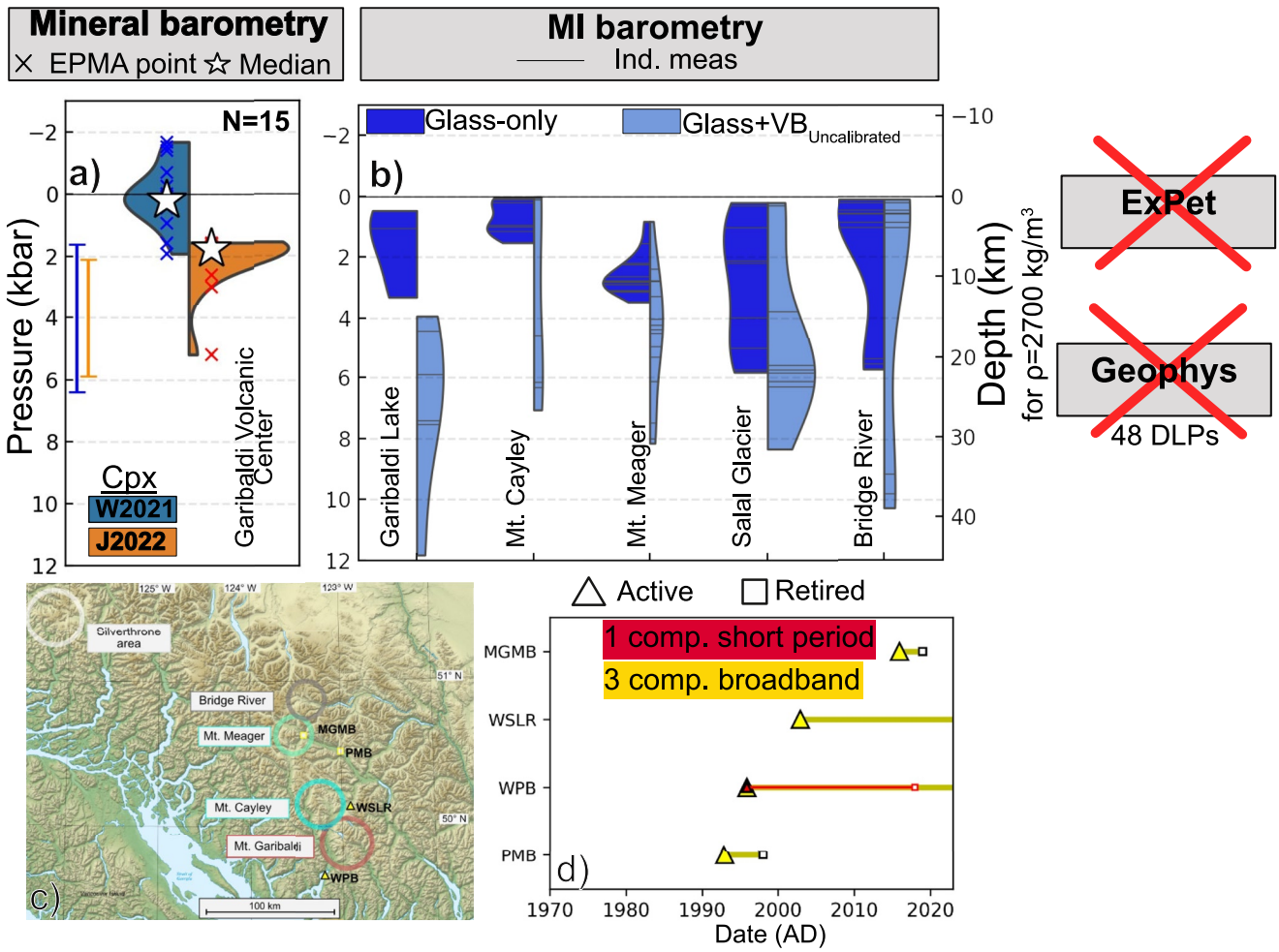

Figure 15. Compilation of magma storage depths for the Canadian Garibaldi Volcanic Belt (a, b) and summary of the seismic network (c, d). Circles in (c) show the approximate location of volcanic fields. Map in (c) adapted from Sémhur (2007).

that numerous intrusions likely occur in the deforming area with a very low probability of eruption (W. C. Evans et al., 2004). Thus, it is unclear if these geodetic estimates are providing useful information on the storage depths of melts beneath the main edifices. In addition, Mount Baker and Glacier Peak, which are both ranked as very high threat (#14 and #15 highest threat in US) have also been greatly understudied from both a petrological and geophysical perspective.

25.2. Probable Trends

With the caveat of the relatively sparse and variable data coverage, we compile the available geophysical (Figure 16a) and mineral (Figure 16b) constraints on magma storage depth as a function of latitude to investigate along-arc trends in magma storage.

From a geophysical perspective, the vast majority of constraints on proximal magma chambers (rather than regional anomalies) are clustered at depths corresponding to ~1–5 kbar, with only magnetotelluric anomalies, LP earthquakes and regional seismic surveys returning higher pressures.

Considering the high imprecision of mineral-only barometers, Cpx-only pressures from J2022 and Amp-only pressures from R2021 are remarkably constant along the arc, although the Amp-only pressures show slightly more scatter. In general, the median pressures from these mineral-only barometers suggest that the vast majority of magma storage occurs in the upper 4 kbar (~0–15 km) of the crust. The general agreement within the ±2–3 kbar uncertainty of Amp and Cpx-based barometers gives us confidence in this result, along with the fact

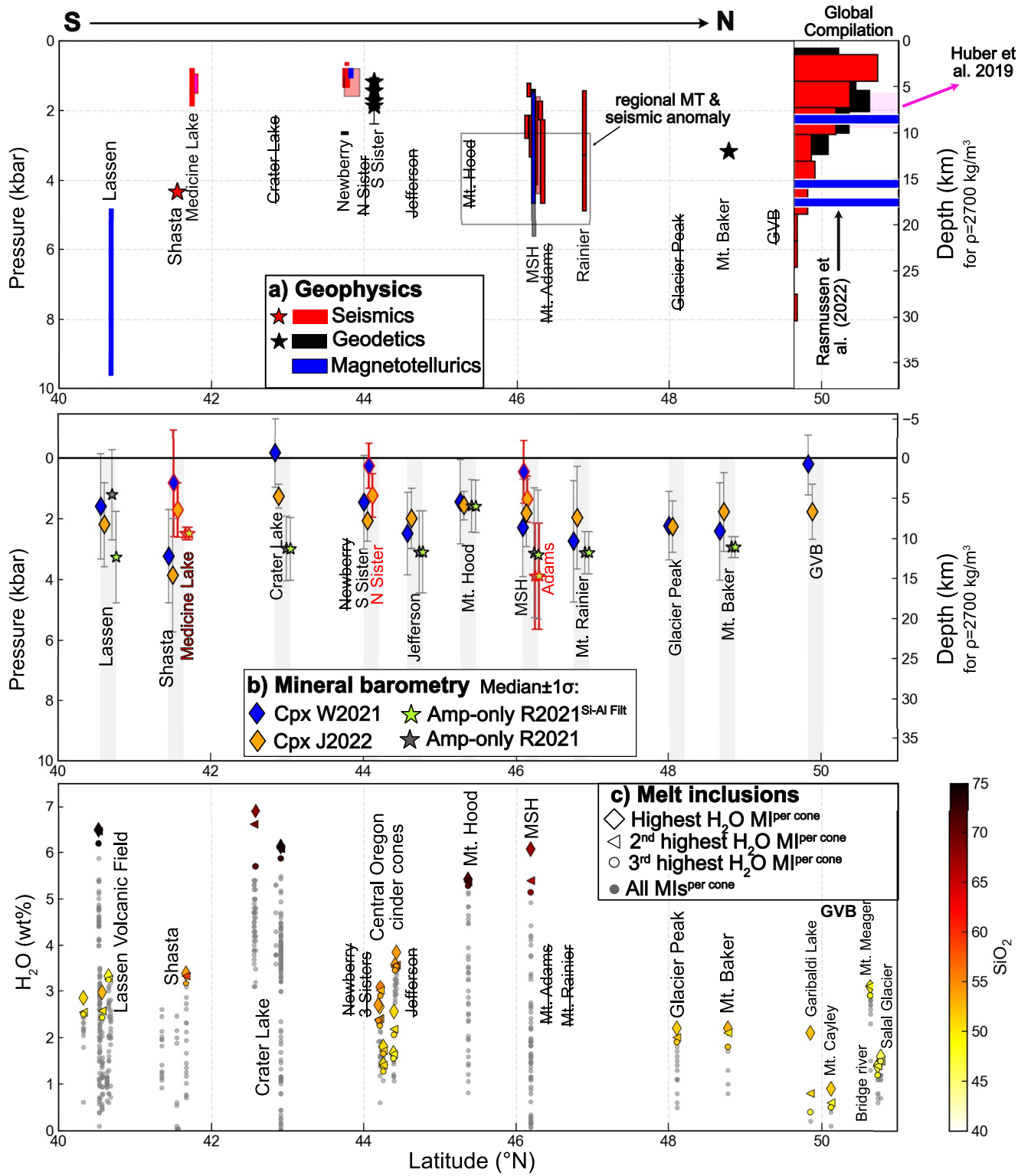

Figure 16. Summary of magma storage depths along the cascades, with the *x* axis showing approximate latitude (Medicine Lake and Mount Adams are shifted slightly from true latitude to avoid overlap with Shasta and MSH respectively). (a) Compilation of geophysics for each center. The histogram shows a global compilation from Rasmussen et al. (2022) using the same color scheme as for the Cascades, and the 2 ± 0.5 kbar from the compilation of Huber et al. (2019). (b) Compilation of mineral barometry. Symbols show the median pressure, and errorbars show the standard deviation of calculated pressures for each volcano. Red outlines on symbols are used for Medicine Lake and MSH because of overlaps in latitude with Shasta and Mount Adams. (c) H_2O contents from melt inclusions (MIs), with the three most H_2O-rich MIs from each volcano/cinder cone colored based on the MI SiO_2 content. Tephra samples collected at different locations but from the same source (e.g., the S17 cone, Mount Shasta) are grouped as one when choosing these three MI. Volcanoes with no reliable constraints are shown with crossed out text.

that geodetic and seismic constraints on magma storage generally have depths equivalent to ~0–5 kbar. With the limitations of the reported information, it is difficult to interpret whether the spread of individual calculated pressures for a given volcanic center represents true transcrustal storage or analytical uncertainty (Wieser et al., 2023b).

The general confinement of magma storage estimates at pressures less than 4 kbar has been noted in a recent global compilation of geophysical estimates of magma storage depths in volcanic arcs, cyan histogram (Figure 16b). Rasmussen et al. (2022) describe a correlation between water contents in MIs from arcs and geophysically determined magma storage depths, with the relationship between depth and H_2O plotting along the water-saturation curve. They propose two possible explanations: (a) H_2O controls magma storage depth through an increase in viscosity accompanying water exsolution (which they refer to as a "mantle control") or (b) H_2O is diffusively reset at a depth determined by a "crustal control." The authors infer that a crustal control would cause correlations between ratios such as Nb/Ce and Ba/La to be lost, while a mantle control would preserve these relationships. Based on the preservation of strong H_2O-incompatible element ratios in the Aleutians, Rasmussen et al. (2022) favor a mantle control, with primary magmatic water contents controlling magma storage depths.

To investigate the hypothesis of Rasmussen et al. (2022), we consider trends in H_2O with latitude along the Cascades, selecting the three most H_2O-rich MIs from each volcanic center (colored diamonds, triangles and circles, Figure 16c) as representative of the H_2O contents most resistant to degassing and diffusive re-equilibration. The relationship of Rasmussen et al. (2022) only applies to mafic magmas, so we color-code the most H_2O-rich MIs by SiO_2 content (Figure 16c). Unlike compiled magma storage depths, H_2O contents in the most mafic samples (yellow and orange colors) show considerable variation along strike.

When considering all MI compositions, a strong positive correlation is present between SiO_2 and H_2O contents (Figure S3 in Supporting Information S1). If a H_2O-saturated mafic magma stalls in the crust and differentiates (as in the model of Rasmussen et al., 2022), the H_2O content in the melt would track the change in volatile solubility from basalt to rhyolite. However, different solubility models show vastly different trends in H_2O solubility over this differentiation interval (see Wieser et al., 2022a; Figure 10), with none predicting an increase as large as that observed here (Figure S10 in Supporting Information S1). Instead, this relationship between SiO_2 and H_2O is more indicative of differentiation in the presence of an exsolved fluid which is relatively CO_2-rich, meaning that CO_2 initially dominates the vapor phase, so H_2O behaves relatively incompatibly during fractional crystallization (Wieser et al., 2022a). This is supported by calculated X_{H_2O} values for Cascade mafic MIs (Figure S11 in Supporting Information S1), which indicate that the exsolved fluid is dominated by CO_2, particularly for MIs where the vapor bubble is accounted for. This is not consistent with the model inferred by Rasmussen et al. (2022), which assumes the volatile system is dominated by a H_2O-rich vapor phase at the point of magma stalling.

Thus, we suggest based on our compilation that it is more likely that a crustal process operating along the entire arc (whether due to a rheological boundary, or density-controlled) is restricting storage of all but the most mafic magmas to the upper 0–5 kbar of the crust (Chaussard & Amelung, 2014; Huber et al., 2019). Our compilation does show hints of deeper crustal magma storage, likely of more mafic magmas. However, due to the very nature of magma differentiation itself, crystals from the mafic predecessors to the more evolved erupted liquids are poorly preserved, meaning deeper magma storage is easily obscured. This preservation bias is particularly hard to see through given the small number of published mineral compositions at many Cascade volcanoes (e.g., $N = 18$ Cpx from Glacier Peak, $N = 16$ Amp from Mount Rainier, $N = 17$ Cpx from Three Sisters). If we imagine that 1% of deeper formed crystals are erupted, we would need thousands of analyses to get a cluster of deeper pressures that we would be able to interpret with confidence, rather than appearing as outliers. Petrologic experiments on predecessor mafic magmas erupted at the periphery of Mount Shasta and Mount Rainer do support a period of mid- to lower-crustal storage that results in crystallization (e.g., Krawczynski et al., 2012) and/or crustal melting (e.g., Blatter et al., 2013, 2017), which is likely important to evolve mantle-derived magmas to the intermediate and silicic compositions characteristic of those stored in the upper crust. Future MI work measuring both the melt and vapor bubble, petrologic experiments, and substantially more mineral analyses are thus required to further investigate the prevalence of deeper storage of mafic melts in the Cascades arc relative to the ubiquitous upper crustal reservoirs recorded by the compiled geophysical studies and available mineral data.

26. Conclusions

A detailed review of available petrological, geochemical and geophysical constraints on the depth of magma storage beneath Cascade arc volcanoes suggest that the majority of magma storage is restricted to the upper 0–5 kbar (0–20 km) of the crust, and at reasonably constant depth along strike. However, further consideration of magma storage at higher resolution, and evaluation of latitudinal variations is not possible because of the large uncertainties on petrological techniques used for estimating storage pressure, and by numerous data gaps that exist along the arc. Considering the number of high-threat volcanoes in the Cascades, the paucity of data to constrain magma storage from geochemical and geophysical perspectives is highly concerning, and a stark contrast to other high-threat volcanoes in the US (e.g., Kilauea, Poland et al., 2014).

Gaps in geophysical data sets result from: (a) difficult access because of terrain, snow and ice cover, (b) the fact many Cascade volcanoes have been relatively quiescent in the last few decades, (c) dense geophysical imaging campaigns are costly and uncommon, and (d) permitting issues in wilderness areas hindering the establishment of dense monitoring networks (Moran & Benjamin, 2021; Poland et al., 2017). Gaps in geochemical and petrological data sets reflect a lack of study of many important systems, specific technique limitations (e.g., neglecting CO_2 vapor bubbles, poor quality EPMA analyses of mineral compositions, Wieser et al., 2023c), and poor data reporting (e.g., publishing only representative mineral analyses). We therefore recommend targeted MI, petrologic, experimental and further geophysical studies of the understudied high threat volcanoes in the Cascades arc to determine their depths of magma storage, which are critical for interpreting future monitoring signals and will influence the style, size, and frequency of future eruptions.

Acknowledgments
The authors acknowledge support from a National Science Foundation Grants 1948862 and 1850779 (to AJRK), 1949173 (to CBT), and 1948834 (to GAA). We also acknowledge support from the National Science Foundation ICER-20-26904 granted to OFM Research (PI. Ghiorso) for maintaining the ENKI server used to perform saturation pressure calculations using VESIcal. This study relies heavily on data provided by corresponding authors, many of whom went to considerable effort to track down decade-old data. We thank Martin Streck for help extracting mineral compositions from his online textural tool, Judy Fierstein for sharing a large quantity of mineral data from Mount Adams, Nicole Moore for sharing mineral data from Mt Baker, Allison Koleszar for sharing amphibole data from Mt Hood, Warner Cribb for sharing pdf tables of mineral data from his thesis on Mount Hood, Heather Wright for sharing mineral data from Crater Lake, Thomas Sisson for sharing data from Rainier, Kristina Walowski and Melissa Scruggs for help reconstructing their Cpx-Liq data sets, Michael Clynne and Bryan Platt for sharing large amounts of data from Brokeoff Volcano, and Tim Druitt and Charlie Bacon for posting large quantities of handwritten EPMA data from Crater Lake. We thank Ellen Aster for help interpreting her vapor bubble data from Lassen. We thank Matthew Gleeson for sending many journal pdfs, which were behind paywalls. We thank Nick Barber for his VMSG QGIS course, which we used to help extract topographic profiles of the Cascades. We are extremely grateful to Julie Donnelly-Nolan, Mellisa Scruggs, and Paul Segall for exceptionally thorough reviews that helped us track down some missing studies, and greatly improved the flow of the draft, and Paul Asimow for editorial handling. Throughout this paper, the post-colonial names are used for Cascade volcanic centres. We acknowledge that Indigenous cultures of the region have names for these volcanoes, and we hope that 1 day the official names of these volcanoes reflect this history.

Data Availability Statement

A compiled data set of mineral compositions, melt inclusions and seismic stations, along with the Jupyter Notebooks used to compile, filter and plot data are available on Penny Wieser's GitHub (https://github.com/PennyWieser/Cascade_data_Compilation/tree/main) and archived on Zenodo at https://doi.org/10.5281/zenodo.8327597 (PennyWieser, 2023).

References

Abers, G. A., & Hacker, B. R. (2016). A MATLAB toolbox and Excel workbook for calculating the densities, seismic wave speeds, and major element composition of minerals and rocks at pressure and temperature. *Geochemistry, Geophysics, Geosystems*, *17*(2), 616–624. https://doi.org/10.1002/2015GC006171

Achauer, U., Evans, J. R., & Stauber, D. A. (1988). High-resolution seismic tomography of compressional wave velocity structure at Newberry Volcano, Oregon Cascade Range. *Journal of Geophysical Research*, *93*(B9), 10135–10147. https://doi.org/10.1029/JB093iB09p10135

Anderson, A. T. (1974). Evidence for a Picritic, volatile-rich magma beneath Mt. Shasta, California. *Journal of Petrology*, *15*(2), 243–267. https://doi.org/10.1093/petrology/15.2.243

Anderson, K., & Segall, P. (2013). Bayesian inversion of data from effusive volcanic eruptions using physics-based models: Application to Mount St. Helens 2004–2008. *Journal of Geophysical Research: Solid Earth*, *118*(5), 2017–2037. https://doi.org/10.1002/jgrb.50169

Applegarth, L. J., Tuffen, H., James, M. R., Pinkerton, H., & Cashman, K. V. (2013). Direct observations of degassing-induced crystallization in basalts. *Geology*, *41*(2), 243–246. https://doi.org/10.1130/G33641.1

Aster, E. M., Wallace, P. J., Moore, L. R., Watkins, J., Gazel, E., & Bodnar, R. J. (2016). Reconstructing CO_2 concentrations in basaltic melt inclusions using Raman analysis of vapor bubbles. *Journal of Volcanology and Geothermal Research*, *323*, 148–162. https://doi.org/10.1016/j.jvolgeores.2016.04.028

Bacon, C. R., & Lanphere, M. A. (2006). Eruptive history and geochronology of Mount Mazama and the crater Lake region, Oregon. *Geological Society of America Bulletin*, *118*(11–12), 1331–1359. https://doi.org/10.1130/B25906.1

Bacon, C. R., Newman, S., & Stolper, E. (1992). Water, CO_2, Cl, and F in melt inclusions in phenocrysts from three Holocene explosive eruptions, Crater Lake, Oregon. *American Mineralogist*, *77*, 1021–1030.

Baggerman, T. D., & DeBari, S. M. (2011). The generation of a diverse suite of Late Pleistocene and Holocene basalt through dacite lavas from the northern Cascade arc at Mount Baker, Washington. *Contributions to Mineralogy and Petrology*, *161*(1), 75–99. https://doi.org/10.1007/s00410-010-0522-2

Baker, M. B., Grove, T. L., & Price, R. (1994). Primitive basalts and andesites from the Mt. Shasta region, N. California: Products of varying melt fraction and water content. *Contributions to Mineralogy and Petrology*, *118*(2), 111–129. https://doi.org/10.1007/BF01052863

Barker, S. E., & Malone, S. D. (1991). Magmatic system geometry at Mount St. Helens modeled from the stress field associated with posteruptive earthquakes. *Journal of Geophysical Research*, *96*(B7), 11883–11894. https://doi.org/10.1029/91JB00430

Barr, J., Grove, T. L., & Elkins-Tanton, L. (2007). High-magnesian andesite from Mount Shasta: A product of magma mixing and contamination, not a primitive melt: Comment and reply: Comment. *Geology*, *35*(1), e147. https://doi.org/10.1130/g24058c.1

Bartels, K. S., Kinzler, R. J., & Grove, T. L. (1991). High pressure phase relations of primitive high-alumina basalts from Medicine Lake volcano, northern California. *Contributions to Mineralogy and Petrology*, *108*(3), 253–270. https://doi.org/10.1007/BF00285935

Beachly, M. W., Hooft, E. E. E., Toomey, D. R., & Waite, G. P. (2012). Upper crustal structure of Newberry Volcano from P-wave tomography and finite difference waveform modeling: Newberry Finite Difference Modeling. *Journal of Geophysical Research*, *117*(B10), B10311. https://doi.org/10.1029/2012JB009458

Bedrosian, P. A., Peacock, J. R., Bowles-Martinez, E., Schultz, A., & Hill, G. J. (2018). Crustal inheritance and a top-down control on arc magmatism at Mount St. Helens. *Nature Geoscience*, *11*, 865–870. https://doi.org/10.1038/s41561-018-0217-2

Benz, H. M., Zandt, G., & Oppenheimer, D. H. (1992). Lithospheric structure of northern California from teleseismic images of the upper mantle. *Journal of Geophysical Research*, *97*(B4), 4791–4807. https://doi.org/10.1029/92JB00067

Blatter, D. L., Sisson, T. W., & Hankins, W. B. (2013). Crystallization of oxidized, moderately hydrous arc basalt at mid- to lower-crustal pressures: Implications for andesite genesis. *Contributions to Mineralogy and Petrology*, *166*(3), 861–886. https://doi.org/10.1007/s00410-013-0920-3

Blatter, D. L., Sisson, T. W., & Hankins, W. B. (2017). Voluminous arc dacites as amphibole reaction-boundary liquids. *Contributions to Mineralogy and Petrology*, *172*(5), 27. https://doi.org/10.1007/s00410-017-1340-6

Blundy, J. (2022). Chemical differentiation by mineralogical buffering in crustal hot zones. *Journal of Petrology*, *63*(7), egac054. https://doi.org/10.1093/petrology/egac054

Blundy, J., & Cashman, K. (2005). Rapid decompression-driven crystallization recorded by melt inclusions from Mount St. Helens volcano. *Geology*, *33*(10), 793. https://doi.org/10.1130/G21668.1

Blundy, J., Cashman, K. V., Rust, A., & Witham, F. (2010). A case for CO_2-rich arc magmas. *Earth and Planetary Science Letters*, *290*(3–4), 289–301. https://doi.org/10.1016/j.epsl.2009.12.013

Bonner, R. (2015). *A magnetotelluric investiagation of shallow conductivity sources beneath the Cascadia Volcanic Arc* (Honors Thesis). Oregon State University.

Bowles-Martinez, E., & Schultz, A. (2020). Composition of magma and characteristics of the hydrothermal system of Newberry Volcano, Oregon, from magnetotellurics. *Geochemistry, Geophysics, Geosystems*, *21*(3), e2019GC008831. https://doi.org/10.1029/2019GC008831

Bullen, T. D., & Clynne, M. A. (1990). Trace element and isotopic constraints on magmatic evolution at Lassen Volcanic Center. *Journal of Geophysical Research*, *95*(B12), 19671–19691. https://doi.org/10.1029/JB095iB12p19671

Cashman, K. V., Sparks, R. S. J., & Blundy, J. D. (2017). Vertically extensive and unstable magmatic systems: A unified view of igneous processes. *Science*, *355*(6331), eaag3055. https://doi.org/10.1126/science.aag3055

Chaussard, E., & Amelung, F. (2014). Regional controls on magma ascent and storage in volcanic arcs. *Geochemistry, Geophysics, Geosystems*, *15*(4), 1407–1418. https://doi.org/10.1002/2013GC005216

Chiarabba, C., Amato, A., & Evans, J. (1995). Variations on the NeHT high-resolution tomography method: A test of technique and results for Medicine Lake volcano, northern California. *Journal of Geophysical Research B3*, *100*, 4035–4052. https://doi.org/10.1029/94jb02771

Christiansen, R. L., Calvert, A., & Champion, D. (2013). Voluminous tholeiitic basalts near Mount Shasta, California, as regional strain markers. In *Presented at the AGU fall meeting abstracts*(p. V11D-03).

Christiansen, R. L., Calvert, A. T., Champion, D. E., Gardner, C. A., Fierstein, J. E., & Vazquez, J. A. (2020). The remarkable volcanism of Shastina, a stratocone segment of Mount Shasta, California. *Geosphere*, *16*(5), 1153–1178. https://doi.org/10.1130/GES02080.1

Christiansen, R. L., Calvert, A. T., & Grove, T. L. (2017). Geologic field-trip guide to Mount Shasta Volcano, Northern California.

Clynne, M. A. (1999). A complex magma mixing origin for rocks erupted in 1915, Lassen peak, California. *Journal of Petrology*, *40*(1), 105–132. https://doi.org/10.1093/petroj/40.1.105

Clynne, M. A., Christiansen, R. L., Trimble, D. A., & McGeehin, J. P. (2008). Radiocarbon dates from volcanic deposits of the Chaos Crags and cinder cone eruptive sequences and other deposits, Lassen volcanic National park and vicinity, California. In *U.S. Geological survey open-file report 02-290*.

Clynne, M. A., & Muffler, L. (2010). *Geologic map of Lassen Volcanic National Park and vicinity, California*. U.S. Geological Survey Scientific Investigations Map 2899.

Conrey, R. (1991). *Geology and petrology of the Mt. Jefferson area, high cascade range, Oregon* (PhD thesis). Washington State University.

Cooper, K. M., & Reid, M. R. (2003). Re-examination of crystal ages in recent Mount St. Helens lavas: Implications for magma reservoir processes. *Earth and Planetary Science Letters*, *213*(1–2), 149–167. https://doi.org/10.1016/S0012-821X(03)00262-0

Couperthwaite, F. K., Wieser, P. E., Kent, A. J. R., Ruth, D. C. S., Gazel, E., & DeVitre, C. L. (2022). Combining Fe-Mg diffusion in olivine and volatile concentrations from olivine-hosted melt inclusions to constrain eruption timescales and magma storage depths beneath Paint Pot Crater, Medicine Lake. In *Presented at the Chapman Conference on distributed volcanism*.

Cribb, J. W. (1997). *A petrologic and geochemical investigation of the evolutionary history of calc-alkaline magmas, Mount Hood, Oregon* (PhD thesis) Ohio State University.

Crider, J. G., Frank, D., Malone, S. D., Poland, M. P., Werner, C., & Caplan-Auerbach, J. (2011). Magma at depth: A retrospective analysis of the 1975 unrest at Mount Baker, Washington, USA. *Bulletin of Volcanology*, *73*(2), 175–189. https://doi.org/10.1007/s00445-010-0441-0

Crosbie, K. J., Abers, G. A., Mann, M. E., Janiszewski, H. A., Creager, K. C., Ulberg, C. W., & Moran, S. C. (2019). Shear velocity structure from ambient noise and teleseismic surface wave tomography in the cascades around Mount St. Helens. *Journal of Geophysical Research: Solid Earth*, *124*(8), 8358–8375. https://doi.org/10.1029/2019JB017836

Danyushevsky, L. V., & Plechov, P. (2011). Petrolog3: Integrated software for modeling crystallization processes. *Geochemistry, Geophysics, Geosystems*, *12*(7), Q07021. https://doi.org/10.1029/2011GC003516

Darr, C. (2006). *Magma chamber processes over the past 475,000 years at Mount Hood, Oregon: Insights from crystal zoning and crystal size distribution studies* (Masters thesis). Oregon State University.

Das, T., & Nolet, G. (1998). Crustal thickness map of the western United States by partitioned waveform inversion. *Journal of Geophysical Research*, *103*(B12), 30021–30038. https://doi.org/10.1029/98JB01119

DeVitre, C. L., Allison, C. M., & Gazel, E. (2021). A high-precision CO_2 densimeter for Raman spectroscopy using a Fluid Density Calibration Apparatus. *Chemical Geology*, *584*, 120522. https://doi.org/10.1016/j.chemgeo.2021.120522

DeVitre, C. L., Dayton, K., Gazel, E., Pamukçu, A., Gaetani, G., & Wieser, P. E. (2023). Laser heating effect on Raman analysis of CO_2 co-existing as liquid and vapor in olivine-hosted melt inclusion bubbles. *Volcanica*, *6*(2), 201–219. https://doi.org/10.30909/vol.06.02.201219

DiGuilio, J. (2015). *Reconstructing the physical record of a four-million-year volcanic system: Geochemistry, thermobarometry, and geologic map of the Mount Jefferson area*. Oregon. Oregon State University Masters Thesis.

Dixon, J. E. (1997). Degassing of alkalic basalts. *American Mineralogist*, *82*(3–4), 368–378. https://doi.org/10.2138/am-1997-3-415

Donnelly-Nolan, J. M. (2008). Chemical analyses of pre-Holocene rocks from Medicine Lake Volcano and vicinity, Northern California. In *U.S. Geological Survey Open-file Report 2008-1094*.

Donnelly-Nolan, J. M., Grove, T. L., Lanphere, M. A., Champion, D. E., & Ramsey, D. W. (2008). Eruptive history and tectonic setting of Medicine Lake Volcano, a large rear-arc volcano in the southern Cascades. *Journal of Volcanology and Geothermal Research*, *177*(2), 313–328. https://doi.org/10.1016/j.jvolgeores.2008.04.023

Donnelly-Nolan, J. M., Stovall, W. K., Ramsey, D. W., Ewert, J., & Jensen, R. (2011). Newberry Volcano—Central Oregon's sleeping giant. USGS Fact Sheet 2011-3145.

Druitt, T. H., & Bacon, C. R. (1989). Petrology of the zoned calcalkaline magma chamber of Mount Mazama, Crater Lake, Oregon. *Contributions to Mineralogy and Petrology*, *101*(2), 245–259. https://doi.org/10.1007/BF00375310

Ducea, M. N., Saleeby, J. B., & Bergantz, G. (2015). The Architecture, chemistry, and evolution of continental magmatic arcs. *Annual Review of Earth and Planetary Sciences*, *43*(1), 299–331. https://doi.org/10.1146/annurev-earth-060614-105049

Dufek, J., Cashman, K., Hooft, E., & Bedrosian, P. (2022). The nature of active magma reservoirs and storage underneath cascade volcanoes. *Elements*, *18*(4), 239–245. https://doi.org/10.2138/gselements.18.4.239

Dzurisin, D. (1999). Results of repeated leveling surveys at Newberry Volcano, Oregon, and near Lassen peak volcano, California. *Bulletin of Volcanology*, *61*(1–2), 83–91. https://doi.org/10.1007/s004450050264

Dzurisin, D., Donnelly-Nolan, J. M., Evans, J. R., & Walter, S. R. (1991). Crustal subsidence, seismicity, and structure near Medicine Lake Volcano, California. *Journal of Geophysical Research*, *96*(B10), 16319–16333. https://doi.org/10.1029/91JB01452

Dzurisin, D., Lisowski, M., & Wicks, C. W. (2009). Continuing inflation at Three Sisters volcanic center, central Oregon Cascade Range, USA, from GPS, leveling, and InSAR observations. *Bulletin of Volcanology*, *71*(10), 1091–1110. https://doi.org/10.1007/s00445-009-0296-4

Dzurisin, D., Lisowski, M., Wicks, C. W., Poland, M. P., & Endo, E. T. (2006). Geodetic observations and modeling of magmatic inflation at the Three Sisters volcanic center, central Oregon Cascade Range, USA. *Journal of Volcanology and Geothermal Research*, *150*(1–3), 35–54. https://doi.org/10.1016/j.jvolgeores.2005.07.011

Dzurisin, D., Poland, M. P., & Bürgmann, R. (2002). Steady subsidence of Medicine Lake volcano, northern California, revealed by repeated leveling surveys. *Journal of Geophysical Research*, *107*(B12), ECV8-1–ECV8-16. https://doi.org/10.1029/2001JB000893

Evans, J. R., & Zucca, J. J. (1988). Active high-resolution seismic tomography of compressional wave velocity and attenuation structure at Medicine Lake Volcano, Northern California Cascade Range. *Journal of Geophysical Research*, *93*(B12), 15016–15036. https://doi.org/10.1029/JB093iB12p15016

Evans, W. C., van Soest, M. C., Mariner, R. H., Hurwitz, S., Ingebritsen, S. E., Wicks, C. W., & Schmidt, M. E. (2004). Magmatic intrusion west of Three Sisters, central Oregon, USA: The perspective from spring geochemistry. *Geology*, *32*(1), 69. https://doi.org/10.1130/G19974.1

Ewert, J., Diefenbach, A. K., & Ramsey, D. W. (2018). 2018 update to the U.S. Geological survey national volcanic threat assessment (Scientific investigations report 2018-5140), Scientific investigations report.

Fierstein, J., Hildreth, W., & Calvert, A. T. (2011). Eruptive history of South Sister, Oregon cascades. *Journal of Volcanology and Geothermal Research*, *207*(3–4), 145–179. https://doi.org/10.1016/j.jvolgeores.2011.06.003

Fillmore, J. A. (2014). *The origin of Adakites in the Garibaldi volcanic complex, southwestern British Columbia, Canada*. Master of Science, University of Regina.

Flinders, A. F., & Shen, Y. (2017). Seismic evidence for a possible deep crustal hot zone beneath Southwest Washington. *Scientific Reports*, *7*(1), 7400. https://doi.org/10.1038/s41598-017-07123-w

Gardner, J. E., Carey, S., Rutherford, M. J., & Sigurdsson, H. (1995). Petrologic diversity in Mount St. Helens dacites during the last 4,000 years: Implications for magma mixing. *Contributions to Mineralogy and Petrology*, *119*(2–3), 224–238. https://doi.org/10.1007/bf00307283

Gerlach, D. C., & Grove, T. L. (1982). Petrology of Medicine Lake highland volcanics: Characterization of endmembers of magma mixing. *Contributions to Mineralogy and Petrology*, *80*(2), 147–159. https://doi.org/10.1007/BF00374892

Geschwind, C.-H., & Rutherford, M. J. (1992). Cummingtonite and the evolution of the Mount St. Helens (Washington) magma system: An experimental study. *Geology*, *20*(11), 1011–1014. https://doi.org/10.1130/0091-7613(1992)020<1011:cateot>2.3.co;2

Ghiorso, M. S., & Gualda, G. A. R. (2015). An H_2O-CO_2 mixed fluid saturation model compatible with rhyolite-MELTS. *Contributions to Mineralogy and Petrology*, *169*(6), 53. https://doi.org/10.1007/s00410-015-1141-8

Gleeson, M. L. M., Gibson, S. A., & Stock, M. J. (2021). Upper mantle mush zones beneath low melt flux ocean island volcanoes: Insights from Isla Floreana, Galápagos. *Journal of Petrology*, *61*(11–12), egaa094. https://doi.org/10.1093/petrology/egaa094

Gross, J. (2012). *Felsic magmas from Mt. Baker in the northern Cascade arc: Origin and role in andesite production* (Masters thesis). Western Washington University. Retrieved from https://cedar.wwu.edu/wwuet/239/.ed

Grove, T. L., Baker, M. B., Price, R. C., Parman, S. W., Elkins-Tanton, L. T., Chatterjee, N., & Müntener, O. (2005). Magnesian andesite and dacite lavas from Mt. Shasta, northern California: Products of fractional crystallization of H_2O-rich mantle melts. *Contributions to Mineralogy and Petrology*, *148*(5), 542–565. https://doi.org/10.1007/s00410-004-0619-6

Grove, T. L., & Donnelly-Nolan, J. M. (1986). The evolution of young silicic lavas at Medicine Lake Volcano, California: Implications for the origin of compositional gaps in calc-alkaline series lavas. *Contributions to Mineralogy and Petrology*, *92*(3), 281–302. https://doi.org/10.1007/BF00572157

Grove, T. L., Donnelly-Nolan, J. M., & Housh, T. (1997). Magmatic processes that generated the rhyolite of Glass Mountain, Medicine Lake volcano, N. California. *Contributions to Mineralogy and Petrology*, *127*(3), 205–223. https://doi.org/10.1007/s004100050276

Grove, T. L., Elkins-Tanton, L. T., Parman, S. W., Chatterjee, N., Müntener, O., & Gaetani, G. A. (2003). Fractional crystallization and mantle-melting controls on calc-alkaline differentiation trends. *Contributions to Mineralogy and Petrology*, *145*(5), 515–533. https://doi.org/10.1007/s00410-003-0448-z

Grove, T. L., Gerlach, D. C., & Sando, T. W. (1982). Origin of calc-alkaline series lavas at Medicine Lake Volcano by fractionation, assimilation and mixing. *Contributions to Mineralogy and Petrology*, *80*(2), 160–182. https://doi.org/10.1007/BF00374893

Grove, T. L., Kinzler, R. J., Baker, M. B., Donnelly-Nolan, J. M., & Lesher, C. E. (1988). Assimilation of granite by basaltic magma at Burnt Lava flow, Medicine Lake volcano, northern California: Decoupling of heat and mass transfer. *Contributions to Mineralogy and Petrology*, *99*(3), 320–343. https://doi.org/10.1007/BF00375365

Grove, T. L., Parman, S., Bowring, S., Price, R., & Baker, M. (2002). The role of an H_2O-rich fluid component in the generation of primitive basaltic andesites and andesites from the Mt. Shasta region, N California. *Contributions to Mineralogy and Petrology*, *142*(4), 375–396. https://doi.org/10.1007/s004100100299

Gualda, G. A. R., Ghiorso, M. S., Lemons, R. V., & Carley, T. L. (2012). Rhyolite-MELTS: A modified calibration of MELTS optimized for silica-rich, fluid-bearing magmatic systems. *Journal of Petrology*, *53*(5), 875–890. https://doi.org/10.1093/petrology/egr080

Guffanti, M., & Weaver, C. S. (1988). Distribution of Late Cenozoic volcanic vents in the Cascade range: Volcanic arc segmentation and regional tectonic considerations. *Journal of Geophysical Research*, *93*(B6), 6513–6529. https://doi.org/10.1029/JB093iB06p06513

Harris, R. A., Iyer, H. M., & Dawson, P. B. (1991). Imaging the Juan de Fuca Plate beneath southern Oregon using teleseismic *P* wave residuals. *Journal of Geophysical Research*, *96*(B12), 19879–19889. https://doi.org/10.1029/91JB02046

Heath, B. A., Hooft, E. E. E., & Toomey, D. R. (2018). Autocorrelation of the seismic wavefield at Newberry Volcano: Reflections from the magmatic and geothermal systems. *Geophysical Research Letters*, *45*(5), 2311–2318. https://doi.org/10.1002/2017GL076706

Heath, B. A., Hooft, E. E. E., Toomey, D. R., & Bezada, M. J. (2015). Imaging the magmatic system of N ewberry V olcano using joint active source and teleseismic tomography. *Geochemistry, Geophysics, Geosystems*, *16*(12), 4433–4448. https://doi.org/10.1002/2015GC006129

Heiken, G. (1978). Plinian-type eruptions in the medicine lake highland, California, and the nature of the underlying magma. *Journal of Volcanology and Geothermal Research*, *4*(3–4), 375–402. https://doi.org/10.1016/0377-0273(78)90023-9

Hildreth, W. (2007). Quaternary magmatism in the cascades- Geological perspectives. In *USGS professional paper 1744*.

Hildreth, W., & Fierstein, J. (1997). Recent eruptions of Mount Adams, Washington cascades, USA. *Bulletin of Volcanology*, *58*(6), 472–490. https://doi.org/10.1007/s004450050156

Hildreth, W., & Fierstein, J. (2015). *Geologic map of the Simcoe Mountains volcanic field, main central segment, Yakama Nation, Washington (Scientific investigations map 3315)*. Scientific Investigations Map.

Hildreth, W., Fierstein, J., Calvert, A. T., Robinson, J. E., Lindquist, T. A., & Nimz, K. (2012). Geologic map of three sisters volcanic cluster, cascade range, Oregon. In *Pamphlet to accompany scientific investigations map 3186, US Geological Survey*.

Hildreth, W., Fierstein, J., & Lanphere, M. (2003). Eruptive history and geochronology of the Mount Baker volcanic field, Washington. *Geological Society of America Bulletin*, *115*, 729–764. https://doi.org/10.1130/0016-7606(2003)115<0729:EHAGOT>2.0.CO;2

Hill, G. J., Caldwell, T. G., Heise, W., Chertkoff, D. G., Bibby, H. M., Burgess, M. K., et al. (2009). Distribution of melt beneath Mount St Helens and Mount Adams inferred from magnetotelluric data. *Nature Geoscience*, *2*(11), 785–789. https://doi.org/10.1038/ngeo661

Hilley, G., Brodsky, E., Roman, D., Shillington, D., & Tobin, H. (2022). SZ4D Implementation plan. *Stanford Digital Repository*. https://doi.org/10.25740/HY589FC7561

Hodge, B. E., & Crider, J. G. (2010). Investigating mechanisms of edifice deflation, 1981–2007, at Mount Baker volcano, Washington, United States. *Journal of Geophysical Research*, *115*(B4), B04401. https://doi.org/10.1029/2009JB006730

Hollyday, A. E., Leiter, S. H., & Walowski, K. J. (2020). Pre-eruptive storage, evolution, and ascent timescales of a high-Mg basaltic andesite in the southern Cascade Arc. *Contributions to Mineralogy and Petrology*, *175*(9), 88. https://doi.org/10.1007/s00410-020-01730-z

Huber, C., Townsend, M., Degruyter, W., & Bachmann, O. (2019). Optimal depth of subvolcanic magma chamber growth controlled by volatiles and crust rheology. *Nature Geoscience*, *12*(9), 762–768. https://doi.org/10.1038/s41561-019-0415-6

Hughes, E. C., Buse, B., Kearns, S. L., Blundy, J. D., Kilgour, G., & Mader, H. M. (2019). Low analytical totals in EPMA of hydrous silicate glass due to sub-surface charging: Obtaining accurate volatiles by difference. *Chemical Geology*, *505*, 48–56. https://doi.org/10.1016/j.chemgeo.2018.11.015

Humphreys, M. C. S., Cooper, G. F., Zhang, J., Loewen, M., Kent, A. J. R., Macpherson, C. G., & Davidson, J. P. (2019). Unravelling the complexity of magma plumbing at Mount St. Helens: A new trace element partitioning scheme for amphibole. *Contributions to Mineralogy and Petrology*, *174*(1), 9. https://doi.org/10.1007/s00410-018-1543-5

Iacono-Marziano, G., Morizet, Y., Le Trong, E., & Gaillard, F. (2012). New experimental data and semi-empirical parameterization of H_2O-CO_2 solubility in mafic melts. *Geochimica et Cosmochimica Acta*, *97*, 1–23. https://doi.org/10.1016/j.gca.2012.08.035

Iacovino, K., Matthews, S., Wieser, P. E., Moore, G., & Begue, F. (2021). VESIcal Part I: An open-source thermodynamic model engine for mixed volatile (H_2O-CO_2) solubility in silicate melt. *Earth and Space Science*, *8*(11), e2020EA001584. https://doi.org/10.1029/2020EA001584

Jiang, C., Schmandt, B., Abers, G. A., Kiser, E., & Miller, M. S. (2023). Segmentation and radial anisotropy of the deep crustal magmatic system beneath the Cascades arc. *Geochemistry, Geophysics, Geosystems*. https://doi.org/10.1002/essoar.10512621.1

Johnson, E. R., & Cashman, K. V. (2020). Understanding the storage conditions and fluctuating eruption style of a young monogenetic volcano: Blue Lake crater (<3 ka), High Cascades, Oregon. *Journal of Volcanology and Geothermal Research*, *408*, 107103. https://doi.org/10.1016/j.jvolgeores.2020.107103

Jones, J., & Malone, S. D. (2005). Mount Hood earthquake activity: Volcanic or tectonic origins? *Bulletin of the Seismological Society of America*, *95*(3), 818–832. https://doi.org/10.1785/0120040019

Jorgenson, C., Higgins, O., Petrelli, M., Bégué, F., & Caricchi, L. (2022). A machine learning-based approach to clinopyroxene thermobarometry: Model optimization and distribution for use in earth sciences. *JGR Solid Earth*, *127*(4), e2021JB022904. https://doi.org/10.1029/2021JB022904

Keith, T. E., Donnelly-Nolan, J., Markman, J., & Beeson, M. (1985). K-Ar ages of rocks in the Mount Hood area, Oregon. *Isochron-West*, *42*, 12–17.

Kent, A. J. R., Darr, C., Koleszar, A. M., Salisbury, M. J., & Cooper, K. M. (2010). Preferential eruption of andesitic magmas through recharge filtering. *Nature Geoscience*, *3*(9), 631–636. https://doi.org/10.1038/ngeo924

Kinzler, R. J. (1985). *A field, petrologic, and geochemical study of the Callahan lava flow, a basaltic andesite from Medicine Lake shield volcano, California* (MSc thesis). MIT.

Kinzler, R. J., Donnelly-Nolan, J. M., & Grove, T. L. (2000). Late Holocene hydrous mafic magmatism at the Paint Pot crater and Callahan flows, Medicine Lake volcano, N. California and the influence of H2O in the generation of silicic magmas. *Contributions to Mineralogy and Petrology*, *138*, 1–16. https://doi.org/10.1007/PL00007657

Kiser, E., Levander, A., Zelt, C., Schmandt, B., & Hansen, S. (2018). Focusing of melt near the top of the Mount St. Helens (USA) magma reservoir and its relationship to major volcanic eruptions. *Geology*, *46*(9), 775–778. https://doi.org/10.1130/G45140.1

Kiser, E., Palomeras, I., Levander, A., Zelt, C., Harder, S., Schmandt, B., et al. (2016). Magma reservoirs from the upper crust to the Moho inferred from high-resolution V_p and V_s models beneath Mount St. Helens, Washington State, USA. *Geology*, *44*(6), 411–414. https://doi.org/10.1130/G37591.1

Koleszar, A. M. (2011). *Controls on eruption style and magma compositions at Mount Hood, Oregon* (PhD thesis). Oregon State University.

Koleszar, A. M., Kent, A. J. R., Wallace, P. J., & Scott, W. E. (2012). Controls on long-term low explosivity at andesitic arc volcanoes: Insights from Mount Hood, Oregon. *Journal of Volcanology and Geothermal Research*, *219*(220), 1–14. https://doi.org/10.1016/j.jvolgeores.2012.01.003

Krawczynski, M. J., Grove, T. L., & Behrens, H. (2012). Amphibole stability in primitive arc magmas: Effects of temperature, H_2O content, and oxygen fugacity. *Contributions to Mineralogy and Petrology*, *164*(2), 317–339. https://doi.org/10.1007/s00410-012-0740-x

Lamadrid, H. M., Moore, L. R., Moncada, D., Rimstidt, J. D., Burruss, R. C., & Bodnar, R. J. (2017). Reassessment of the Raman CO_2 densimeter. *Chemical Geology*, *450*, 210–222. https://doi.org/10.1016/j.chemgeo.2016.12.034

Lee, C.-T. A., & Anderson, D. L. (2015). Continental crust formation at arcs, the arclogite "delamination" cycle, and one origin for fertile melting anomalies in the mantle. *Science Bulletin*, *60*(13), 1141–1156. https://doi.org/10.1007/s11434-015-0828-6

Lerner, A. H., O'Hara, D., Karlstrom, L., Ebmeier, S. K., Anderson, K. R., & Hurwitz, S. (2020). The prevalence and significance of offset magma reservoirs at arc volcanoes. *Geophysical Research Letters*, *47*(14), e2020GL087856. https://doi.org/10.1029/2020GL087856

Le Voyer, M., Rose-Koga, E. F., Shimizu, N., Grove, T. L., & Schiano, P. (2010). Two contrasting H_2O-rich components in primary melt inclusions from Mount Shasta. *Journal of Petrology*, *51*(7), 1571–1595. https://doi.org/10.1093/petrology/egq030

Linneman, S. R., & Myers, J. D. (1990). Magmatic inclusions in the Holocene rhyolites of Newberry volcano, central Oregon. *Journal of Geophysical Research*, *95*(B11), 17677–17691. https://doi.org/10.1029/jb095ib11p17677

Lipman, P. W., Banks, N. G., & Rhodes, J. M. (1985). Degassing-induced crystallization of basaltic magma and effects on lava rheology. *Nature*, *317*(6038), 604–607. https://doi.org/10.1038/317604a0

Lisowski, M., Dzurisin, D., Denlinger, R. P., & Iwatsubo, E. (2008). Analysis of GPS-measured deformation associated with the 2004–2006 dome-building eruption of Mount St. Helens, Washington. In *A volcano Rekindled: The renewed eruption of Mount St. Helens, 2004–2006, USGS professional paper 1750*.

Loewen, M. W. (2012). *Volatile mobility of trace metals in volcanic systems* (PhD dissertation) (p. 237). Oregon State University.

Lowenstern, J. B. (2003). Melt inclusions come of age: Volatiles, volcanoes, and sorby's legacy. In *Developments in volcanology* (pp. 1–21). Elsevier. https://doi.org/10.1016/S1871-644X(03)80021-9

Lu, L., & Bostock, M. G. (2022). Deep long-period earthquakes near Mount Meager, British Columbia. *Canadian Journal of Earth Sciences*, *59*(7), 407–417. https://doi.org/10.1139/cjes-2021-0103

Lu, Z., Wicks, C., Dzurisin, D., Thatcher, W., Freymueller, J. T., McNutt, S. R., & Mann, D. (2000). Aseismic inflation of Westdahl volcano, Alaska, revealed by satellite radar interferometry. *Geophysical Research Letters*, *27*(11), 1567–1570. https://doi.org/10.1029/1999gl011283

Magee, C., Stevenson, C. T. E., Ebmeier, S. K., Keir, D., Hammond, J. O. S., Gottsmann, J. H., et al. (2018). Magma plumbing systems: A geophysical perspective. *Journal of Petrology*, *59*(6), 1217–1251. https://doi.org/10.1093/petrology/egy064

Mandeville, C. W., Webster, J. D., Tappen, C., Taylor, B. E., Timbal, A., Sasaki, A., et al. (2009). Stable isotope and petrologic evidence for open-system degassing during the climactic and pre-climactic eruptions of Mt. Mazama, Crater Lake, Oregon. *Geochimica et Cosmochimica Acta*, *73*(10), 2978–3012. https://doi.org/10.1016/j.gca.2009.01.019

Mandler, B. E., Donnelly-Nolan, J. M., & Grove, T. L. (2014). Straddling the tholeiitic/calc-alkaline transition: The effects of modest amounts of water on magmatic differentiation at Newberry Volcano, Oregon. *Contributions to Mineralogy and Petrology*, *168*(4), 1066. https://doi.org/10.1007/s00410-014-1066-7

Mastin, L. G., Roeloffs, E., Beeler, N. M., & Quick, J. E. (2008). Constraints on the size, overpressure, and volatile content of the Mount St. Helens magma system from geodetic and dome-growth measurements during the 2004–2006+ eruption. A volcano Rekindled: The renewed eruption of Mount St. Helens, 2004–2006. In *U.S. geological survey professional paper 1750* (pp. 461–488).

McCrory, P. A., Blair, J. L., Waldhauser, F., & Oppenheimer, D. H. (2012). Juan de Fuca slab geometry and its relation to Wadati-benioff zone seismicity: JDF slab geometry and WBZ seismicity. *Journal of Geophysical Research*, *117*(B9), B09306. https://doi.org/10.1029/2012JB009407

McGary, R. S., Evans, R. L., Wannamaker, P. E., Elsenbeck, J., & Rondenay, S. (2014). Pathway from subducting slab to surface for melt and fluids beneath Mount Rainier. *Nature*, *511*(7509), 338–340. https://doi.org/10.1038/nature13493

Mercer, C. N., & Johnston, A. D. (2008). Experimental studies of the P–T–H_2O near-liquidus phase relations of basaltic andesite from North Sister volcano, high Oregon cascades: Constraints on lower-crustal mineral assemblages. *Contributions to Mineralogy and Petrology*, *155*(5), 571–592. https://doi.org/10.1007/s00410-007-0259-8

Mironov, N. L., Tobelko, D. P., Smirnov, S. Z., Portnyagin, M. V., & Krasheninnikov, S. P. (2020). Estimation of CO_2 content in the gas phase of melt inclusions using Raman spectroscopy: Case study of inclusions in olivine from the Karymsky volcano (Kamchatka). *Russian Geology and Geophysics*, *61*(5–6), 600–610. https://doi.org/10.15372/RGG2019169

Moore, L. R., Gazel, E., Tuohy, R., Lloyd, A. S., Esposito, R., Steele-MacInnis, M., et al. (2015). Bubbles matter: An assessment of the contribution of vapor bubbles to melt inclusion volatile budgets. *American Mineralogist*, *100*(4), 806–823. https://doi.org/10.2138/am-2015-5036

Moore, L. R., Mironov, N., Portnyagin, M., Gazel, E., & Bodnar, R. J. (2018). Volatile contents of primitive bubble-bearing melt inclusions from Klyuchevskoy volcano, Kamchatka: Comparison of volatile contents determined by mass-balance versus experimental homogenization. *Journal of Volcanology and Geothermal Research*, *358*, 124–131. https://doi.org/10.1016/j.jvolgeores.2018.03.007

Moore, N. E., & DeBari, S. M. (2012). Mafic magmas from Mount Baker in the northern Cascade arc, Washington: Probes into mantle and crustal processes. *Contributions to Mineralogy and Petrology*, *163*(3), 521–546. https://doi.org/10.1007/s00410-011-0686-4

Moran, S. C., & Benjamin, P. (2021). Permitting Volcano monitoring stations in wilderness/restricted areas: A case study from Mount Hood, Oregon. In *D138. Presented at the GSA meeting*.

Moran, S. C., Lees, J. M., & Malone, S. D. (1999). *P* wave crustal velocity structure in the greater Mount Rainier area from local earthquake tomography. *Journal of Geophysical Research*, *104*(B5), 10775–10786. https://doi.org/10.1029/1999JB900036

Mordensky, S. P., & Wallace, P. J. (2018). Magma storage below cascades shield volcanoes as inferred from melt inclusion data: A comparison of long-lived and short-lived magma plumbing systems. *Journal of Volcanology and Geothermal Research*, *368*, 1–12. https://doi.org/10.1016/j.jvolgeores.2018.10.011

Mullen, E. K., & McCallum, I. S. (2014). Origin of basalts in a hot subduction setting: Petrological and geochemical insights from Mt. Baker, Northern Cascade Arc. *Journal of Petrology*, *55*(2), 241–281. https://doi.org/10.1093/petrology/egt064

Mullineaux, D. R. (1974). *Pumice and other pyroclastic deposits in Mount Rainier National Park*. US Government Printing Office.

Musumeci, C., Gresta, S., & Malone, S. D. (2002). Magma system recharge of Mount St. Helens from precise relative hypocenter location of microearthquakes: Magma recharge of St. Helens from hypocenters. *Journal of Geophysical Research*, *107*(B10), ESE16-1–ESE16-9. https://doi.org/10.1029/2001JB000629

Nakada, S., Bacon, C. R., & Gartner, A. E. (1994). Origin of phenocrysts and compositional diversity in pre-Mazama rhyodacite lavas, Crater Lake, Oregon. *Journal of Petrology*, *35*(1), 127–162. https://doi.org/10.1093/petrology/35.1.127

NASA/METI/AIST/Japan Space systems and U.S./Japan ASTER Science Team. (2019). ASTER global digital elevation model V003. https://doi.org/10.5067/ASTER/ASTGTM.003

Neave, D. A., & Putirka, K. D. (2017). A new clinopyroxene-liquid barometer, and implications for magma storage pressures under Icelandic rift zones. *American Mineralogist*, *102*(4), 777–794. https://doi.org/10.2138/am-2017-5968

Nichols, M. L., Malone, S. D., Moran, S. C., Thelen, W. A., & Vidale, J. E. (2011). Deep long-period earthquakes beneath Washington and Oregon volcanoes. *Journal of Volcanology and Geothermal Research*, *200*(3–4), 116–128. https://doi.org/10.1016/j.jvolgeores.2010.12.005

Obrebski, M., Abers, G. A., & Foster, A. (2015). Magmatic arc structure around M ount R ainier, WA, from the joint inversion of receiver functions and surface wave dispersion. *Geochemistry, Geophysics, Geosystems*, *16*(1), 178–194. https://doi.org/10.1002/2014gc005581

O'Hara, D., Karlstrom, L., & Ramsey, D. W. (2020). Time-evolving surface and subsurface signatures of Quaternary volcanism in the Cascades arc. *Geology*, *48*(11), 1088–1093. https://doi.org/10.1130/G47706.1

Pallister, J. S., Clynne, M. A., Wright, H. M., Van Eaton, A. R., Vallance, J. W., Sherrod, D. R., & Kokelaar, B. P. (2017). *Field-trip guide to Mount St. Helens, Washington-An overview of the eruptive history and petrology, tephra deposits, 1980 pyroclastic density current deposits, and the crater*. Scientific Investigations Report.

Park, S. K., & Ostos, L. C. (2013). Constraints from magnetotelluric measurements on magmatic processes and upper mantle structure in the vicinity of Lassen volcanic center, northern California. *Geosphere*, *9*(3), 382–393. https://doi.org/10.1130/GES00799.1

Parker, A. L., Biggs, J., & Lu, Z. (2014). Investigating long-term subsidence at Medicine Lake Volcano, CA, using multitemporal InSAR. *Geophysical Journal International*, *199*(2), 844–859. https://doi.org/10.1093/gji/ggu304

Parker, A. L., Biggs, J., & Lu, Z. (2016). Time-scale and mechanism of subsidence at Lassen volcanic center, CA, from InSAR. *Journal of Volcanology and Geothermal Research*, *320*, 117–127. https://doi.org/10.1016/j.jvolgeores.2016.04.013

Parsons, T., Trehu, A. M., Luetgert, J. H., Miller, K., Kilbride, F., Wells, R. E., et al. (1998). A new view into the Cascadia subduction zone and volcanic arc: Implications for earthquake hazards along the Washington margin. *Geology*, *26*(3), 199. https://doi.org/10.1130/0091-7613(1998)026<0199:ANVITC>2.3.CO;2

PennyWieser. (2023). PennyWieser/Cascade_data_Compilation: Cascade_Supplementary_Data (v.1.1) [Dataset]. Zenodo. https://doi.org/10.5281/zenodo.8327609

Phillips, M., & Till, C. B. (2022). Crustal storage and ascent history of the Mt. Shasta primitive magnesian andesite: Implications for arc magma crustal flux rates. *Contributions to Mineralogy and Petrology*, *177*(1), 9. https://doi.org/10.1007/s00410-021-01853-x

Pitcher, B. W., & Kent, A. J. R. (2019). Statistics and segmentation: Using big data to assess Cascades arc compositional variability. *Geochimica et Cosmochimica Acta*, *265*, 443–467. https://doi.org/10.1016/j.gca.2019.08.035

Pitt, A. M., Hill, D. P., Walter, S. W., & Johnson, M. J. S. (2002). Midcrustal, long-period Earthquakes beneath northern California volcanic areas. *Seismological Research Letters*, *73*(2), 144–152. https://doi.org/10.1785/gssrl.73.2.144

Platt, B. (2020). *Constraining Internal eruption trigger mechanisms for flows at Brokeoff Volcano, Lassen volcanic center, California* (Masters thesis). California State Fresno

Poland, M. P., Bawden, G., Liwoski, M., & Dzurisin, D. (2004). Newly discovered subsidence at Lassen peak, southern cascade range, California, from InSAR and GPS. In *Presented at the AGU fall meeting, San Fran. Abstract G51A-0068*.

Poland, M. P., Bürgmann, R., Dzurisin, D., Lisowski, M., Masterlark, T., Owen, S., & Fink, J. (2006). Constraints on the mechanism of long-term, steady subsidence at Medicine Lake volcano, northern California, from GPS, leveling, and InSAR. *Journal of Volcanology and Geothermal Research*, *150*(1–3), 55–78. https://doi.org/10.1016/j.jvolgeores.2005.07.007

Poland, M. P., Lisowski, M., Dzurisin, D., Kramer, R., McLay, M., & Pauk, B. (2017). Volcano geodesy in the Cascade arc, USA. *Bulletin of Volcanology*, *79*(8), 59. https://doi.org/10.1007/s00445-017-1140-x

Poland, M. P., Miklius, A., & Emily, M.-B. (2014). Magma supply, storage, and transport at shield-stage Hawaiian volcanoes. In *Characteristics of Hawaiian volcanoes, professional paper 1801* (pp. 179–234). U.S. Geological Survey.

Priest, G. R., Hladky, F. R., Mertzman, S. A., Murray, R. B., & Wiley, T. J. (2013). Volcanic signature of Basin and range extension on the shrinking Cascade arc, Klamath falls-Keno area, Oregon. *Journal of Geophysical Research: Solid Earth*, *118*(8), 4013–4038. https://doi.org/10.1002/jgrb.50290

Pritchard, M. E., Mather, T. A., McNutt, S. R., Delgado, F. J., & Reath, K. (2019). Thoughts on the criteria to determine the origin of volcanic unrest as magmatic or non-magmatic. *Philosophical Transactions of the Royal Society A*, *377*(2139), 20180008. https://doi.org/10.1098/rsta.2018.0008

Prueher, L. M., & McBirney, A. R. (1988). Relations of cinder cones to the magmatic evolution of Mount Mazama, Crater Lake National park, Oregon. *Journal of Volcanology and Geothermal Research*, *35*(3), 253–268. https://doi.org/10.1016/0377-0273(88)90021-2

Putirka, K. D. (2008). Thermometers and barometers for volcanic systems. *Reviews in Mineralogy and Geochemistry*, *69*(1), 61–120. https://doi.org/10.2138/rmg.2008.69.3

Putirka, K. D., Johnson, M., Kinzler, R., Longhi, J., & Walker, D. (1996). Thermobarometry of mafic igneous rocks based on clinopyroxene-liquid equilibria, 0–30 kbar. *Contributions to Mineralogy and Petrology*, *123*(1), 92–108. https://doi.org/10.1007/s004100050145

QGIS.org. (2022). QGIS geographic information system. Retrieved from http://www.qgis.org

Quinn, E. (2014). *Experimental determination of pre-eruptive storage conditions and continuous decompression of rhyodacite magma erupted from Chaos Crags, Lassen volcanic center, California* (MSci thesis). Hombold State University.

Rasmussen, D. J., Plank, T. A., Roman, D. C., & Zimmer, M. M. (2022). Magmatic water content controls the pre-eruptive depth of arc magmas. *Science*, *375*(6585), 1169–1172. https://doi.org/10.1126/science.abm5174

Reeg, H. (2008). *Seismic structure of the crust and upper mantle of the Sierra Nevada, California* (MSci thesis). University of Colorado.

Riddick, S. N., & Schmidt, D. A. (2011). Time-dependent changes in volcanic inflation rate near Three Sisters, Oregon, revealed by InSAR. *Geochemistry, Geophysics, Geosystems*, *12*, 12. https://doi.org/10.1029/2011GC003826

Ridolfi, F. (2021). Amp-TB2: An updated model for calcic amphibole thermobarometry. *Minerals*, *11*(3), 324. https://doi.org/10.3390/min11030324

Ritter, J. R. R., & Evans, J. R. (1997). Deep structure of Medicine Lake volcano, California. *Tectonophysics*, *275*(1–3), 221–241. https://doi.org/10.1016/S0040-1951(97)00022-X

Rohay, A., & Malone, S. D. (1977). Seismic velocity anomalies in the vicinity of Mt. Baker, Washington (Abstract). In *Presented at the Geological Society of America* (Vol. 9).

Rowe, M., Thornber, C. R., Gooding, D., & Pallister, J. (2008). *Catalog of Mount St. Helens 2004–2005 tephra samples with major- and trace-element geochemistry*. U.S. Geological Survey Open-File Report 2008-1131.

Rudnick, R. L. (1995). Making continental crust. *Nature*, *378*(6557), 571–578. https://doi.org/10.1038/378571a0

Ruscitto, D. M., Wallace, P. J., Johnson, E. R., Kent, A. J. R., & Bindeman, I. N. (2010). Volatile contents of mafic magmas from cinder cones in the Central Oregon High Cascades: Implications for magma formation and mantle conditions in a hot arc. *Earth and Planetary Science Letters*, *298*(1–2), 153–161. https://doi.org/10.1016/j.epsl.2010.07.037

Ruscitto, D. M., Wallace, P. J., & Kent, A. J. R. (2011). Revisiting the compositions and volatile contents of olivine-hosted melt inclusions from the Mount Shasta region: Implications for the formation of high-Mg andesites. *Contributions to Mineralogy and Petrology*, *162*(1), 109–132. https://doi.org/10.1007/s00410-010-0587-y

Rutherford, M. J., & Devine, J. D. (1988). The May 18, 1980, eruption of Mount St. Helens: 3. Stability and chemistry of amphibole in the magma chamber. *Journal of Geophysical Research*, *93*(B10), 11949–11959. https://doi.org/10.1029/JB093iB10p11949

Rutherford, M. J., & Devine, J. D. (2008). Chapter 31: Magmatic conditions and processes in the storage zone of the 2004–2006 Mount St. Helens dacite. In *A volcano Rekindled: The renewed eruption of Mount St. Helens, 2004–2006. Professional paper 1750-31*.

Rutherford, M. J., Sigurdsson, H., Carey, S., & Davis, A. (1985). The May 18, 1980, eruption of Mount St. Helens: 1. Melt composition and experimental phase equilibria. *Journal of Geophysical Research*, *90*(B4), 2929–2947. https://doi.org/10.1029/JB090iB04p02929

Ryan, W. B. F., Carbotte, S. M., Coplan, J. O., O'Hara, S., Melkonian, A., Arko, R., et al. (2009). Global multi-resolution topography synthesis. *Geochemistry, Geophysics, Geosystems*, *10*(3), Q03014. https://doi.org/10.1029/2008GC002332

Sas, M., DeBari, S., Clynne, M., & Rusk, B. (2017). Using mineral geochemistry to decipher slab, mantle, and crustal input in the generation of high-Mg andesites and basaltic andesites from the northern Cascade Arc. *American Mineralogist*, *102*(5), 948–965. https://doi.org/10.2138/am-2017-5756

Scandone, R., & Malone, S. D. (1985). Magma supply, magma discharge and readjustment of the feeding system of Mount St. Helens during 1980. *Journal of Volcanology and Geothermal Research*, *23*(3–4), 239–262. https://doi.org/10.1016/0377-0273(85)90036-8

Schmidt, M. E., & Grunder, A. L. (2011). Deep mafic Roots to arc volcanoes: Mafic recharge and differentiation of basaltic andesite at North Sister volcano, Oregon cascades. *Journal of Petrology*, *52*(3), 603–641. https://doi.org/10.1093/petrology/egq094

Schmidt, M. E., Grunder, A. L., & Rowe, M. C. (2008). Segmentation of the Cascade Arc as indicated by Sr and Nd isotopic variation among diverse primitive basalts. *Earth and Planetary Science Letters*, *266*(1–2), 166–181. https://doi.org/10.1016/j.epsl.2007.11.013

Schwab, B., & Castro, J. (2007). Pre-eruptive storage conditions of 1915 Lassen peak dacite. In *Presented at the GSA Denver annual meeting*.

Scott, S. (2010). Processes controlling Magma Chamber Evolution beneath Mt. Rainier, Washington (Thesis). Central Washington University.

Scott, W. E., & Gardner, C. (2017). Field-trip guide to Mount Hood, Oregon, highlighting eruptive history and hazards.

Scott, W. E., Gardner, C., Tilling, R. I., & Lanphere, M. A. (1997). Geologic history of Mount Hood volcano. Oregon: A field-trip guidebook: U.S. Geological survey open-file report (pp. 97–263).

Scruggs, M. A., & Putirka, K. D. (2018). Eruption triggering by partial crystallization of mafic enclaves at Chaos Crags, Lassen volcanic center, California. *American Mineralogist*, *103*(10), 1575–1590. https://doi.org/10.2138/am-2018-6058

Sémhur. (2007). Map of Garibaldi volcanic belt. Retrieved from https://commons.wikimedia.org/wiki/File:Garibaldi_Volcanic_Belt-en.svg

Shaw, S. (2011). *H_2O contents in olivine-hosted melt inclusions from primitive magmas in the Northern Cascade arc* (Masters thesis). Western Washington University.

Shehata, M. A., & Mizunaga, H. (2022). Moho depth and tectonic implications of the western United States: Insights from gravity data interpretation. *Geoscience Letters*, *9*(1), 23. https://doi.org/10.1186/s40562-022-00233-y

Sheppard, P. R., Ort, M. H., Anderson, K. C., Clynne, M. A., & May, E. M. (2009). Multiple dendrochronological responses to the eruption of cinder cone, Lassen volcanic National park, California. *Dendrochronologia*, *27*(3), 213–221. https://doi.org/10.1016/j.dendro.2009.09.001

Sherrod, D., Mastin, L., Scott, W., & Schilling, S. (1997). Volcano hazards at Newberry Volcano, Oregon. In *USGS open file report 97-513*.

Shishkina, T. A., Botcharnikov, R. E., Holtz, F., Almeev, R. R., Jazwa, A. M., & Jakubiak, A. A. (2014). Compositional and pressure effects on the solubility of H_2O and CO_2 in mafic melts. *Chemical Geology*, *388*, 112–129. https://doi.org/10.1016/j.chemgeo.2014.09.001

Sisson, T. W., & Lanphere, M. A. (2000). The geologic history of Mount Rainier volcano.

Sisson, T. W., & Layne, G. D. (1993). H_2O in basalt and basaltic andesite glass inclusions from four subduction-related volcanoes. *Earth and Planetary Science Letters*, *117*(3–4), 619–635. https://doi.org/10.1016/0012-821x(93)90107-k

Sisson, T. W., Salters, V. J. M., & Larson, P. B. (2014). Petrogenesis of Mount Rainier andesite: Magma flux and geologic controls on the contrasting differentiation styles at stratovolcanoes of the southern Washington Cascades. *Geological Society of America Bulletin*, *126*(1–2), 122–144. https://doi.org/10.1130/B30852.1

Sisson, T. W., Schmitt, A. K., Daníšík, M., Calvert, A. T., Pempena, N., Huang, C.-Y., & Shen, C.-C. (2019). Age of the dacite of Sunset Amphitheater, a voluminous Pleistocene tephra from Mount Rainier (USA), and implications for cascade glacial stratigraphy. *Journal of Volcanology and Geothermal Research*, *376*, 27–43. https://doi.org/10.1016/j.jvolgeores.2019.03.003

Sisson, T. W., & Vallance, J. W. (2009). Frequent eruptions of Mount Rainier over the last ~2,600 years. *Bulletin of Volcanology*, *71*(6), 595–618. https://doi.org/10.1007/s00445-008-0245-7

Smith, D., & Leeman, W. P. (1993). The origin of Mount St. Helens andesites. *Journal of Volcanology and Geothermal Research*, *55*(3), 271–303. https://doi.org/10.1016/0377-0273(93)90042-p

Stanley, W. D. (1984). Tectonic study of cascade range and Columbia plateau in Washington State based upon magnetotelluric soundings. *Journal of Geophysical Research*, *89*(B6), 4447–4460. https://doi.org/10.1029/JB089iB06p04447

Stauber, D. A., Green, S. M., & Iyer, H. M. (1988). Three-dimensional *P* velocity structure of the crust below Newberry Volcano, Oregon. *Journal of Geophysical Research*, *93*(B9), 10095–10107. https://doi.org/10.1029/JB093iB09p10095

Stockstill, K. (1999). *The origin and evolution of the Burroughs Mountain lava flow, Mount Rainier, Washington* (Masters thesis). Michigan State University.

Streck, M. J., & Leeman, W. P. (2018). Petrology of "Mt. Shasta" high-magnesian andesite (HMA): A product of multi-stage crustal assembly. *American Mineralogist*, *103*(2), 216–240. https://doi.org/10.2138/am-2018-6151

Taira, T., & Brenguier, F. (2016). Response of hydrothermal system to stress transients at Lassen Volcanic Center, California, inferred from seismic interferometry with ambient noise. *Earth Planets and Space*, *68*(1), 162. https://doi.org/10.1186/s40623-016-0538-6

Thornber, C. R., Pallister, J., Rowe, M., McConnell, S., Herriott, T. M., & Eckberg, A. (2008). Catalog of Mount St. Helens 2004–2007 dome samples with major- and trace-element chemistry.

Thurber, C., Zhang, H., Brocher, T., & Langenheim, V. (2009). Regional three-dimensional seismic velocity model of the crust and uppermost mantle of northern California: N. California 3-D seismic velocity model. *Journal of Geophysical Research*, *114*(B1), B01304. https://doi.org/10.1029/2008JB005766

Till, C. B., Kent, A. J. R., Abers, G. A., Janiszewski, H. A., Gaherty, J. B., & Pitcher, B. W. (2019). The causes of spatiotemporal variations in erupted fluxes and compositions along a volcanic arc. *Nature Communications*, *10*(1), 1350. https://doi.org/10.1038/s41467-019-09113-0

Turner, S. J., Izbekov, P., & Langmuir, C. (2013). The magma plumbing system of Bezymianny Volcano: Insights from a 54year time series of trace element whole-rock geochemistry and amphibole compositions. *Journal of Volcanology and Geothermal Research*, *263*, 108–121. https://doi.org/10.1016/j.jvolgeores.2012.12.014

Ulberg, C. W., Creager, K. C., Moran, S. C., Abers, G. A., Thelen, W. A., Levander, A., et al. (2020). Local source V_p and V_s tomography in the Mount St. Helens region with the iMUSH broadband array. *Geochemistry, Geophysics, Geosystems*, *21*(3), e2019GC008888. https://doi.org/10.1029/2019GC008888

Underwood, S. J., Feeley, T. C., & Clynne, M. A. (2012). Hydrogen isotope investigation of amphibole and biotite phenocrysts in silicic magmas erupted at Lassen Volcanic Center, California. *Journal of Volcanology and Geothermal Research*, *227*(228), 32–49. https://doi.org/10.1016/j.jvolgeores.2012.02.019

USGS. (2022). Mt Shasta hazards.

Ustunisik, G., Loewen, M. W., Nielsen, R. L., & Tepley, F. J. (2016). Interpretation of the provenance of small-scale heterogeneity as documented in a single eruptive unit from Mt. Jefferson, Central Oregon Cascades. *Geochemistry, Geophysics, Geosystems*, *17*(8), 3469–3487. https://doi.org/10.1002/2016GC006297

Venezky, D. Y., & Rutherford, M. J. (1997). Preeruption conditions and timing of dacite-andesite magma mixing in the 2.2 ka eruption at Mount Rainier. *Journal of Geophysical Research*, *102*(B9), 20069–20086. https://doi.org/10.1029/97JB01590

Venugopal, S., Schiavi, F., Moune, S., Bolfan-Casanova, N., Druitt, T., & Williams-Jones, G. (2020). Melt inclusion vapour bubbles: The hidden reservoir for major and volatile elements. *Scientific Reports*, *10*(1), 9034. https://doi.org/10.1038/s41598-020-65226-3

Wagner, T. P., Donnelly-Nolan, J. M., & Grove, T. L. (1995). Evidence of hydrous differentiation and crystal accumulation in the low-MgO, high-Al_2O_3 Lake Basalt from Medicine Lake volcano, California. *Contributions to Mineralogy and Petrology*, *121*(2), 201–216. https://doi.org/10.1007/s004100050099

Waite, G. P., & Moran, S. C. (2009). VP Structure of Mount St. Helens, Washington, USA, imaged with local earthquake tomography. *Journal of Volcanology and Geothermal Research*, *182*(1–2), 113–122. https://doi.org/10.1016/j.jvolgeores.2009.02.009

Waite, R., Mastin, L. G., & Beget, J. (1995). Volcanic hazard zonation for Glacier Peak volcano, Washington (USGS open file report 95-499), open-file report.

Walowski, K. J., Wallace, P. J., Cashman, K. V., Marks, J. K., Clynne, M. A., & Ruprecht, P. (2019). Understanding melt evolution and eruption dynamics of the 1666 C.E. eruption of Cinder Cone, Lassen Volcanic National Park, California: Insights from olivine-hosted melt inclusions. *Journal of Volcanology and Geothermal Research*, *387*, 106665. https://doi.org/10.1016/j.jvolgeores.2019.106665

Walowski, K. J., Wallace, P. J., Clynne, M. A., Rasmussen, D. J., & Weis, D. (2016). Slab melting and magma formation beneath the southern Cascade arc. *Earth and Planetary Science Letters*, *446*, 100–112. https://doi.org/10.1016/j.epsl.2016.03.044

Wang, X., Hou, T., Wang, M., Zhang, C., Zhang, Z., Pan, R., et al. (2021). A new clinopyroxene thermobarometer for mafic to intermediate magmatic systems. *European Journal of Mineralogy*, *33*(5), 621–637. https://doi.org/10.5194/ejm-33-621-2021

Wanke, M., Clynne, M. A., von Quadt, A., Vennemann, T. W., & Bachmann, O. (2019). Geochemical and petrological diversity of mafic magmas from Mount St. Helens. *Contributions to Mineralogy and Petrology*, *174*(1), 10. https://doi.org/10.1007/s00410-018-1544-4

Waters, L. E., Andrews, B. J., & Frey, H. M. (2021). Daly gaps at South Sister, Oregon, USA, generated via partial melting. *Contributions to Mineralogy and Petrology*, *176*(7), 52. https://doi.org/10.1007/s00410-021-01805-5

Weaver, C. S., Green, S. M., & Iyer, H. M. (1982). Seismicity of Mount Hood and structure as determined from teleseismic *P* wave delay studies. *Journal of Geophysical Research*, *87*(B4), 2782–2792. https://doi.org/10.1029/JB087iB04p02782

Weaver, C. S., Norris, R., & Jonientz-Trisler, C. (1990). Results of seismological monitoring in the cascade range, 1962–1989: Earthquakes, eruptions, avalanches and other curiosities. *Geoscience Canada*, *17*(3), 158–162.

White, R., & McCausland, W. (2016). Volcano-Tectonic earthquakes: A new tool for estimating intrusive volumes and forecasting eruptions. *Journal of Volcanology and Geothermal Research*, *309*, 139–155. https://doi.org/10.1016/j.jvolgeores.2015.10.020

Wicks, C. W. (2002). Magmatic activity beneath the quiescent Three Sisters volcanic center, central Oregon Cascade Range, USA. *Geophysical Research Letters*, *29*(7), 1122. https://doi.org/10.1029/2001GL014205

Wieser, P. E., Edmonds, M., Gansecki, C., Maclennan, J., Jenner, F. E., Kunz, B., et al. (2022a). Explosive activity on Kīlauea's lower east rift zone Fueled by a volatile-rich, dacitic melt. *Geochemistry, Geophysics, Geosystems*, *23*(2), e2021GC010046. https://doi.org/10.1029/2021GC010046

Wieser, P. E., Gleeson, M. L. M., Matthews, S., DeVitre, C. L., & Gazel, E. (2023a). Determining the pressure-Temperature-Composition (P-T-X) conditions of magma storage. *EarthArxiv Preprint*. https://doi.org/10.31223/X50M44

Wieser, P. E., Iacovino, K., Matthews, S., Moore, G., & Allison, C. (2022b). VESIcal Part II: A critical approach to volatile solubility modelling using an open-source Python3 engine (preprint). *Earth Sciences*. https://doi.org/10.1029/2021EA001932

Wieser, P. E., Kent, A. J., & Till, C. (2023b). Barometers behaving badly II: A critical evaluation of Cpx-only and Cpx-Liq thermobarometry in variably-hydrous arc magmas. *EarthArxiv*. https://doi.org/10.31223/X59655

Wieser, P. E., Kent, A. J. R., Till, C. B., Donovan, J., Neave, D. A., Blatter, D. L., & Krawczynski, M. J. (2023c). Barometers behaving badly I: Assessing the influence of analytical and experimental uncertainty on clinopyroxene thermobarometry calculations at crustal conditions. *Journal of Petrology*, *64*(2), egac126. https://doi.org/10.1093/petrology/egac126

Wieser, P. E., Lamadrid, H., Maclennan, J., Edmonds, M., Matthews, S., Iacovino, K., et al. (2021). Reconstructing magma storage depths for the 2018 Kīlauean eruption from melt inclusion CO_2 contents: The importance of vapor bubbles. *Geochemistry, Geophysics, Geosystems*, *22*(2), e2020GC009364. https://doi.org/10.1029/2020GC009364

Wieser, P. E., Petrelli, M., Lubbers, J., Wieser, E., Ozaydin, S., Kent, A., & Till, C. (2022c). Thermobar: An open-source Python3 tool for thermobarometry and hygrometry. *Volcanica*, *5*(2), 349–384. https://doi.org/10.30909/vol.05.02.349384

Wong, Y., & Segall, P. (2020). Joint inversions of ground deformation, extrusion flux, and gas emissions using physics-based models for the Mount St. Helens 2004–2008 eruption. *Geochemistry, Geophysics, Geosystems*, *21*(12), e2020GC009343. https://doi.org/10.1029/2020GC009343

Wright, H. M., Bacon, C. R., Vazquez, J. A., & Sisson, T. W. (2012). Sixty thousand years of magmatic volatile history before the caldera-forming eruption of Mount Mazama, Crater Lake, Oregon. *Contributions to Mineralogy and Petrology*, *164*(6), 1027–1052. https://doi.org/10.1007/s00410-012-0787-8

Zhang, H., Thurber, C. H., Shelly, D., Ide, S., Beroza, G. C., & Hasegawa, A. (2004). High-resolution subducting-slab structure beneath northern Honshu, Japan, revealed by double-difference tomography. *Geology*, *32*(4), 361. https://doi.org/10.1130/G20261.2

Zucca, J. J., & Evans, J. R. (1992). Active high-resolution compressional wave attenuation tomography at Newberry Volcano, central cascade range. *Journal of Geophysical Research*, *97*(B7), 11047–11055. https://doi.org/10.1029/92JB00492

References From the Supporting Information

Moore, G., Vennemann, T., & Carmichael, I. S. E. (1998). An empirical model for the solubility of H_2O in magmas to 3 kilobars. *American Mineralogist*, *83*(1–2), 36–42. https://doi.org/10.2138/am-1998-1-203

Newman, S., & Lowenstern, J. B. (2002). VolatileCalc: A silicate melt-H_2O-CO_2 solution model written in visual basic for excel. *Computers & Geosciences*, *28*(5), 597–604. https://doi.org/10.1016/S0098-3004(01)00081-4

Papale, P., Moretti, R., & Barbato, D. (2006). The compositional dependence of the saturation surface of H_2O+CO_2 fluids in silicate melts. *Chemical Geology*, *229*(1–3), 78–95. https://doi.org/10.1016/j.chemgeo.2006.01.013